

For Reference

NOT TO BE TAKEN FROM THIS ROOM

For Reference

NOT TO BE TAKEN FROM THIS ROOM

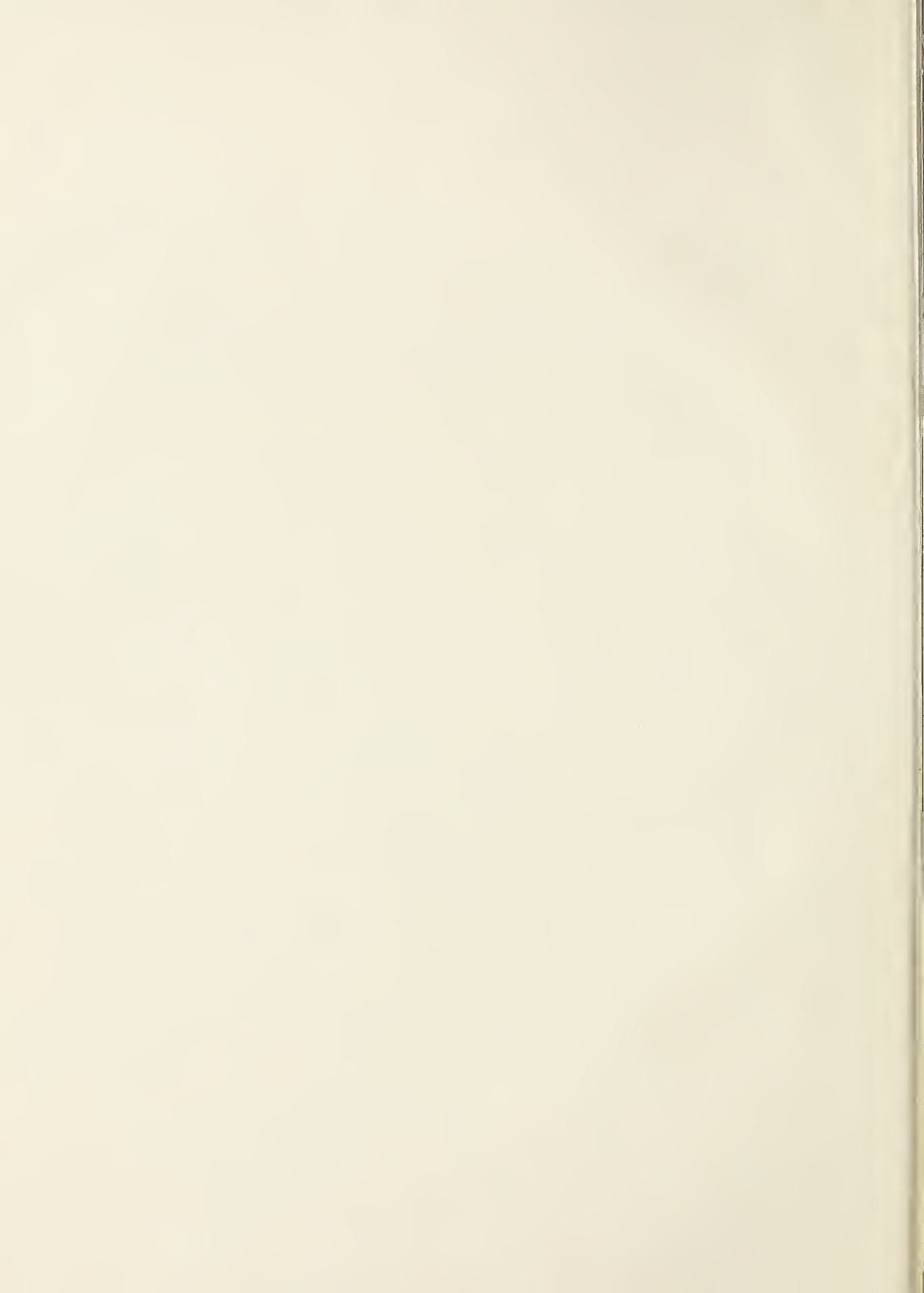
Ex LIBRIS
UNIVERSITATIS
ALBERTAENSIS





Digitized by the Internet Archive
in 2018 with funding from
University of Alberta Libraries

<https://archive.org/details/Adler1963>



thesis
963
1D

THE UNIVERSITY OF ALBERTA

ELECTRON TUNNELING INTO SUPERCONDUCTORS

by

J. G. Adler

A THESIS

SUBMITTED TO THE FACULTY OF GRADUATE STUDIES
IN PARTIAL FULFILLMENT OF THE REQUIREMENTS FOR THE DEGREE
OF DOCTOR OF PHILOSOPHY

DEPARTMENT OF PHYSICS

EDMONTON, ALBERTA

APRIL, 1963

ABSTRACT

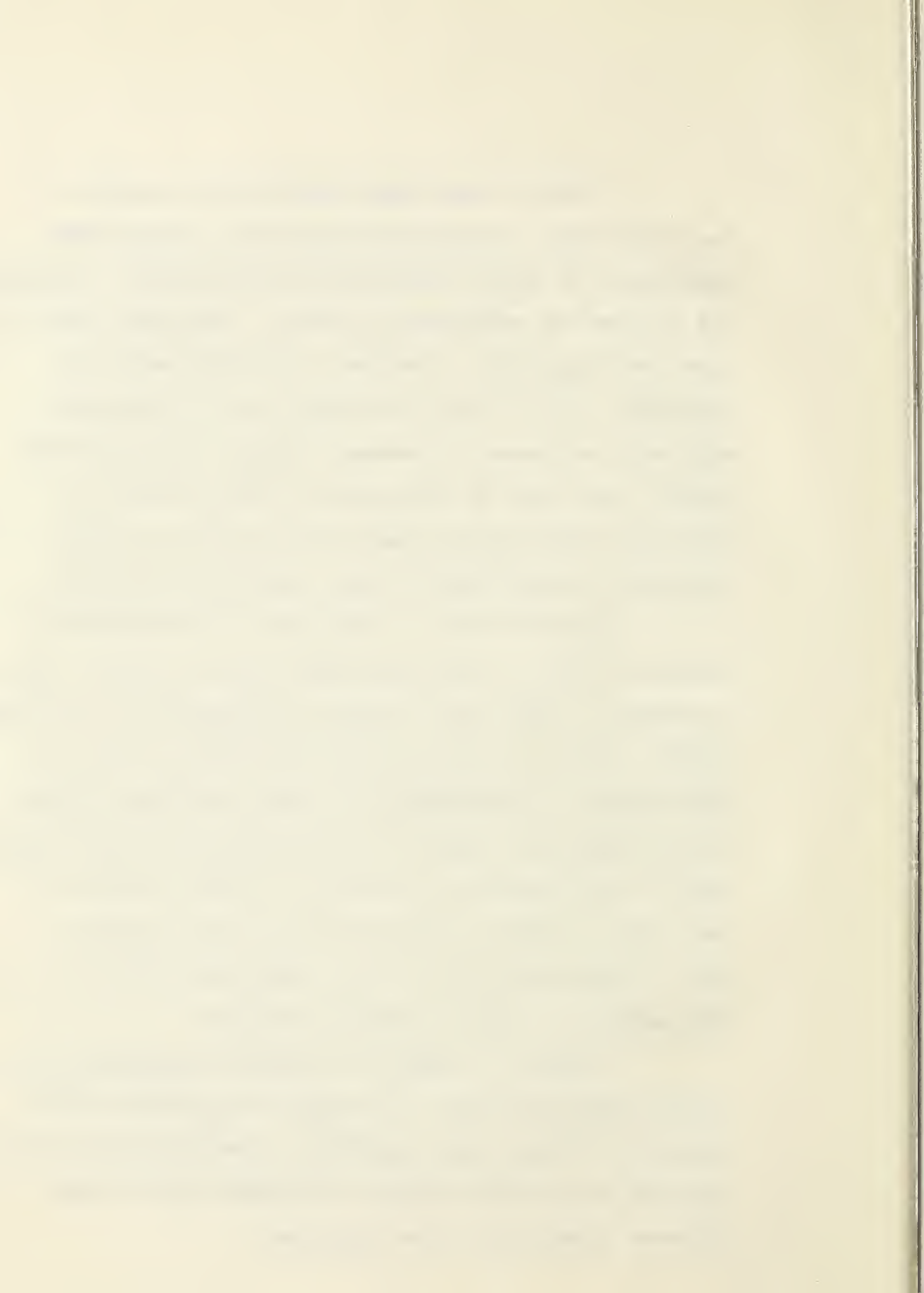
Since 1960 there has been a great deal of interest in experiments involving electron tunneling into superconductors. This new technique, which is very simple in principle, provides a direct method of observing the energy gap in the density of electron states of a superconductor. More recently this technique has also been applied to the study of detailed variation in the density of states in a superconductor. The theory of electron tunneling, as it applies to the study of superconductors, is discussed.

In order to be able to observe small variations in the density of states of superconductors a new method for measuring the dynamic conductance of tunnel junctions had to be devised. This method involves a very sensitive bridge technique and is described in detail. Since some of the experiments of interest had to be performed at temperatures below, 1°K a He^3 cryostat was used. A description of the design and operation as well as proposed modifications of this apparatus is given. Although the cryostat has so far only been used in tunneling experiments, it was designed in such a way that it would be used to investigate other phenomena, particularly transport properties in metals.

Initial experiments involved measurements of the energy gap in superconducting lead. During these experiments we gained familiarity with tunneling techniques and refined our experimental method. The energy gaps of superconducting zinc, aluminum, and indium were also measured. All of these are found to be in good agreement with the theory of Bardeen, Cooper, and Schrieffer (1957b), and with the exception of zinc for which no published tunneling data were found, with the values obtained by other workers using tunneling techniques.

The discovery of structure in the density of electron states of superconducting lead by Giaever, Hart, and Megerle (1962) and by Rowell, Chynoweth, and Phillips (1962), stimulated us to search for similar effects in other metals. Investigation by Adler and Rogers (1963) of the density of states of superconducting indium showed that if such structure is present it must be smaller by more than an order of magnitude than that observed in lead. However new and thus far unexplained structure in the density of states of indium was found.

Finally, a number of tunneling experiments involving superconductors, and which should lead to more definitive results, are proposed. A new method for investigation of the Fermi surface of normal metals using electron tunneling is also suggested.



ACKNOWLEDGEMENTS

It is a pleasure to express my gratitude to Dr. S.B. Woods, my research supervisor, for his cheerful help and encouragement during my years as a graduate student.

I am indebted to Drs. F.D. Manchester and D.D. Betts for many informative discussions.

Special thanks are due to Mr. J.S. Rogers for his assistance in the preparation and mounting of the specimens as well as help during some of the runs. It should also be noted that the design and analysis of the electrical measuring apparatus (Chapter III) was a joint project to which he and I contributed equally.

I wish to thank Mr. R.H. Enns for some helpful discussions concerning tunneling integrals.

Acknowledgements are also due to our expert glassblower, Mr. J. Legge, for his prompt and patient handling of the glassblowing. I am indebted to Messrs. H. McClung and P. Crouse for producing the necessary liquid air and liquid helium. Thanks are also due to the Computing Center for allowing me to use their facilities.

It is a pleasure to acknowledge the financial support of the National Research Council without which this project could not have been carried out.

Last but not least I wish to express my deep gratitude to my wife, Marilyn, and to Richie and Wendy for their patient endurance of the past years.

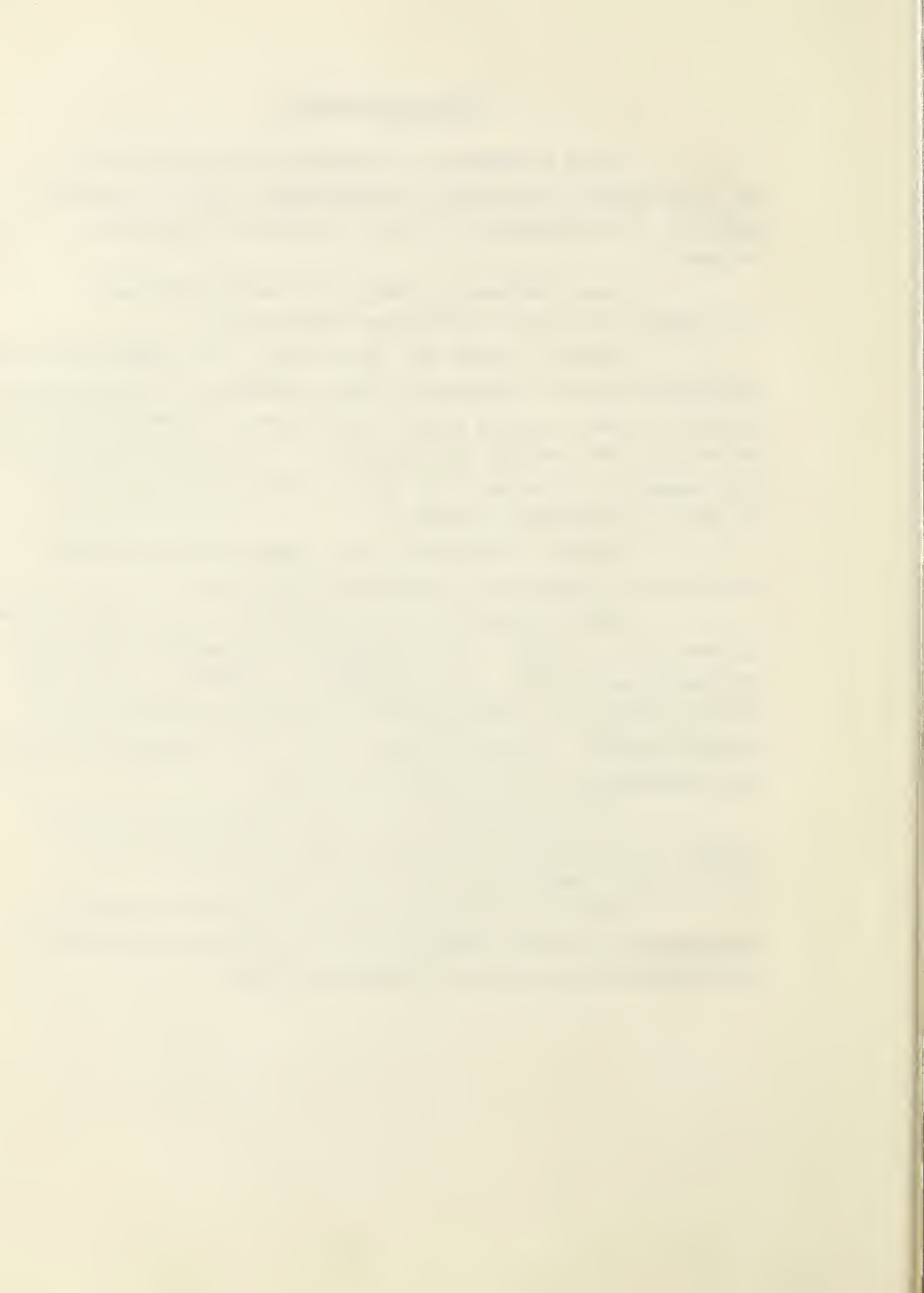


TABLE OF CONTENTS

Chapter		Page
I	THEORETICAL APPROACH TO SUPERCONDUCTIVITY	
	A. Historical Introduction	1
	B. Attempts at a Microscopic Theory of Superconductivity	3
	C. Experimental Evidence of an Energy gap in Superconductors	5
	D. The BCS Theory	6
	E. The Density of Electron States in a Superconductor	12
II	A SURVEY OF THE THEORY OF ELECTRON TUNNELING INTO SUPERCONDUCTORS	
	A. Introduction	13
	B. A Model of Tunneling	14
	C. Modification of the BCS Density of States in the Vicinity of the Energy Gap as indicated by Tunneling Measurements	23
	D. Multiphonon Effects Observed in Tunneling Experiments	26
III	ELECTRICAL APPARATUS AND MEASUREMENT CIRCUITS	
	A. Introduction	28
	B. The Tunneling Curve Tracer	29
	C. Data Processing	38
IV	DESIGN, CONSTRUCTION, AND OPERATION OF A He^3 CRYOSTAT	
	A. Introduction	42
	B. Sources of He^3	44
	C. General Features of He^3 Cryostats	46
	D. Description of the He^3 Cryostat	47
	E. Discussion of some of the Design Parameters of the Liquid He^3 Cryostat	53
	F. Thermometer Calibration	59
	G. Operating Procedure of the He^3 Cryostat	60
	H. Proposed Modifications to the He^3 Cryostat	63

Chapter		Page
V	EXPERIMENTAL METHOD	
	A. Preparation of Tunnel Junctions	66
	B. Specimen Mounting	75
	C. Procedure	77
VI	EXPERIMENTAL RESULTS	
	A. Current-Voltage Curves	79
	B. The Energy Gap	84
	C. Measurements of Relative Conductance	87
VII	CONCLUSIONS AND DISCUSSIONS	
	A. The Energy Gaps	95
	B. The relative Conductance Measurements	97
	C. Suggestions for Further Investigation	98
	D. A Proposed New Application of Electron Tunneling to Normal Metals	100
	BIBLIOGRAPHY	102

Appendices

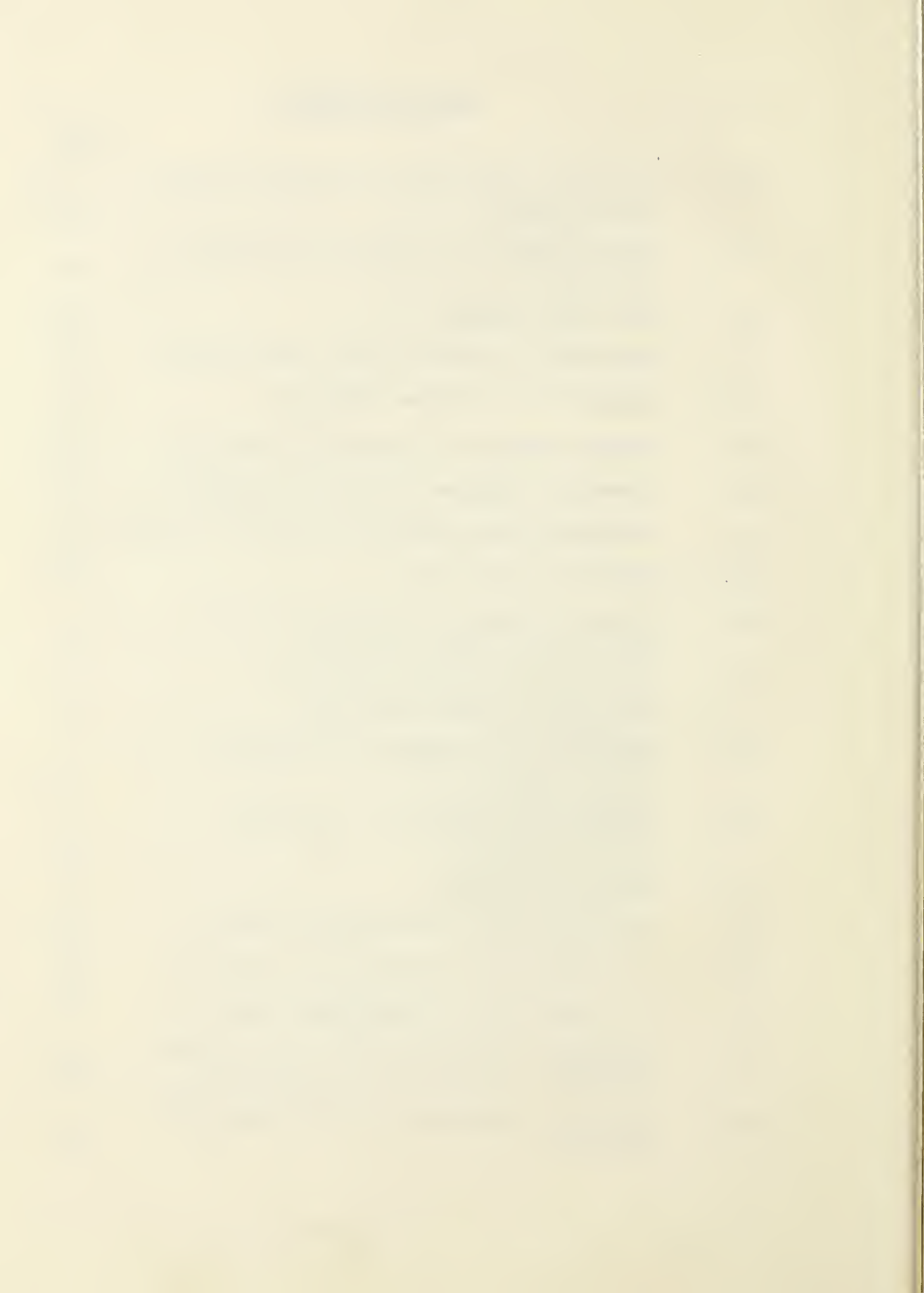
I	Evaluation of Some Integrals Occuring in Tunneling Problems	107
II	Numerical Evaluation of the Normalized Current and Relative Conductance for the Case of Two Identical Superconductors at the Absolute Zero	111
III	Machine Drawings of the Low Temperature Part of the He ³ Cryostat	116
IV	Summary of Results and Conclusions for the Experiments Involving Indium	126

LIST OF TABLES

I	Values of the Energy Gap	87
II	Normalized Current and Relative Conductance	112

LIST OF FIGURES

	Page
2.1 Schematic description of various tunneling processes	15
3.1 Block diagram of electrical measuring apparatus	30
3.2 The curve tracer	33
3.3 Equivalent circuit of the curve tracer	35
3.4 Example curve tracer operation	39
4.1 Vapour pressure of the helium isotopes	43
4.2 Schematic diagram of the He ³ cryostat	48
4.3 Proposed modifications of the He ³ cryostat	64
5.1 Specimen preparation	67
5.2 Current-voltage curve for a typical Al-Al ₂ O ₃ -Al tunnel junction	70
5.3 Semi-log plot of I-V curves for Al-Al ₂ O ₃ -Al tunnel junctions	71
5.4 Linearity of a typical Al-Al ₂ O ₃ -Al tunnel junction	72
5.5 Symmetry of a typical Al-Al ₂ O ₃ -Al tunnel junction	73
5.6 Specimen Mounting	76
6.1 I-V curves for a Pb-Al ₂ O ₃ -Al junction	80
6.2 I-V curves for a Zn-Al ₂ O ₃ -Al junction	85
6.3 I-V curves for a Al-Al ₂ O ₃ -Al junction	86
6.4 Relative conductance of an In-Al ₂ O ₃ -Al junction	89
6.5 Relative conductance of an In-Al ₂ O ₃ -Al junction	91

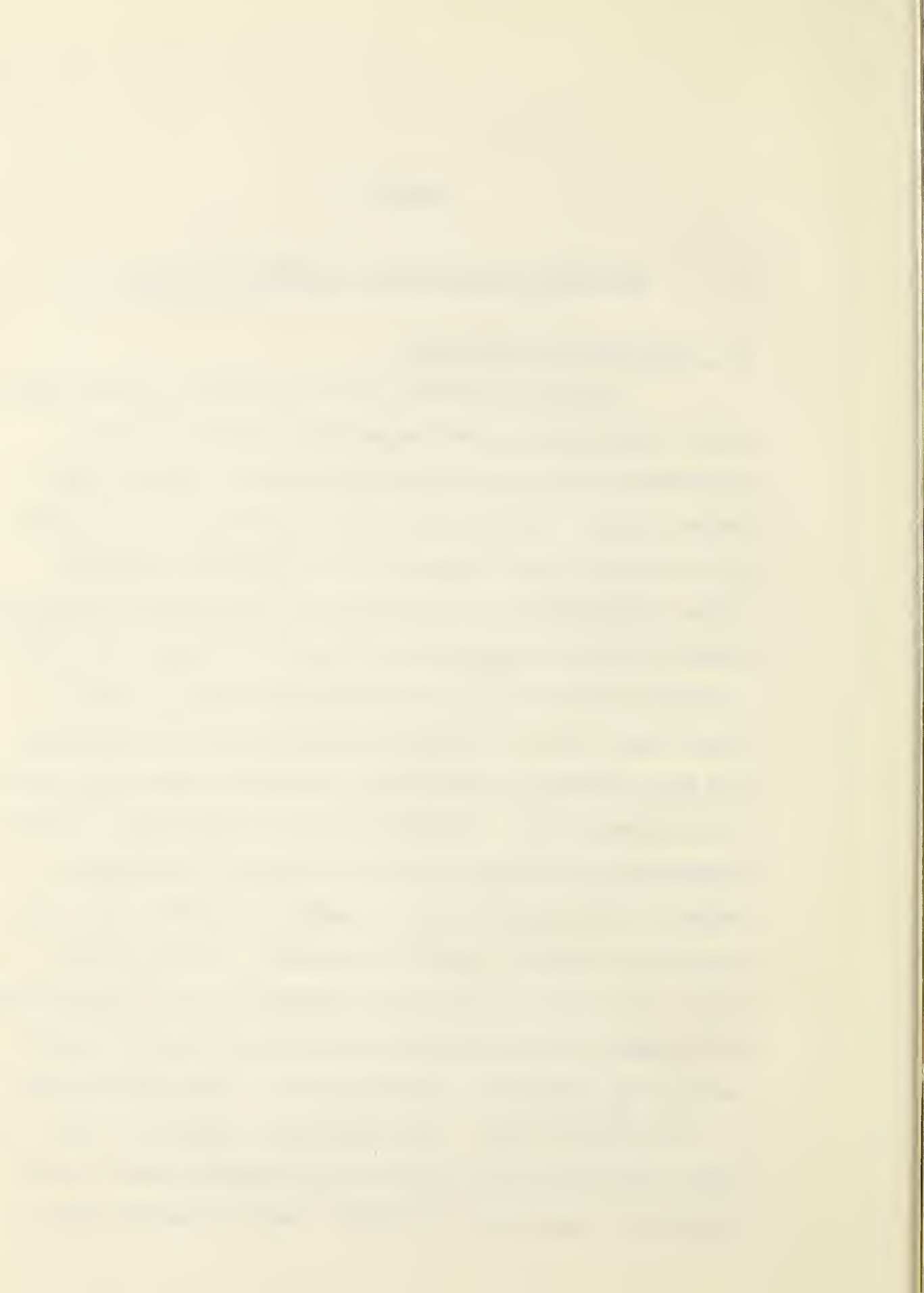


		Page
6.6	Relative conductance of an Al-Al ₂ O ₃ -Al junction	93
A-1	Assembly view of He ³ cryostat	117
A-2	He ⁴ Radiation trap	118
A-3	He ³ Radiation trap	119
A-4	He ³ Chamber	120
A-5	Top of outer can	121
A-6	He ⁴ Chamber	122
A-7	Ferrules	123
A-8	Outer can	124
A-9	Dewar cap	125
I	Relative Conductance of an In-Al ₂ O ₃ -Al Tunnel Junction	132

CHAPTER I

THEORETICAL APPROACH TO SUPERCONDUCTIVITYA. Historical Introduction

Superconductivity was discovered by Onnes (1911) while investigating the temperature variation of the electrical resistance of mercury wires at liquid helium temperatures. He found that the resistance of the wires he was using became residual (i.e. reached a constant value determined by the scattering of electrons by lattice imperfections or impurities) at about 14°K and then quite abruptly at about 4°K the resistance dropped to zero. Since that time the complete disappearance of resistance has been observed in about two dozen pure metals and over one hundred alloys. Shortly after the discovery of this superconductive state it was found that by applying a magnetic field greater than a certain critical value, H_c , resistive behaviour could be restored. It was further found that the critical field increased as the temperature was lowered, from an initial value of zero at the superconducting transition temperature, T_c , to a finite value at the absolute zero. This behaviour, along with the almost discontinuous change in the specific heat at the transition temperature indicated that the change which



a metal undergoes in becoming a superconductor is a phase transition in the thermodynamic sense. This transformation is of the second order if there is no magnetic field present, while a first order transition takes place in non-zero magnetic fields.

Application of Maxwell's electromagnetic equations to materials of infinite conductivity indicates that the magnetic flux density, B , is a constant in such media. If this constant were other than zero the normal to superconducting transition would be dependent on the previous history of the specimen, and reversible thermodynamics could not then be applied to this problem. However the experiments of Meissner and Oschenfeld (1933) showed that indeed the superconducting state is one of perfect diamagnetism (i.e. $B = \text{const.} = 0$) and hence the transition is a thermodynamically reversible one. In the period between 1933 and 1956 a number of "two fluid models" flourished. These models treated the electrons in the superconductor as if they were constituents of two interpenetrating gases. One of these gases, the normal component, consisted of ordinary electrons not unlike those considered in the Sommerfeld model of a metal. The second component consisted of "super-electrons", which did not contribute to the entropy of the electron gas and were responsible for the superconducting properties. The

theories of the Londons (cf. London (1950)) gave a fairly good macroscopic explanation of the electromagnetic properties of superconductors based on a modification and expansion of Maxwell's equations. Many phenomenological two fluid models describing the thermodynamic behaviour of superconductors appeared starting with the Casimir and Gorter (1934) model. All of these have since been shown to be special cases of a more general model due to Marcus (1952 a, 1952b, 1953) and Lewis (1956).

Very little progress toward a microscopic theory was made before 1950. Until that time two problems in particular eluded explanation: (i) only the electronic properties and not the lattice properties were affected by the transition, (ii) many metals in spite of their vastly different band structure became superconductors.

B. Attempts at a Microscopic Theory of Superconductivity

Significant progress towards a microscopic theory of superconductivity occurred with the almost simultaneous discovery by Reynolds et al. (1950) and prediction by Fröhlich (1950 a,b) of the isotope effect. This effect demonstrated that in many superconductors the superconducting transition temperature, T_c , is dependent on the isotopic mass, M , according to the relation

$$T_c M^{1/2} = \text{const.} \quad (1.1)$$



for a given element. Thus it was conclusively shown that although the lattice remained unaffected by the transition it does play an important role in superconductivity.

Fröhlich (1950 a,b) proposed a theory of superconductivity based on an attractive electron-electron interaction. The mechanism of this interaction was due to the exchange of phonons* between the interacting electrons. This interaction is possible because the ions are neither rigidly bound in the lattice, nor infinitely heavy. Thus an electron passing through the lattice slightly distorts the periodic potential. Another electron traveling through the distorted (polarized) lattice does not experience the same periodic potential which the first electron saw; in this way the two electrons interact via the lattice. Fröhlich further showed that if the energy difference between the electron states in such phonon exchange interactions is less than the phonon energy the interaction is attractive. He was also able to establish the criterion for the occurrence of superconductivity, i.e. that if such an attractive electron-electron interaction dominates over repulsive Coulomb interaction between electrons, a metal becomes superconducting. He was able to explain,

* Strictly speaking "virtual" phonons since superconductivity presumably exists at $T = 0^{\circ}\text{K}$.

qualitatively, why poor conductors (having strong electron-phonon coupling) became superconductors while good conductors (e.g. group one metals) did not. His theory also accounted for the isotope effect. The quantitative features of the theory failed however because these involved calculating the energy of the superconducting state using perturbation theory. The difficulty of this approach is evident if we consider that the energies of the normal and superconducting states are both about one electron-volt per atom, while the energy difference between them is less than 10^{-7} of this value. The calculation of the energy difference by perturbation methods could not be carried out with sufficient accuracy. Attempts at a similar theory by Bardeen (1950 a,b) using the variational approach also resulted in mathematical difficulties. Various attempts by other authors to produce a microscopic theory of superconductivity are reviewed by Bardeen (1956).

C. Experimental Evidence of an Energy Gap in Superconductors

In the ensuing seven years a great deal of experimental evidence accumulated indicating an energy gap, 2Δ , in the density of electron states of a superconductor such that no excited electronic states exist whose energy is less than 2Δ above the ground state.

(i) Corak et al. (1956) observed that the low temperature specific heat of superconductors is proportional to $\exp(-\Delta/kT)$.

(ii) Blevins, Gordy, and Fairbank (1955) observed that the absorption of electromagnetic radiation increases sharply when the frequency, ω , is greater than a critical value $2\Delta/\hbar$. They also demonstrated that the energy gap, 2Δ , increases from zero at the transition temperature to a limiting value of $2\Delta \approx 3.5 kT_c$ at absolute zero.

(iii) Experiments by Glover and Tinkham (1956, 1957) involving infrared transmission in thin superconducting films also indicated an energy gap.

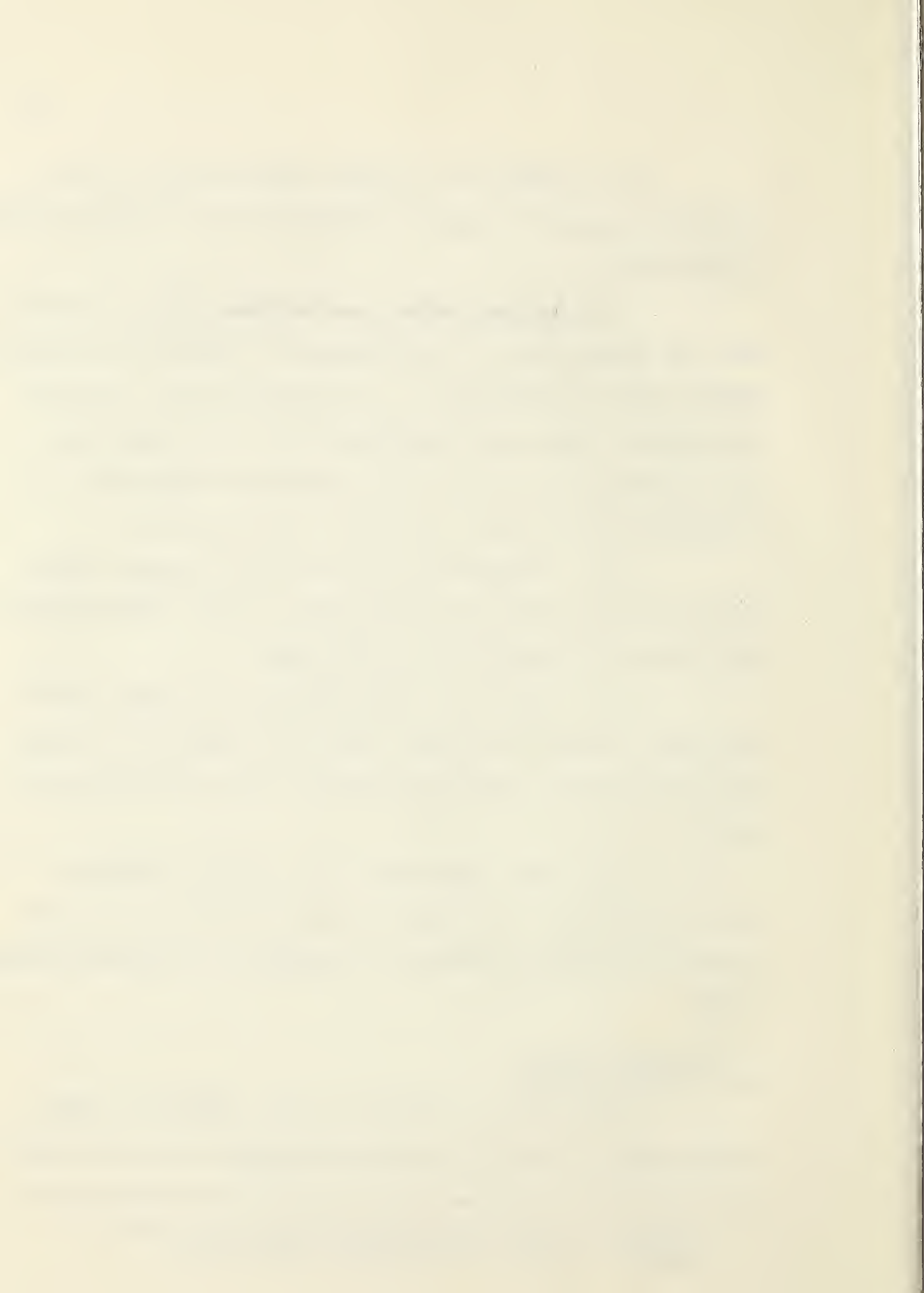
(iv) Mackinnon (1955), Mason and Bommel (1955), and Morse, Tamerkin and Bohm (1955) all showed that ultrasonic attenuation decreases sharply in the superconducting state.

Many other experiments gave further evidence for an energy gap. A complete and lucid account of these is given by Biondi, Forrester, Garfunkel, and Satterthwaite (1958).

D. The BCS* Theory

This theory, although in some respects a simplified model, is able to account for most of the phenomena

* Throughout this thesis BCS refers to the theory of Bardeen, Cooper and Schrieffer (1957 a,b).



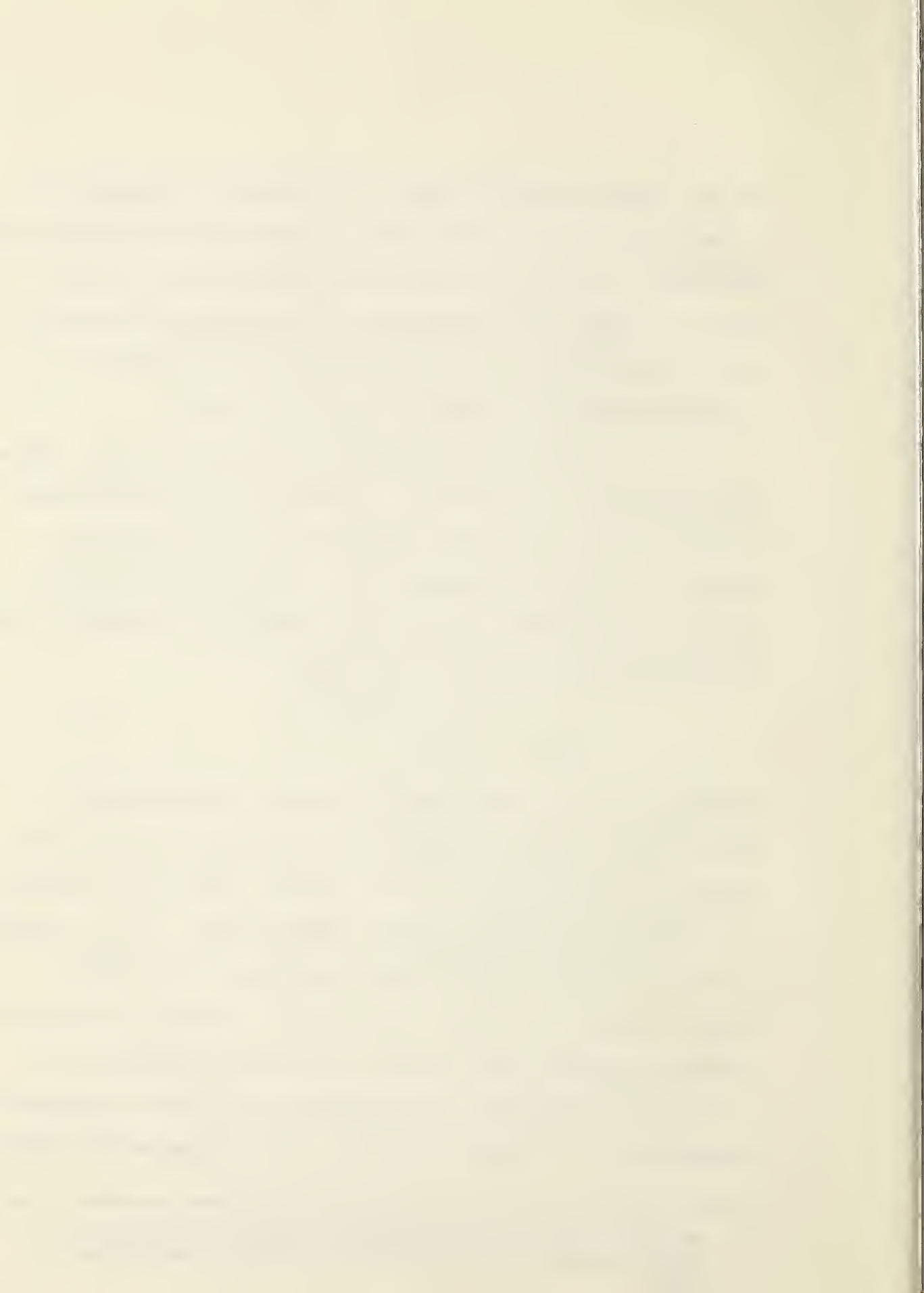
of the superconducting state. No attempt to describe it in any detail will be made here, instead only those aspects pertinent to electron tunneling phenomena will be dealt with. We begin by considering the behaviour of electrons in a normal metal, and then describe how this differs in a superconductor according to the BCS theory.

It is indeed striking that in spite of the complex band structure and diversity of metals which become superconductors there is great similarity in their behaviour below the transition temperature. We know from Bloch's theorem that normal metals may be described in terms of one electron wave functions of the form

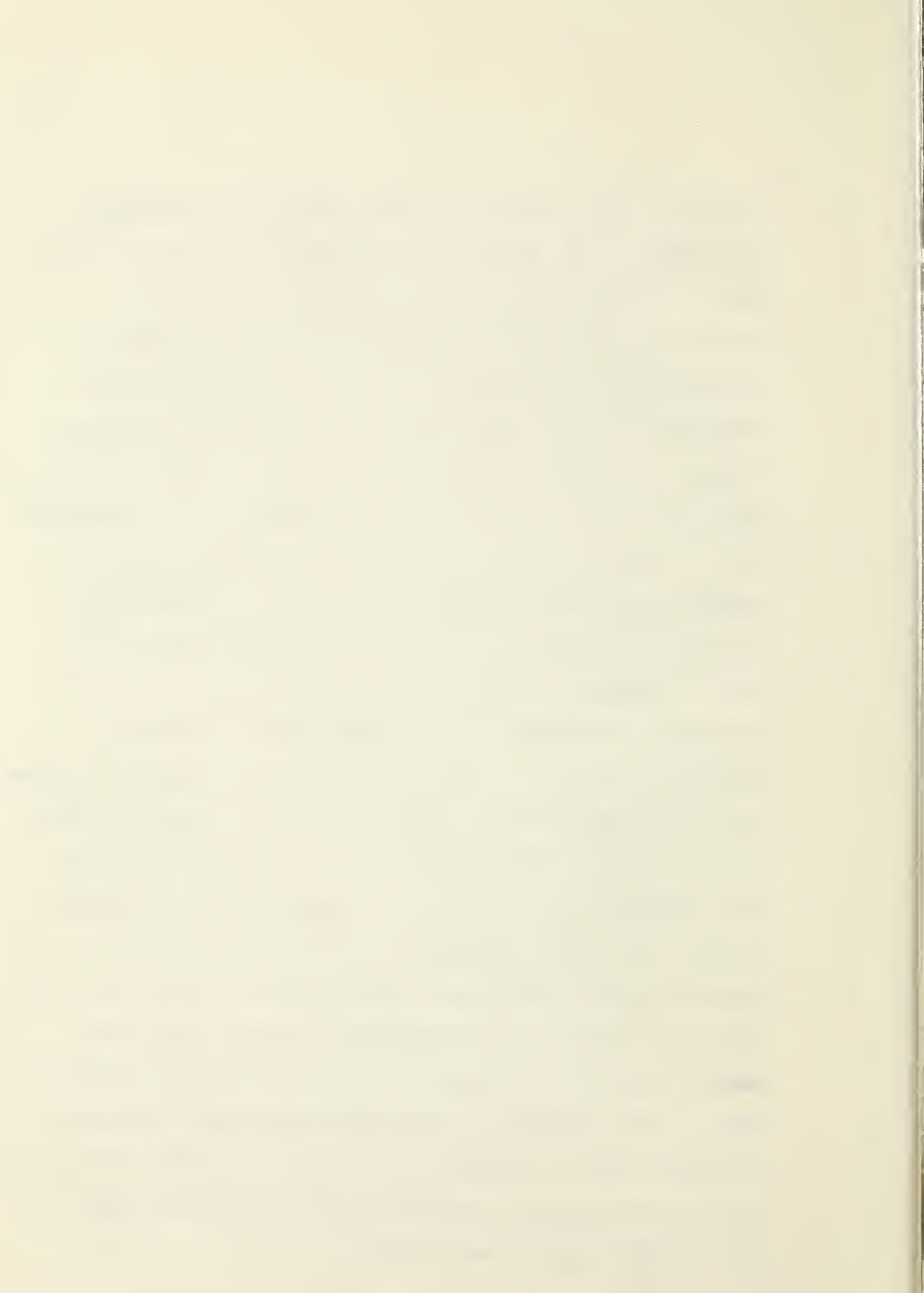
$$\psi_{\vec{k},s} = U_{\vec{k},s} e^{-i\vec{k} \cdot \vec{r}} \quad , \quad (1.2)$$

where \vec{k}, s are the four quantum numbers corresponding to wave vector and spin respectively, and $U_{\vec{k},s}$ is a function having the periodicity of the lattice. Since the electrons are Fermions, the many-electron system will consist of all the energy levels being filled up to the Fermi level (energy ϵ_F and wave vector \vec{k}_F)*. The only correlations between electrons dealt with in the Bloch description of a metal are statistical ones arising due to the antisymmetry requirement of the wave function. In a normal metal there

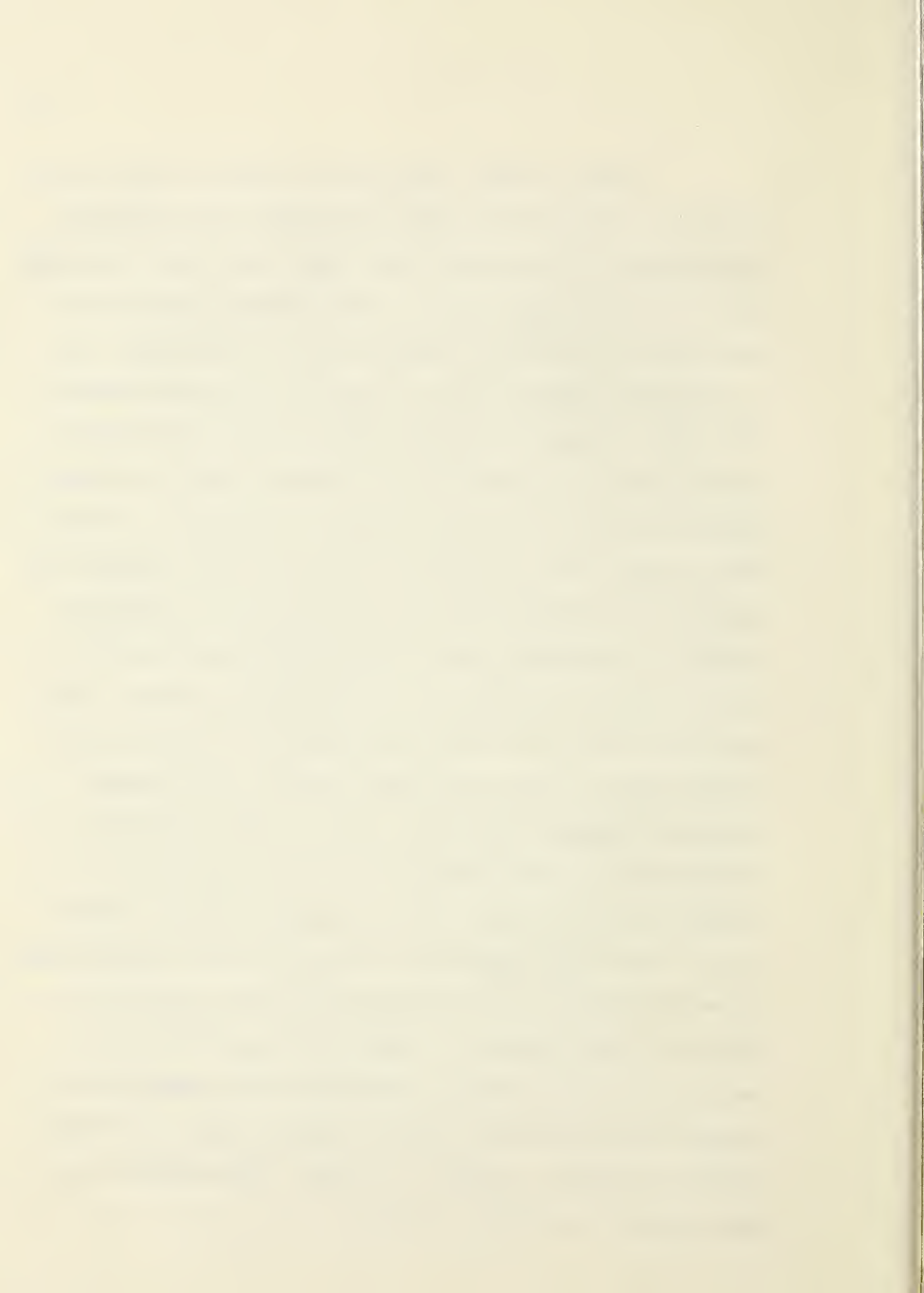
* We deal here with the special case of a spherical Fermi surface since that is the only case treated by BCS.



will be a large number of single particle excitations (of energy $\approx kT$) in which an electron in a state $k_i < k_F$ will be replaced by one in a state $k_j > k_F$. Such excitations may be conveniently described in terms of "quasi-particle" energies, i.e. the excitation energy measured from the Fermi surface. The energy difference between the ground state and an excited state is then given in terms of the sum of such quasi-particle energies, $\epsilon(\vec{k})$. Phenomena such as the electrical resistance of a normal metal arise through interactions, in particular the electron-phonon and electron-impurity interactions. Both of these processes provide a mechanism by which the electrons can readily be scattered from one momentum state into another. Such a mechanism, for example, assures that any ordered state, such as a current carrying state, will be quickly randomized in the absence of the field which produced it. Herein lies the essential difference between the normal and superconducting state, for in the superconducting case such single particle excitations are far less frequent and consequently ordered states may persist even in the absence of the fields which produced them. This difference between the normal and superconducting states is assumed to be due to electron correlations. It is by introducing correlations that the BCS theory is able to treat superconductivity.



Cooper (1956) showed that if there exists a net attractive interaction between electrons, then pairs of electrons may form a bound state with a net gain in energy over the Fermi ground state. Such binding arises from long range correlations between pairs of electrons, and is strongest between pairs of opposite spins and momenta ($-\vec{k} \uparrow, \vec{k} \downarrow$; where the arrows indicate spin orientation). Unfortunately as pointed out by Frölich (1962) no simple physical picture of these correlations appears to exist. Some insight into the physical basis for such binding can however be obtained through an argument due to Frölich (1962) if one assumes that the attractive interaction exists only for electrons above the Fermi surface. Consider two electrons that in the absence of mutual interaction would be above the Fermi surface, thus having energies slightly above ϵ_F . Owing to the attractive interaction the resultant energy of the pair will be somewhat less than $2\epsilon_F$. The pair cannot however break up into two single particles because all the energetically accessible states are occupied (since such states lie below the Fermi surface). This pairing of electrons accounts for the different features of the normal and superconducting phases since it takes a small but finite amount of energy to break up a pair. This results in a high degree of coherence of the



wave functions of the superconducting state, which makes single particle excitations difficult in the superconducting state.

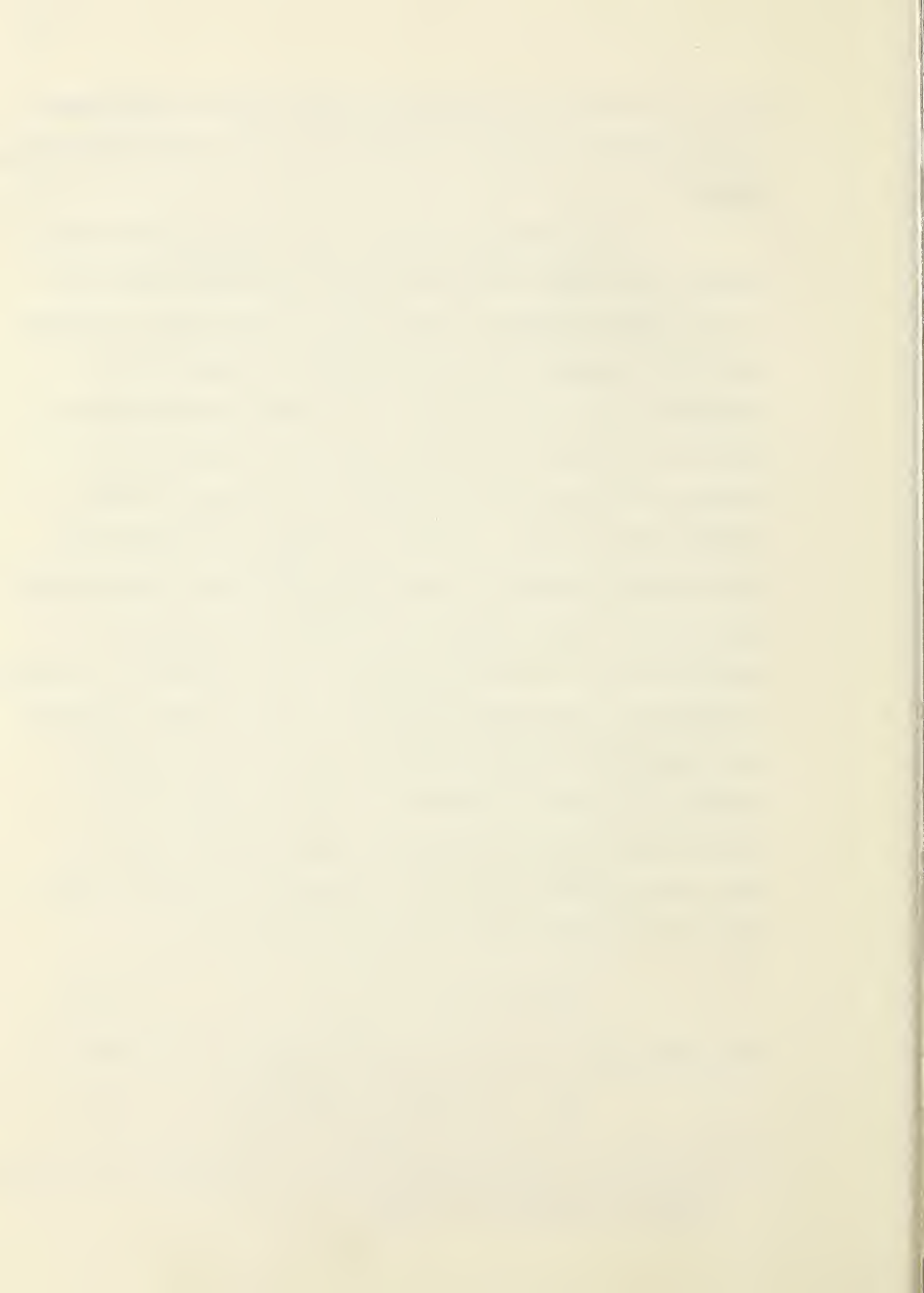
The BCS theory assumes that the major difference between the normal and superconducting states arises due to this added dynamical correlation between such electron pairs with opposite spin and momentum. They make no assumption about the nature of the interaction giving rise to such pairs, save that there is some constant attractive interaction at temperatures below T_c which vanishes for $T = T_c$. On this basis they calculate the free energy difference between the normal and superconducting states. Their theory results in an energy gap 2Δ centered about the Fermi surface. This energy gap is given in terms of a non-linear integral equation which involves the attractive electron-electron interaction, $-V$, the density of states at the Fermi surface of the normal metal, $\rho(0)$, and an average phonon frequency, ω_{ave} , which they choose to be half the Debye frequency. They are able to solve this equation in the limit

$$\rho(0) V \ll 1^* \quad (1.3)$$

The energy gap $2\Delta_0$ at the absolute zero is then given by

$$2\Delta_0 = 4 (\hbar\omega)_{ave} e^{-1/\rho(0)V} \quad (1.4)$$

* This is the weak coupling limit, i.e. where the electron-phonon interaction is weak.



and the single particle energy with respect to the Fermi surface is

$$E = (\epsilon^2 + \Delta^2)^{1/2} \quad . \quad (1.5)$$

It is evident that (1.5) reduces to the appropriate quasi-particle energy, ϵ , for a normal metal since in that case the energy gap is zero. They are able from the above to deduce the thermodynamic properties of superconductors, as well as the temperature variation of the energy gap. They obtain the relation $2\Delta_0 = 3.52 kT_c$ which is in reasonable agreement with the experimental values. Further extensions of this theory by Mattis and Bardeen (1958), and by Rickayzen (1958, 1959) are able to account for the electromagnetic properties of superconductors. A thorough review of the theory and recent experimental results is given by Bardeen and Schrieffer (1961).

It should be stressed that since the nature of the attractive interaction does not explicitly enter in the BCS theory, the framework of the theory should in principle also be able to deal with the problems of transition metal superconductors (cf. Geballe, Mathias, Hull, and Corenzwit 1961) in which the attractive potential does not arise from the electron-phonon interaction. The effect of explicit types of interactions have been treated by Swihart (1962).

E. The Density of Electron States in a Superconductor

A quantity of prime interest in electron tunneling into superconductors is the density of states. This may be obtained directly from (1.5).

$$\begin{aligned}\frac{dN(E)}{dE} &= \frac{dN(\epsilon)}{d\epsilon} \frac{d\epsilon}{dE} \\ &= \rho_n(0) \frac{d\epsilon}{dE}\end{aligned}$$

where $\rho_n(0)$ is the density of states of the normal metal evaluated at the Fermi surface. Carrying out the differentiation of (1.5) we obtain

$$\rho_s(E) = \rho_n(0) \text{RP} \frac{|E|}{\sqrt{E^2 - \Delta^2}}^*, \quad (1.6)$$

where $\rho_s(E)$ is the density of states of the superconductor. It is evident from (1.6) that the density of states of the superconductor is singular at the edges of the energy gap, where $E = \Delta$. The total number of states remains unaltered by the transition to the superconducting state.

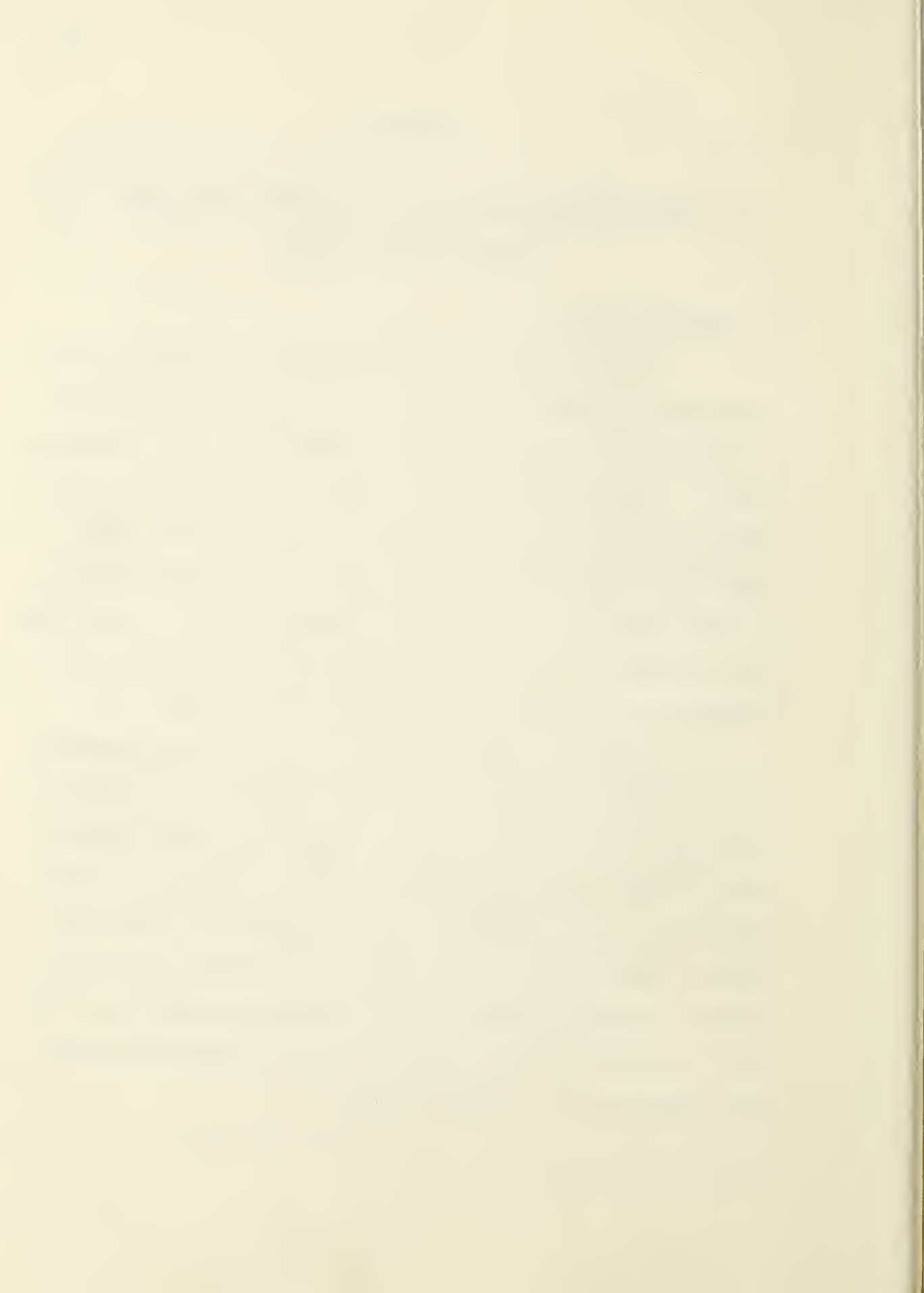
* RP denotes the real part

CHAPTER II

A SURVEY OF THE THEORY OF ELECTRON TUNNELING
INTO SUPERCONDUCTORSA. Introduction

Until August 1960 far infrared transmission and ultrasonic attenuation presented the most direct methods of observing the superconducting energy gap. At that time Giaever (1960a) published the results of his first experiments on electron tunneling into superconductors. His technique, simple in principle, provides a direct method of observing the energy gap of superconductors. Since then this technique has also been applied to determining the density of electronic states in superconductors.

Basically what is done in tunneling experiments is to inject electrons of various energies into a superconductor; due to the energy gap those electrons having their energies in the gap region will be rejected. Such injection is done through a very thin ($<100 \text{ \AA}$) insulating barrier which allows one to vary the potential difference between the metal from which the electrons emanate and the one into which they are injected. In this way the injection energy may be varied at will.



B. A Model of Tunneling*

It has long been known (cf. Sommerfeld and Bethe 1933) that a current can flow through a thin insulating film between two metals due to quantum-mechanical tunneling. A short qualitative description of the tunneling process is given below for the following three cases: (i) two normal metals, (ii) a normal metal and a superconductor, and (iii) two superconductors.

(i) Fig. 2.1 (a) shows two normal metals separated by a thin insulating film at $T = 0^\circ\text{K}$. Energy is represented on the abscissa, while the density of states near the Fermi level is shown on the ordinate**, the corresponding current-voltage (I-V) characteristic is also shown. The transmission probability for a particle tunneling through a potential barrier depends exponentially on both the square root of the barrier height and the thickness of the barrier. If the applied voltage is kept small, neither the barrier height nor its thickness are affected. The current will increase linearly with applied

* The treatment given below, in the main parallels that given by Giaever (1961) and by Shapiro, Smith, Nicol, Miles, and Strong (1962). Since no review article on the subject is yet available, I attempt in this section to summarize the theory briefly, stressing some of the underlying assumptions. Some of the integrations, the results of which are merely stated in the current literature are carried out in detail in Appendix I.

** Only the energy region within a few kT of the Fermi surface is shown in Fig. 2.1 the lower levels are assumed to be completely filled.

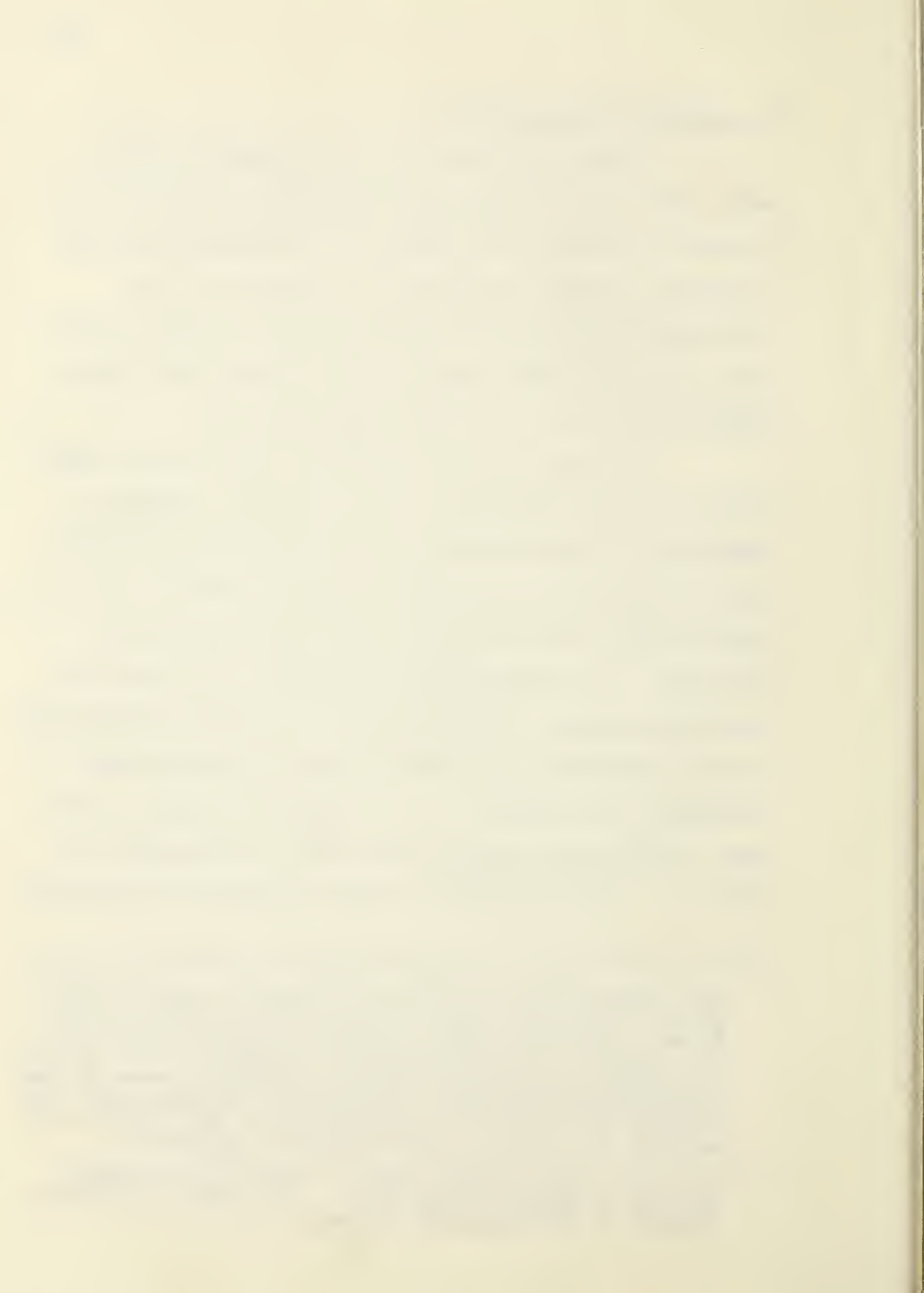
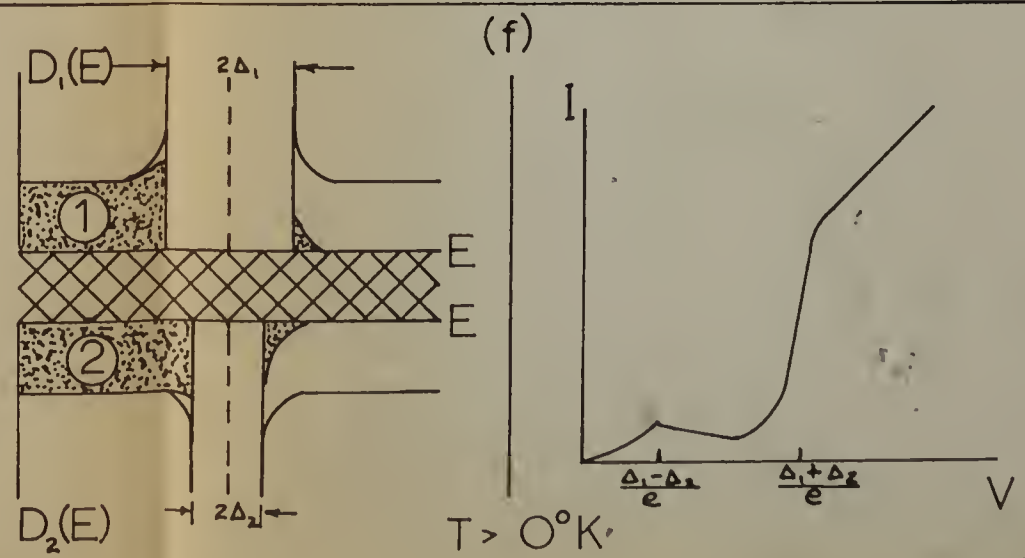
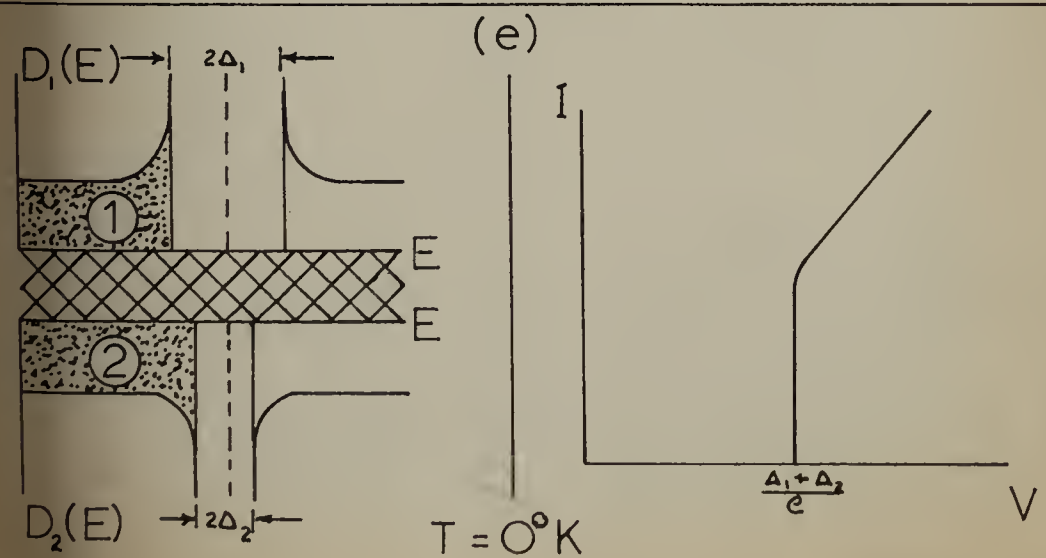
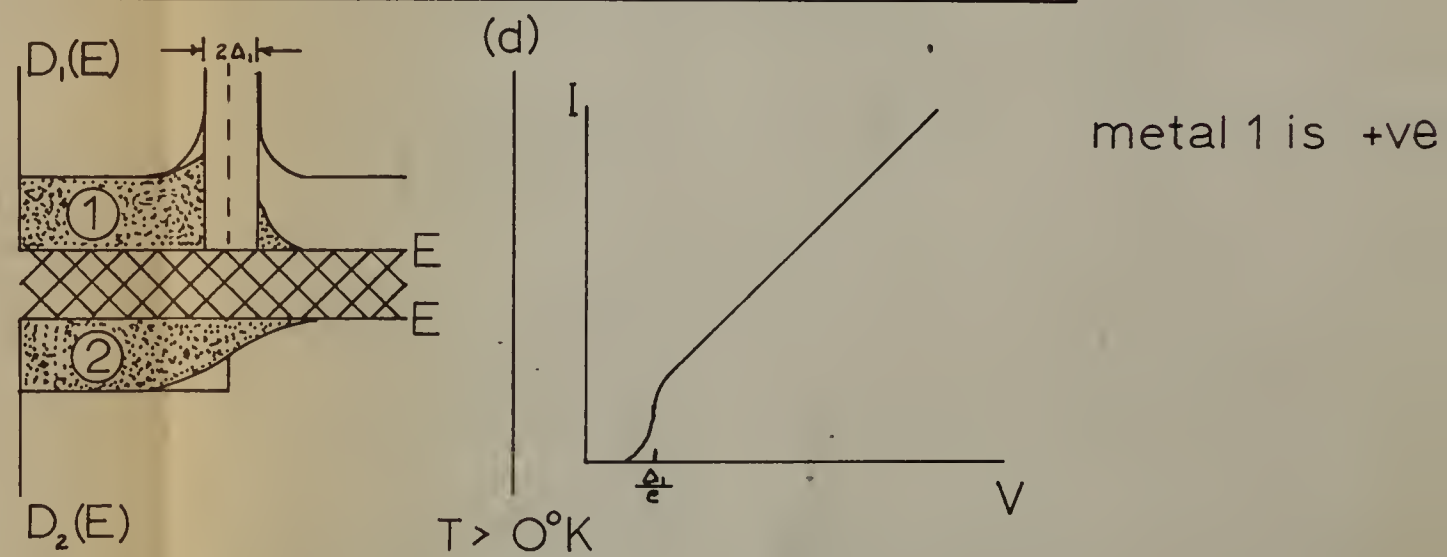
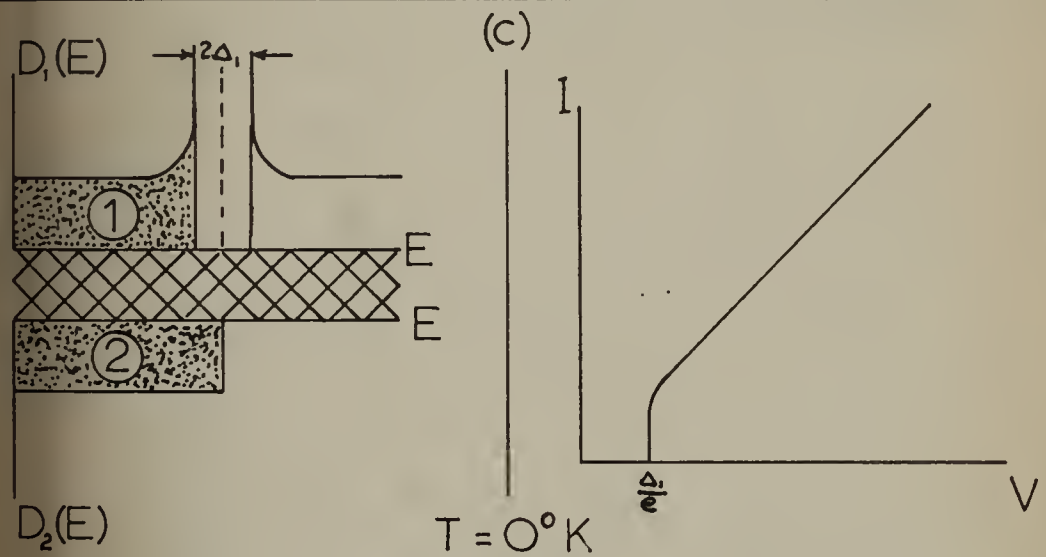
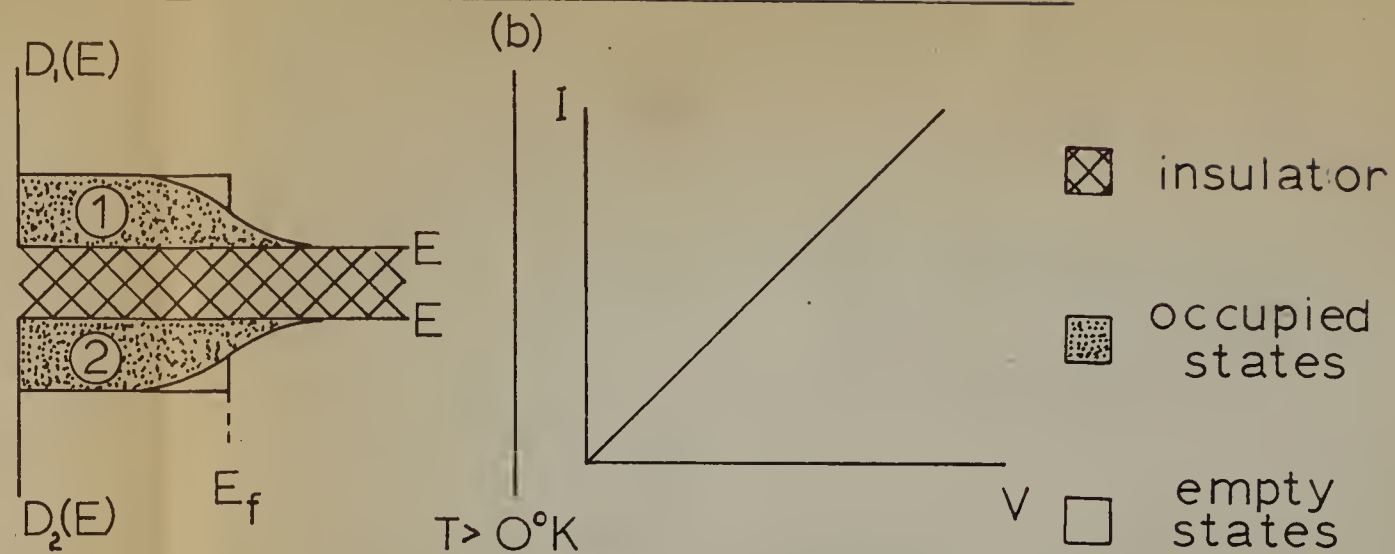
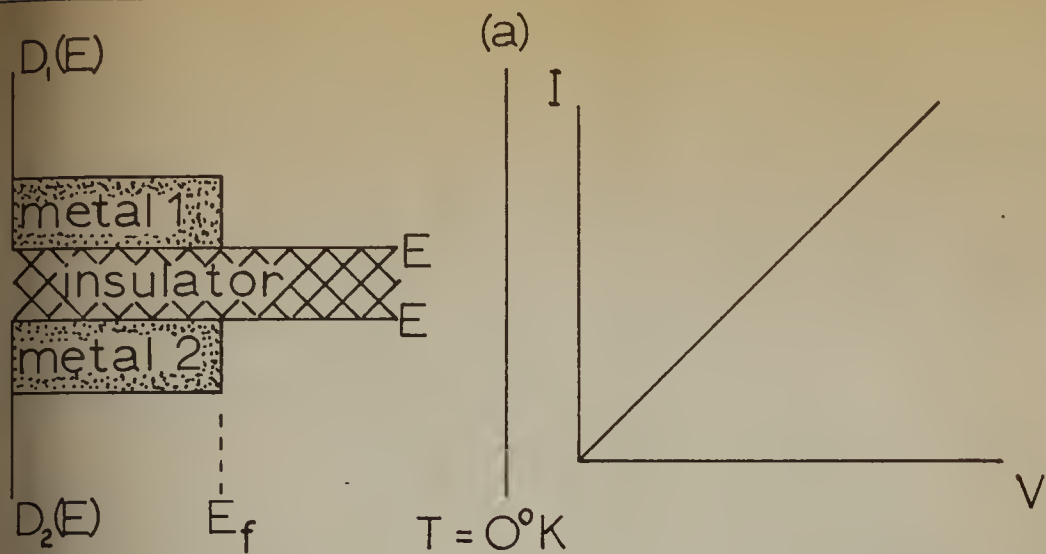


FIGURE 2.1

Schematic description of various tunneling processes. This figure shows the density of states, $D(E)$, near the Fermi surface plotted against energy, E . The corresponding current-voltage curves are also shown.



voltage^{*}, since the number of electrons which flow is proportional to the potential difference between the two sides of the barrier.^{**} Since kT is small compared with the barrier height in our work the tunneling process is temperature independent.

(ii) Consider now the situation which would exist at $T = 0^\circ\text{K}$ with one of the metals superconducting (Fig. 2.1(c)). The density of states of the superconductor (metal 1) has an energy gap $2\Delta_1$ centered about the Fermi level. Thus no current will flow until the applied voltage is at least $V = \Delta_1/e$. Assuming that the number of electrons tunneling is proportional to the density of states, then as V increases ($V > \Delta_1/e$) the current increases rapidly at first. Finally, as the electrons face a less favourable density of states, the current approaches asymptotically that obtained when both metals are normal. At non-zero temperatures (Fig. 2.1(d)) there are always some thermally excited electrons above the energy gap. These will give a temperature dependent contribution to the current even for applied voltages, $V < \Delta_1/e$.

* This is true for the small applied voltages involved. For detailed analysis see Holm (1951).

** N.B. For zero applied voltage the Fermi levels in both metals lie at the same level. For an applied voltage, V , the Fermi levels are displaced by an amount eV from one another, e being the electronic charge.

(iii) This situation is one in which both metals are superconducting as shown in Fig. 2.1(e) and (f). Again we consider first the case at $T = 0^\circ\text{K}$. As the applied voltage is increased no current flows until $V = (\Delta_1 + \Delta_2)/e$. For larger applied voltages the current rises sharply at first, and finally approaches the I-V curve obtained when both metals were normal. For $T > 0^\circ\text{K}$ there are again a few normal electrons above the gap. At any given temperature their relative numbers will be proportional to Δ_1/Δ_2 . These normal electrons give rise to a current flow even for the smallest applied voltages, this current increases until $V = (\Delta_1 - \Delta_2)/e$. As the voltage is further increased only the same number of electrons can flow, but these now face a less favourable density of states, and the current therefore decreases with increasing voltage. This part of the I-V curve is called the "negative resistance" region. Finally when the applied voltage reaches a value of $(\Delta_1 + \Delta_2)/e$ the current again rises sharply at first and then gradually approaches the I-V curve obtained for both metals in the normal state.

We shall now derive the I-V characteristics for tunnel junctions based on the model outlined above. Tunneling through a potential barrier is treated as an ordinary quantum transition. The transition probability per unit time for the transition from an occupied state k_1 on one

side of the barrier to an unoccupied state k_f on the other is given by:

$$P_{k_i \rightarrow k_f} = 2\pi/\hbar |M|^2 f_i (1-f_f) \rho_f, \quad (2.1)^*$$

where ρ_f is the density of final states, f_f is the probability that the final state is occupied, and f_i is the probability of occupation of the initial state. M is the matrix element for the transition. Before proceeding it is necessary to make the following assumptions:

- (i) M is independent of energy for the small energy differences involved,
- (ii) M remains unaltered in the transition from the normal to the superconducting state.

Bardeen (1961) has examined these assumptions from the many-body point of view, and using the W.K.B. approximation has shown them to be reasonable. A more detailed theoretical justification of these assumptions has been given by Cohen, Falicov, and Phillips (1962). It should be noted however that Harrison (1961) has also shown that in normal metals these assumptions can not be justified on the basis of the independent particle model alone. If these two assumptions are made, then the only variable that enters in the transition probability is the density of final states.

* See any standard quantum mechanics text, eg.: L.I. Schiff. Quantum Mechanics, McGraw-Hill Co., New York (1955); Sec. 29.

If we now consider a voltage, V , applied to one of the metals, equation (2.1) enables us to calculate the tunneling current. The net tunneling current will be given by the sum of the two one way currents, i.e.

$$I = (4\pi e)/\hbar \int_{-\infty}^{\infty} |M|^2 \left\{ \rho_2(E+eV) f(E) \rho_1(E)[1-f(E+eV)] \right\} dE \\ - (4\pi e)/\hbar \int_{-\infty}^{\infty} |M|^2 \left\{ \rho_2(E+eV) f(E+eV) \rho_1(E)[1-f(E)] \right\} dE. \quad (2.2)$$

The subscripts 1 and 2 refer to metals 1 and 2 respectively, E is the energy measured with respect to the Fermi level, and e is the electronic charge. The extra factor of two is present due to the two possible spin states of the electrons. The assumptions about M allow us to take it out of the integral and then

$$I = \alpha \int_{-\infty}^{\infty} \rho_2(E+eV) \rho_1(E) [f(E)-f(E+eV)] dE, \quad (2.3)$$

where $\alpha = (4\pi e |M|^2)/\hbar$.

For the case when both metals are normal and at $T = 0^\circ\text{K}$ this reduces to:

$$I_{nn} = \alpha \rho_1(0) \rho_2(0) eV, \quad (2.4)^*$$

where $\rho_1(0)$ and $\rho_2(0)$ are the densities of states of metals 1 and 2 at the Fermi surface. This expression is valid only for small applied voltages as is the case in

* See Appendix I(a) for integration (section (1))

our work. A further assumption, that the density of states in the vicinity of the Fermi surface is constant, had to be made in order to obtain equation 2.4.

Similarly for the case in which one metal is in the normal state while the other is in the superconducting state at $T = 0^\circ\text{K}$ one obtains:*

$$I_{\text{ns}} = 0 \quad \text{for } eV < \Delta \quad (2.5)$$

$$I_{\text{ns}} = \alpha\rho_1(0)\rho_2(0)[(eV)^2 - \Delta^2]^{1/2} \quad \text{for } eV > \Delta \quad (2.5a)$$

Glaever and Megerle (1961) have evaluated I_{ns} for $T > 0^\circ\text{K}$ and $eV < \Delta$ based on the BCS theory. They obtain:

$$I_{\text{ns}} = \alpha\rho_1(0)\rho_2(0) 2\Delta \sum_m (-1)^{m+1} K_1(m\Delta/kT) \sinh(meV/kT), \quad (2.5b)$$

where K_1 is the first order modified Bessel function of the second kind. It is evident from the above that the superconducting energy gap as well as its variation with temperature can be determined by tunneling experiments. The results of such experiments** are in good agreement with the values predicted by the BCS theory. Good qualitative agreement is also obtained between the experimental I-V

* See Appendix I(a) section (11) for derivation.

** cf. Glaever (1960a and 1960b), Glaever and Megerle (1961), Glaever, Hart, and Megerle (1962), Nicol, Shapiro, and Smith (1960), Shapiro, et al. (1962), Townsend and Sutton (1962), Taylor, and Burstein (1963).

curves and those predicted using the BCS density of states in conjunction with the model of tunneling outlined above, thus giving strong support to the BCS theory. Having made the assumption that the matrix element, M , is constant the current becomes proportional to the density of states. Then ratio of the conductance, $(dI/dV)_{ns}$, when one of the metals is superconducting to the conductance, $(dI/dV)_{nn}$, when both metals are normal gives the relative change in the density of states. This quantity, called the relative conductance, $G_{ns} = (dI/dV)_{ns}/(dI/dV)_{nn}$, may be calculated from equations (2.4, 2.5, and 2.5a), for $T = 0^{\circ}\text{K}$:

$$G_{ns} = \frac{(dI/dV)_{ns}}{(dI/dV)_{nn}} = (eV)[(eV)^2 - \Delta^2]^{-1/2}. \quad (2.6)$$

Experiments of Giaever and Megerle (1961) show that in spite of "kT smearing"* measured values of relative conductance also give good agreement with the BCS density of states. Thus relative conductance measurements on tunnel junctions consisting of a normal metal and a superconductor provide a sensitive tool for studying the energy gap, its temperature dependence, and the ratio of the density

- * The physical reason for this smearing being that for $T > 0^{\circ}\text{K}$ there are some thermally excited normal electrons above the gap.

of states of the superconducting to normal phases of a superconductor. In the temperature region below $1/2 T_c$ the energy gap is almost temperature independent and kT smearing is small for energies $eV > \Delta$. Thus equation (2.6) may be used for comparison with experimental data; this avoids laborious numerical integrations on a computer which are required to calculate the relative conductance for $T > 0^\circ K$.

We now turn our attention to the case of two superconductors separated by a thin insulating film. A scheme by which numerical evaluation of the integrals arising in a calculation of the current for cases in which $T > 0^\circ K$ has been given by Shapiro, et al. (1962). For simplicity we shall limit ourselves here only to the case of two identical superconductors at $T = 0^\circ K$. The I-V characteristic for this case is given below, for a detailed derivation see Appendix I (a) section (iii).

$$I_{ss} = 0 \quad \text{for } eV > 2\Delta \quad (2.7)$$

$$I_{ss} = \alpha_p^2(0) \left\{ \frac{(eV)^2}{eV + 2\Delta} K\left(\frac{eV-2\Delta}{eV+2\Delta}\right) + (eV+2\Delta) \left[E\left(\frac{eV-2\Delta}{eV+2\Delta}\right) - K\left(\frac{eV-2\Delta}{eV+2\Delta}\right) \right] \right\}, \quad (2.7a)$$

where K and E are complete elliptic integrals of the first and second kind respectively. This expression has been

evaluated on the IBM 1620 computer and a table of relative conductance as a function of voltage is given in Appendix II. A comparison of the relative conductance, G_{ss} , for this case with experiment is shown in Fig. 6.6.

It is indeed gratifying that good qualitative agreement is obtained between this simple model and experiment. Recalling that the basic assumption of the model was that the transition probability is energy independent, and this led to the current being proportional to the densities of states of the superconductors, it is surprising that no density of states variations have yet been detected in normal metals using tunneling techniques. Such variations would be expected to be rather pronounced in some of the transition metals. Experimental attempts to observe such variations (Giaever, Hart, and Megerle (1962)) in nickel have led to negative results.

C. Modifications to the BCS Density of States in the Vicinity of the Energy Gap as indicated by Tunneling Measurements.

With one exception it has not been possible to show any major discrepancy between the BCS theory and tunneling experiments. Equations (2.7) and (2.7a) show that for two superconductors at $T = 0^{\circ}\text{K}$ there ought to be a current jump at $eV = 2\Delta$. Experiments by Giaever, Hart,

and Megerle (1962) on various tunnel junctions (particularly Sn-SnO_x-Sn) show that the I-V curve has a finite slope at $eV = 2\Delta$. This slope is less than the expected after the fact that the measurements are made at $T > 0^\circ\text{K}$ is taken into account. This unexpected slope introduces an uncertainty in the determination of the energy gap from the I-V characteristics. Giaever et al. were able to improve the agreement between theory and experiment by assuming that the energy levels are not sharply defined but instead have a non-zero width. Such a modification tends to smear the density of states in the region of the gap. This alteration to the BCS theory was first introduced by Hebel and Slichter (1959) to explain the results of nuclear spin relaxation experiments in superconductors. We shall now describe this modification referring to it as HS smearing and the resulting density of states as the HS density of states respectively. The change is introduced into the theory by replacing the sharp energy levels of BCS by others having a width δ . δ is later adjusted to obtain best fit with the experimental results. The energy level breadth function used has a width 2δ and a height $1/2\delta$. The HS density of states is then given by:

$$\rho_{\text{HS}} = \frac{1}{2\delta} \int_{E-\delta}^{E+\delta} \rho_{\text{BCS}} dE' \quad . \quad (2.9)$$

Carrying out the integration one obtains:

$$\rho_{\text{HS}} = 0 \quad \text{for } |E| < \Delta - \delta \quad (2.10)$$

$$\rho_{\text{HS}} = 1/2\delta[(E+\delta)^2 - \Delta^2]^{1/2} \quad \text{for } \Delta - \delta < |E| < \Delta + \delta \quad (2.10a)$$

$$\rho_{\text{HS}} = 1/2\delta\left\{[(E+\delta)^2 - \Delta^2]^{1/2} - [(E-\delta)^2 - \Delta^2]^{1/2}\right\} \\ \text{for } |E| > \Delta + \delta. \quad (2.10b)$$

It can be seen that (2.10b) goes over to the BCS density of states as the energy, E , increases. The important effect of this treatment is the removal of the singularity in the BCS density of states. Giaever et al. found improved agreement between theory and experiment using a value of $\delta/\Delta = .03$. If the smearing is attributed to finite lifetime effects*, they then obtain a lower limit of 10^{-11} sec. for the lifetime.

In conclusion it is evident that the superconducting energy gap as well as the density of states in a superconductor may be studied by the technique of electron tunneling. The good qualitative agreement between such experiments and the BCS theory is one of the major triumphs of that theory. The discrepancy which does arise in the vicinity of the energy gap can be reduced by introduction of a level breadth. Further discussion is given in the chapter dealing with our own results.

* Assuming the lifetime to be given by the uncertainty principle, $\tau \sim \hbar/\delta$.

D. Multiphonon Effects Observed in Tunneling Experiments

Giaever, Hart, Megerle (1962) and more recently Rowell, Chynoweth, and Phillips (1962) have reported humps in the relative conductance curves obtained from measurements on tunnel junctions in which at least one of the metals is lead. Rowell, et al. were able to resolve harmonic structure in the conductance curves which consisted of peaks occurring at energies:

$$E_n = \Delta + nE_t, \quad (2.11)$$

where E_t is the energy of the transverse acoustic phonon in lead, n is an integer, and the energy $E_n = eV$ is the electron energy. They also observe that the magnitude of the peaks decreases with increasing voltage. They attribute this observed structure to multiphonon effects (emission or absorption of one or more phonons by the tunneling electrons). In arriving at their explanation they had to assume an Einstein phonon spectrum, the energy of each harmonic oscillator being the transverse phonon energy. Assuming such a spectrum a simple qualitative model of this effect can be given. Consider electrons tunneling from one metal to another and having some energy E . Even if there are many available states of energy, E , only those electrons having the appropriate spin and momentum will be able to participate in the

tunneling process and thus contribute to the tunneling current. Electrons whose energy is E_n can cross the barrier, emit a phonon, and thereby reduce their energy to $E' \doteq \Delta$. In this manner such electrons arrive into a region where the density of states available to them is high, hence by virtue of an Einstein spectrum the conduction can be enhanced at voltages, $V = E_n/e$. The reason for the decreasing amplitude of successive peaks is a consequence of the fact that in general an $n + 1$ phonon process is less probable than an n phonon process. It is not surprising that such structure has thus far only been observed in lead since this metal has the strongest electron-phonon interaction of all superconductors.

CHAPTER III.

ELECTRICAL APPARATUS AND MEASUREMENT CIRCUITSA. Introduction

One of the initially appealing aspects about electron tunneling measurements is that it is relatively simple to determine the I-V curves for a tunnel junction. Since I is of the order of microamperes, while V is in the millivolt range, a good quality VTVM will suffice to measure both I and V (I being obtained by measuring the voltage developed across a calibrated resistor). Such a procedure is tedious, but can be remedied by replacing the VTVM with an oscilloscope and simultaneously displaying V on the abscissa and voltage proportional to I on the ordinate. Two ways of carrying out such a measurement are possible. The first of these involves a variable dc voltage supply by which the bias across the tunneling junction may be manually varied. The second method uses an oscillator to sweep the voltage across the junction and displays the I-V curve on the scope screen as a continuous trace. Either method leads to accurate results provided that four terminal measurements are made. In our experiments we have employed both of these methods. In order to record this data we employed an oscilloscope camera and

negative film. The use of negative material is particularly convenient since it can readily be enlarged for closer inspection. When using the oscillator technique care must be taken to keep the sweep frequencies low (below a few cycles per second) because at higher frequencies junction capacity effects become visible.

The measurement of relative conductance on the other hand is not quite so simple. Giaever, Hart, and Megerle (1962) have used fairly complex circuitry to record the dynamic resistance of tunnel junctions directly on an X-Y plotter. They carried out such measurements by superimposing a small alternating current signal on the bias current through the junction and observing the ac voltage developed across the junction.

We have used a completely different method for obtaining the relative conductance. By keeping the apparatus simple we have been able to obtain much higher sensitivity than other workers in this field, although the reduction of the data to its final form is still somewhat laborious.

B. The Tunneling Curve Tracer

A complete block diagram of the circuitry is given in figure 3.1. The Hewlett Packard oscillator provided a triangular waveform which was used for the

FIGURE 3.1

Block diagram of the electrical apparatus used in measuring the relative conductance and the current-voltage curves of tunnel junctions.

automatic sweep. The specimen in the cryostat was connected to the external apparatus by a four conductor shielded cable. Leads 1 and 4 are the current leads; 2 and 3 are the potential leads. The heavier black lines denote ground bus wiring. Extreme care was taken to ground all equipment and shields at a single point so that ac pickup was kept to a minimum. The potentiometer served a dual purpose. With the switch across the galvanometer closed it was used as a standard voltage source to calibrate the oscilloscope and the galvanometer amplifier. It also served as a bias source so that any segment of the I-V or relative conductance curves could be shifted in voltage for a more detailed display on the oscilloscope screen. For relative conductance measurements a quantity, δV , which is the voltage difference between some known linear I-V relation and the specimen voltage at the same current was recorded on the vertical input. Simultaneous recording of the specimen voltage, V , was carried out on the horizontal input.

The galvanometer amplifier,* used to pre-amplify δV , is a highly stable feedback amplifier. These amplifiers are discussed extensively by Rogers (1962) but the one

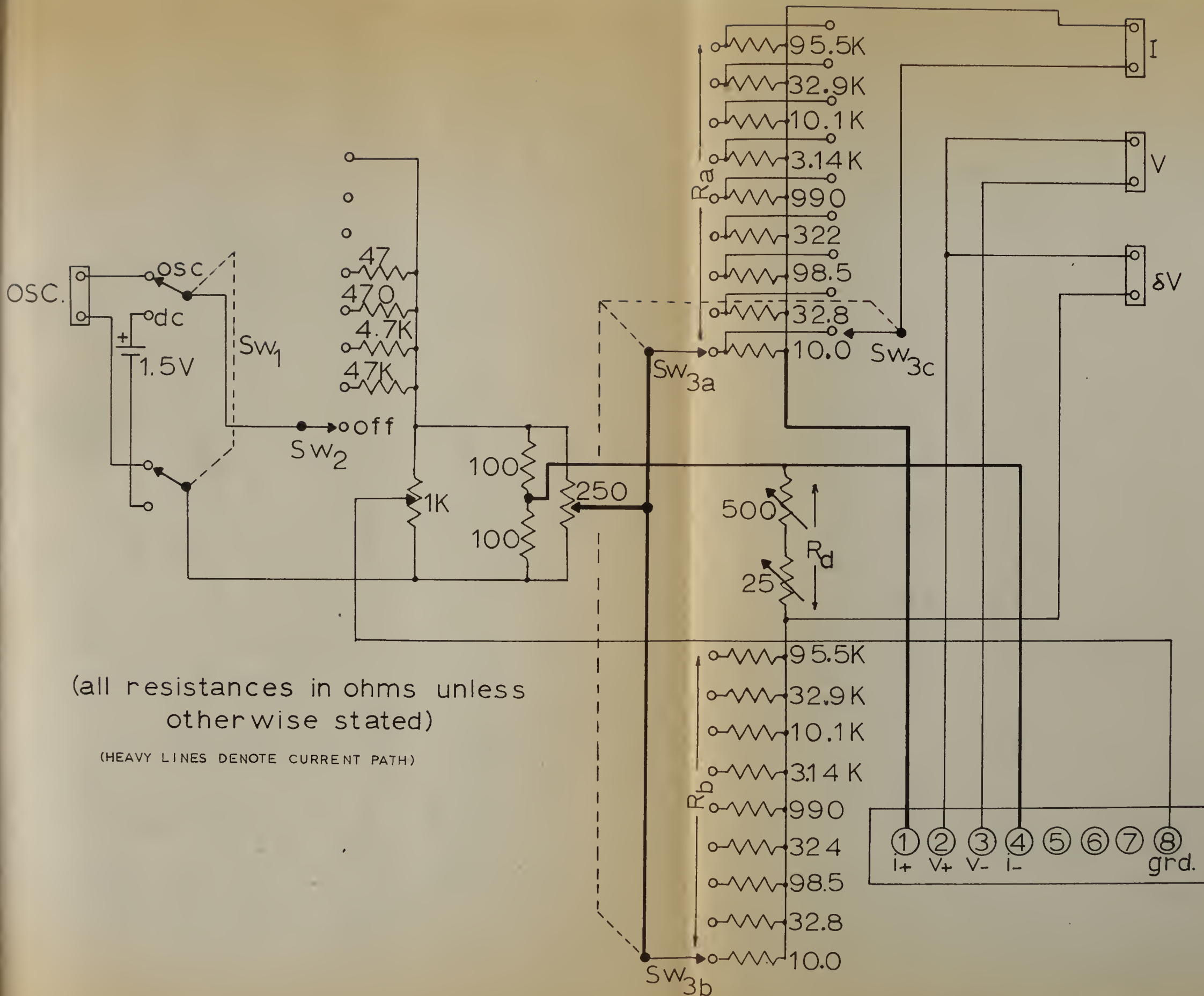
* It is a pleasure to acknowledge my gratitude to Mr. J. S. Rogers for designing and building the amplifier specifically for this application.

used here is somewhat unconventional in that the output galvanometer is replaced by an oscilloscope. Excellent stability is achieved due to high feedback and the consequent sacrifice in gain is not serious because an amplification factor greater than 10^3 has never been required. At this gain a voltage, δV , of one microvolt produces a displacement of one centimeter on the oscilloscope screen.

A detailed diagram of the curve tracer appears in Fig. 3.2. As can be seen there is provision for both an automatic and a manual sweep, depending on the position of switch Sw_1 . The magnitude of the voltage bias across the specimen can be controlled by adjusting Sw_2 and the 250 ohm variable resistor. The ground connections are all made at terminal 8 and the 1000 ohm potentiometer can be adjusted so that the circuit is at some level above ground potential. This potentiometer was adjusted so that the ac pick-up visible on the oscilloscope screen was a minimum. The I-V curves are obtained by the four terminal method; the current wiring is shown by the heavy black lines. The voltage proportional to current is generated across R_a , which may be adjusted to any one of nine values, thus providing variable current sensitivity.

FIGURE 3.2

Circuit diagram of the curve tracer.



(all resistances in ohms unless otherwise stated)

(HEAVY LINES DENOTE CURRENT PATH)

The remainder of the circuit is for obtaining the curves of δV as a function of V , from which the relative conductance may be calculated. An equivalent circuit for this part of the curve tracer appears in Fig. 3.3. It is essentially a bridge, one arm of which (the tunnel junction) is a non-linear element. If we let R_g be the input resistance of the galvanometer amplifier then we may write $\delta V = i_g R_g$. The loop equations describing the circuit may then be written:

$$e - V = R_a i - R_a i_g \quad (3.1)$$

$$e = -(R_b + R_d) i + (R_b + R_d) i_o + R_b i_g \quad (3.2)$$

$$o = -(R_a + R_b) i + R_b i_o + (R_a + R_b + R_g) i_g \quad (3.3)$$

This particular set of loops is used in the analysis since the form of V as a function of i is not known. Replacing $i_g R_g$ by δV and combining (3.1) with (3.2) we have

$$V - (R_a + R_b) \frac{\delta V}{R_g} = -(R_a + R_b + R_d) i + (R_b + R_d) i_g \quad (3.4)$$

and

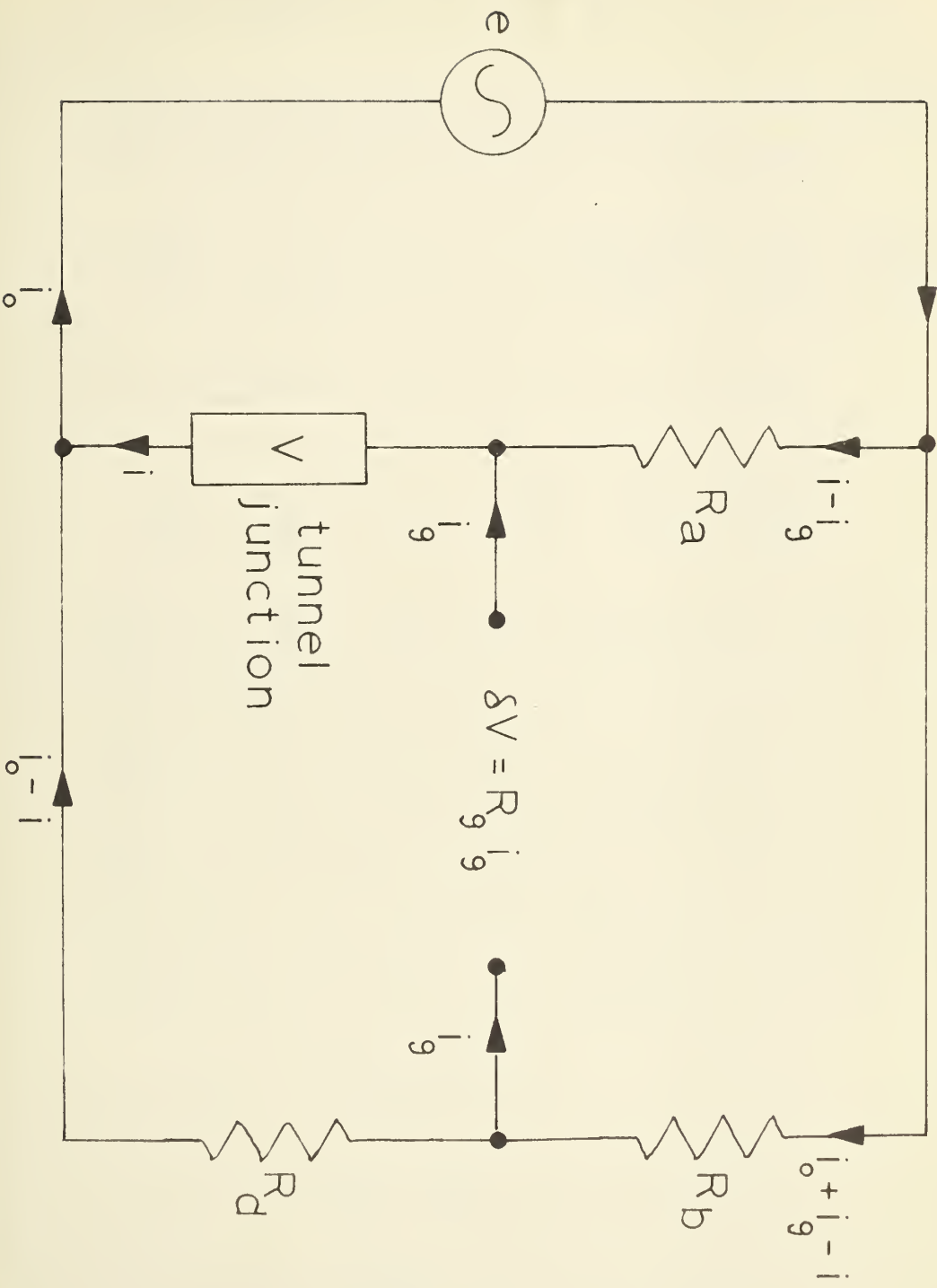
$$(R_a + R_b + R_g) \frac{\delta V}{R_g} = (R_a + R_b) i - R_b i_o. \quad (3.3a)$$

Solving these equations for the current in the tunnel junction we obtain

FIGURE 3.3

Equivalent circuit of the relative conductance
measuring part of the curve tracer.

$$(di/dV) = \frac{1 + [(2R_d + R_g)/R_g + R_d/R] dsV/dV}{R_d}$$



$$i = \frac{1}{R_a} \left\{ \frac{R_b}{R_d} (V + \delta V) + \left[\frac{(R_a + R_b)}{R_g} + 1 \right] \delta V \right\}. \quad (3.5)$$

Differentiating (3.5) with respect to the voltage across the junction gives the dynamic conductance,

$$\frac{di}{dV} = \frac{R_b}{R_d R_a} \left\{ 1 + \left[1 + \frac{R_d (R_a + R_b)}{R_b R_g} + \frac{R_d}{R_b} \right] \frac{d(\delta V)}{dV} \right\}. \quad (3.6)$$

In our case $R_a = R_b = R$ so (3.6) becomes:

$$\frac{di}{dV} = \frac{1}{R_d} \left\{ 1 + \left[1 + \frac{2R_d}{R_g} + \frac{R_d}{R} \right] \frac{d(\delta V)}{dV} \right\}. \quad (3.7)$$

Note that R_d in Fig. 3.2 is adjustable. Let us designate the setting of R_d by R_n when the measurements are being carried out with specimens in the normal state, and by R_s for the measurements with superconducting specimens. Let δV_s and δV_n denote values of δV obtained from measurements with superconducting and normal specimens respectively. Further let us make the following definitions:

$$\lambda = \frac{(R_n - R_s)}{R_s},$$

$$\mu = \frac{2R_s}{R_g} + \frac{R_s}{R},$$

$$\eta_s = \frac{d(\delta V_s)}{dV},$$

$$\eta_n = \frac{d(\delta V_n)}{dV} ,$$

and

$$G = \frac{(di/dV)_s}{(di/dV)_n} ,$$

the ratio of dynamic conductance in the superconducting phase to the dynamic conductance in the normal phase. Then it follows from (3.7) that:

$$G = (1 + \lambda) [1 + (1+\mu)\eta_s] [1 + (1+\mu)(1+\lambda)\eta_n]^{-1}. \quad (3.8)$$

Whenever the nature of the I-V characteristic of the tunnel junction being measured permitted, the experiment was carried out using $R_s = R_n$, and thus $\lambda = 0$. This simplifies the evaluation of G , since for our specimens η_s and η_n were small ($\doteq 10^{-3}$) while μ was usually about 10^{-1} or less. For this special case we have:

$$G = 1 + (1+\mu) \frac{d(\delta V_s - \delta V_n)}{dV} . \quad (3.9)$$

In other cases when $R_s \neq R_n$ and an uncertainty of $\Delta G \doteq G\lambda\eta_s$ could be tolerated in G we used the expression

$$G \doteq (1 + \lambda) [1 + (1+\mu) \frac{d(\delta V_s - \delta V_n)}{dV}] . \quad (3.10)$$

Fortunately we could keep $\lambda \doteq 0.01$ in these cases and then (3.10) was accurate enough. Where greater precision

is required and $\lambda \neq 0$ ^{one} must calculate G by (3.8) which is a tedious procedure indeed.

In order to show more clearly the nature of our bridge measurements we give the following simple example. Fig. 3.4 (a) shows a non-linear current-voltage characteristic, as well as the voltage, V' , across R_d . The δV - V curve appears in Fig. 3.4 (b). Now if we let $R_a = R_b \gg R_d$ and $R_g \gg R_d$ then:

$$V \doteq iR_d - \delta V$$

and

$$\begin{aligned} \frac{dV}{di} &= R_d - \frac{d(\delta V)}{di} \\ &= R_d - \frac{d(\delta V)}{dV} \frac{dV}{di} . \end{aligned}$$

Thus

$$\frac{di}{dV} = \frac{1 + \frac{d(\delta V)}{V}}{R_d} \quad (3.7a)$$

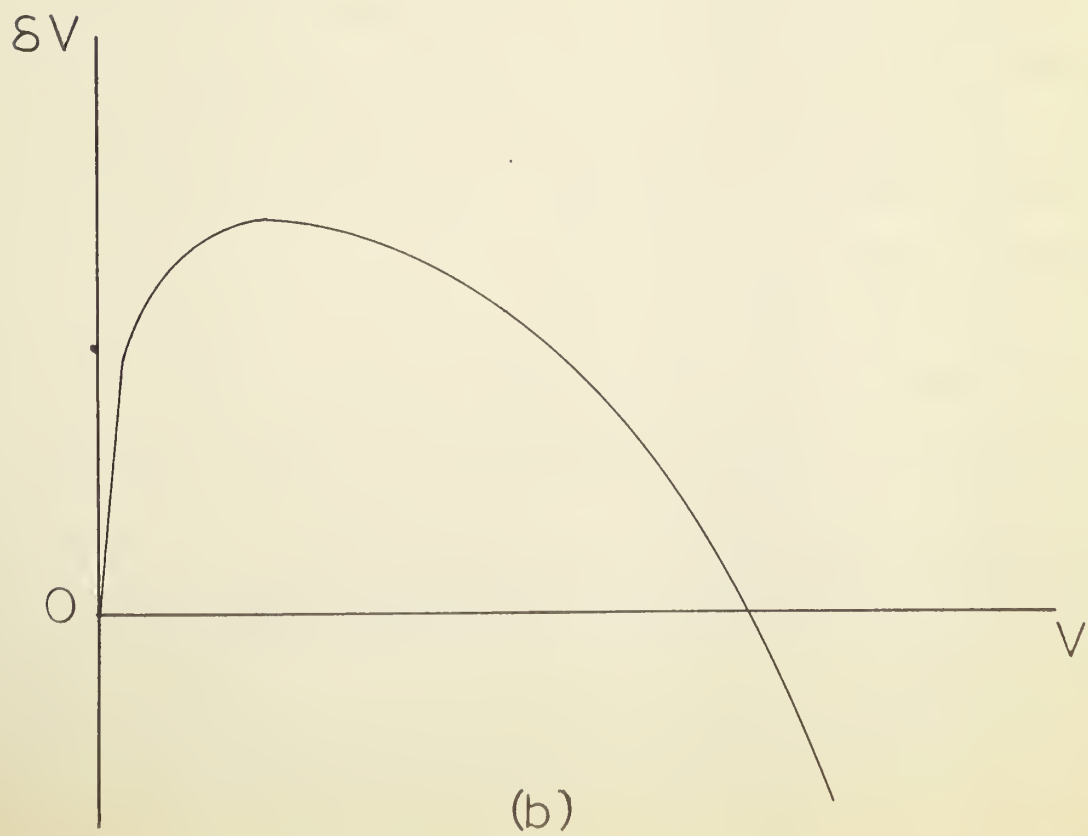
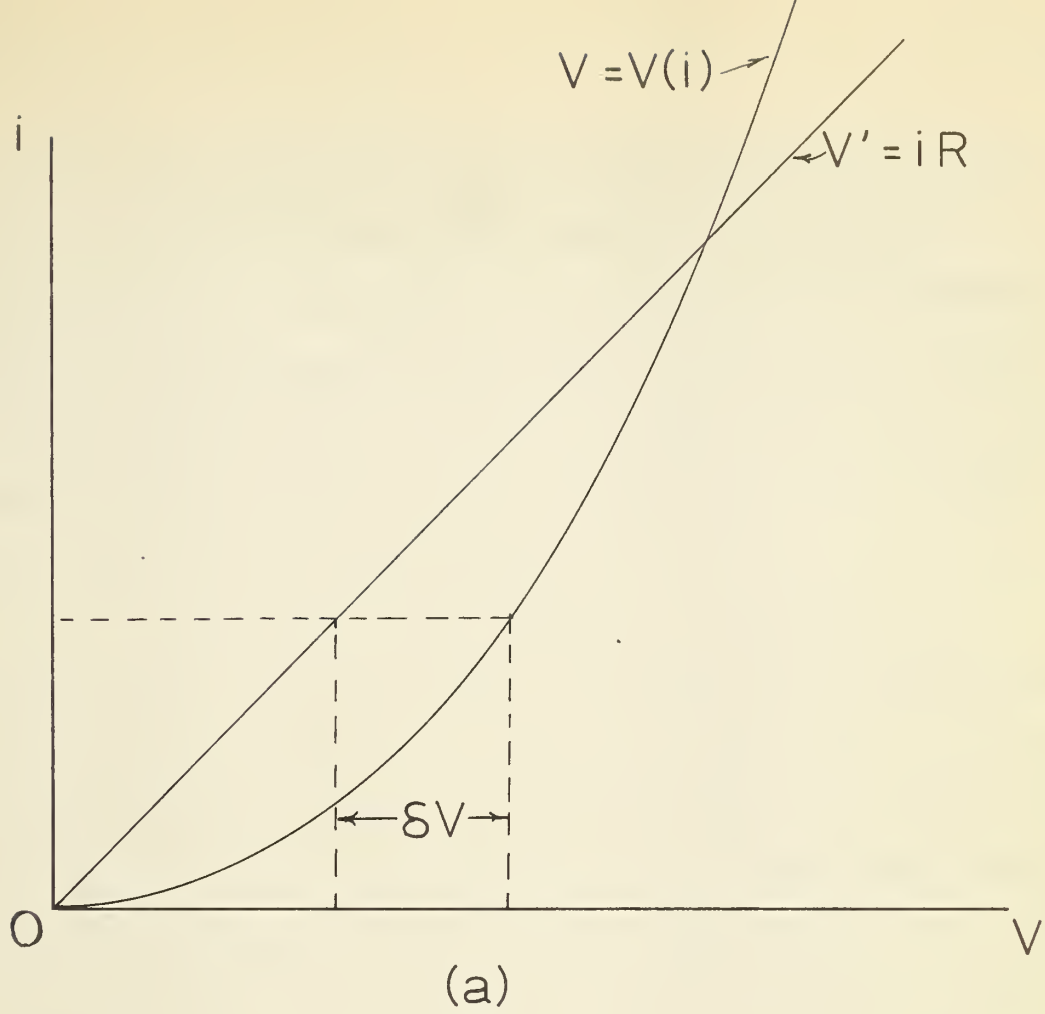
which is identical to (3.7) under similar assumptions.

C. Data Processing

All curves were traced with increasing voltage and also with decreasing voltage. This assured us that there was no appreciable phase shift in the galvanometer amplifier at the sweep rates we used and any spurious

FIGURE 3.4

Schematic showing how a δV - V curve (b) is obtained from the current-voltage curve (a).



signals which affected the two traces differently could be distinguished from stable specimen characteristics. Any effects due to seismic disturbances in the neighbourhood of the galvanometer amplifier, or to heating in the tunnel junction, were readily detected in this way. Only those events present in both traces at the same voltage were used in the data analysis.

The curves were recorded on negative film^{*} using an oscilloscope camera. The negatives were projected through an enlarger onto a sheet of graph paper. Linear magnifications as high as five were used. Two negatives, one taken in the normal state and one in the superconducting state, having the same scales, were traced on one sheet of graph paper. The separation between two such curves, along the ordinate direction, is proportional to $(\delta V_s - \delta V_n)$. This separation was measured as a function of junction voltage with as many as 500 points being obtained on some of our experimental runs. The relative conductance was then obtained easily when the separations were multiplied by the appropriate scale factor to allow for the magnification. This calculation was carried out using the IBM 1620 digital computer. We were able to adjust our sensitivity

* Kodak Contrast Process Ortho sheet film was used and developed in Kodak D-8 developer for about 45 seconds.

for δV up to a maximum of about $1 \mu V/cm$ on the oscilloscope screen, whereas the sensitivity for V was variable up to $200 \mu V/cm$ which was ample. In some instances as many as thirty-five photographs were taken to obtain a relative conductance curve.

CHAPTER IV

DESIGN, CONSTRUCTION, AND OPERATION OF A He^3 CRYOSTATA. Introduction

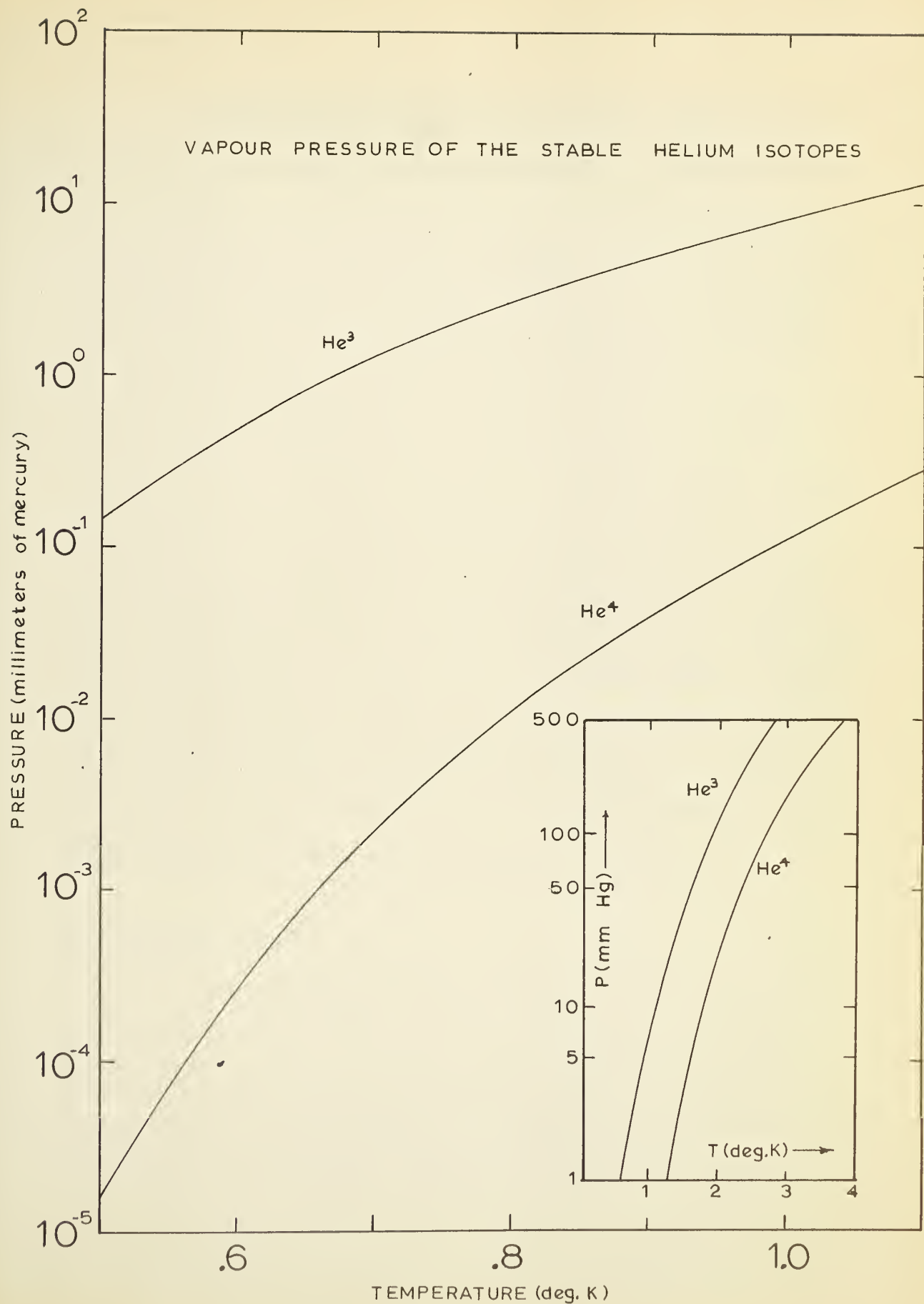
The use of He^3 instead of He^4 to obtain low temperatures by allowing the liquid helium to evaporate under its saturated vapour pressure* has two distinct advantages. (i) As can be seen in Fig. 4.1, the vapour pressure of He^3 is very much higher than that of He^4 , thus much smaller vacuum pumps may be used. (ii) In the temperature region of interest (above 0.25°K) He^3 does not exhibit superfluidity, thus the phenomenon of film flow which gives rise to a large heat influx to a He^4 bath at temperatures below 2.2°K is absent. Such heat influx arises as a direct consequence of the superfluidity of He^4 . It is due to the rapid flow of a thin film of superfluid He^4 from the bath along the walls of the pumping tube to regions of higher temperature. This film evaporates and has to be pumped away, otherwise it will condense again on the surface of the bath where it will deliver its heat of vapourization. These reasons make the use of He^4 impractical as a refrigerant below 1°K .

* The pressure is reduced below atmospheric by the use of a vacuum pump. The temperature is then varied by adjusting the pressure over the boiling liquid.

FIGURE 4.1

Vapour Pressures of the Stable Helium Isotopes.
Data for the He^3 scale was obtained from Sydoriak and Roberts (1957). Data for the He^4 scale was obtained from van Dijk, Durieux, Clement, and Logan (1958).

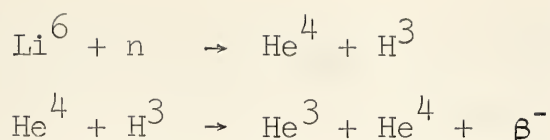
VAPOUR PRESSURE OF THE STABLE HELIUM ISOTOPES



Temperatures below 1°K could have been attained by the use of adiabatic demagnetization of a paramagnetic salt. However a He^3 cryostat has the advantage of simplicity in that no large electromagnet is required. For experiments in which the magnetic state of the specimen prior to cooling is of importance, magnetic cooling has an added disadvantage. For example if work is being carried out on superconductors some magnetic flux is trapped in the specimen during the cooling process. Thus some type of thermal switch must be incorporated in the cryostat in order to isolate the specimen from the salt pill. The specimen must then be warmed to some temperature above the superconducting transition temperature to expel the trapped flux, and then allowed to cool again. For these reasons the use of a He^3 cryostat has a decided advantage over other methods of refrigeration when investigating properties of superconductors below 1°K .

B. Sources of He^3

The natural abundance of He^3 is extremely low, constituting only 10^{-3} to 10^{-6} of helium gas obtained from natural gas wells (cf. Aldrich and Nier 1948). Commercially available He^3 is obtained artificially as a by-product of tritium production in nuclear reactors.



As the above equations show, even with artificially produced He^3 , one must still separate the two isotopes. Early methods of separation involved thermal diffusion. Daunt, Probst and Johnston (1947 and 1948) showed that He^3 does not participate in superfluid flow and thus showed the way to low temperature methods for the separation of the stable helium isotopes. Many methods of separation have since been devised and are described by Peshkov and Zinov'eva (1959). At the present time the only producer of He^3 on this continent is the U. S. Atomic Energy Commission.* The consumption of He^3 for cryogenic applications has been greatly increased in the past two years due to a reduction in the price of He^3 from about \$1500 to \$150 per liter (N.T.P.).

Commercial He^3 contains small traces of H^3 , a beta emitter with a half life of 12 1/2 years, and for this reason some precautions should be taken in the initial handling of He^3 . Since the beta particles are of low energy (18 keV) no shielding other than that provided by the gas container and the metallic or glass pumping tubes of the cryostat need be used. However precautions should be taken to prevent the possible ingestion of tritium,

* He^3 is distributed through contract with the Monsanto chemical Company, Mound Laboratory, Miamisburg, Ohio.

e.g. glassblowing on sections of a cryostat which have been in contact with H^3 should be avoided.

C. General Features of He^3 Cryostats

A number of He^3 cryostats* have been described in the literature. In all cases the principle of their operation is very similar, consisting of a He^3 stage that operates within a He^4 cryostat which has been cooled to $\approx 1.25^\circ\text{K}$. The He^3 is liquefied in a condenser at 1.25°K and the liquid is then allowed to enter a chamber (He^3 chamber). The experimental specimen is placed in thermal contact with the He^3 chamber. Variation of the pressure above the liquid He^3 allows one to control the temperature of the specimen. Two types of these cryostats have been built. (i) The "single shot" cryostats in which the He^3 is allowed to condense in the He^3 pumping tube until sufficient liquid has accumulated in the He^3 chamber. The temperature may then be reduced by pumping on the He^3 . After all the He^3 is pumped away it is necessary to recondense it again at 1.25°K . (ii) The "refrigerator" in which the He^3 is condensed in a special condensing capillary and is allowed to enter the He^3 chamber con-

* Roberts and Sydoriak (1955), Seidel and Keesom (1958), Reich and Garwin (1958), Ambler and Dove (1961), Martin (1961), de Bruyn Ouboter, Taconis, LePair, and Beenakker (1960), van den Meijdenberg, Taconis, and Le Pair (1961), and Zinov'eva and Peshkov (1959).

tinuously, i.e. while the He^3 is being pumped. The He^3 which is pumped away is recondensed in a cyclic manner. This type of cryostat allows maintenance of a particular temperature for prolonged periods. Because it is cyclic it requires smaller amounts of He^3 , since the coolant is continuously replenished. Due to the price and scarcity of He^3 it is always recovered and re-used. This puts a very stringent requirement on the He^3 system in that it has to be free even of "superleaks", which are leaks that are too small to allow ordinary fluids to pass, but permit superfluid He^4 to pass. Such leaks would contaminate the He^3 and if they were large enough the He^3 - He^4 mixture would exhibit a lambda transition, the temperature of which increases with He^4 concentration. Such mixtures tend to limit the ultimate temperature attainable with a He^3 cryostat. Our He^3 cryostat was designed in such a way that it served both as a refrigerator and a single shot cryostat.

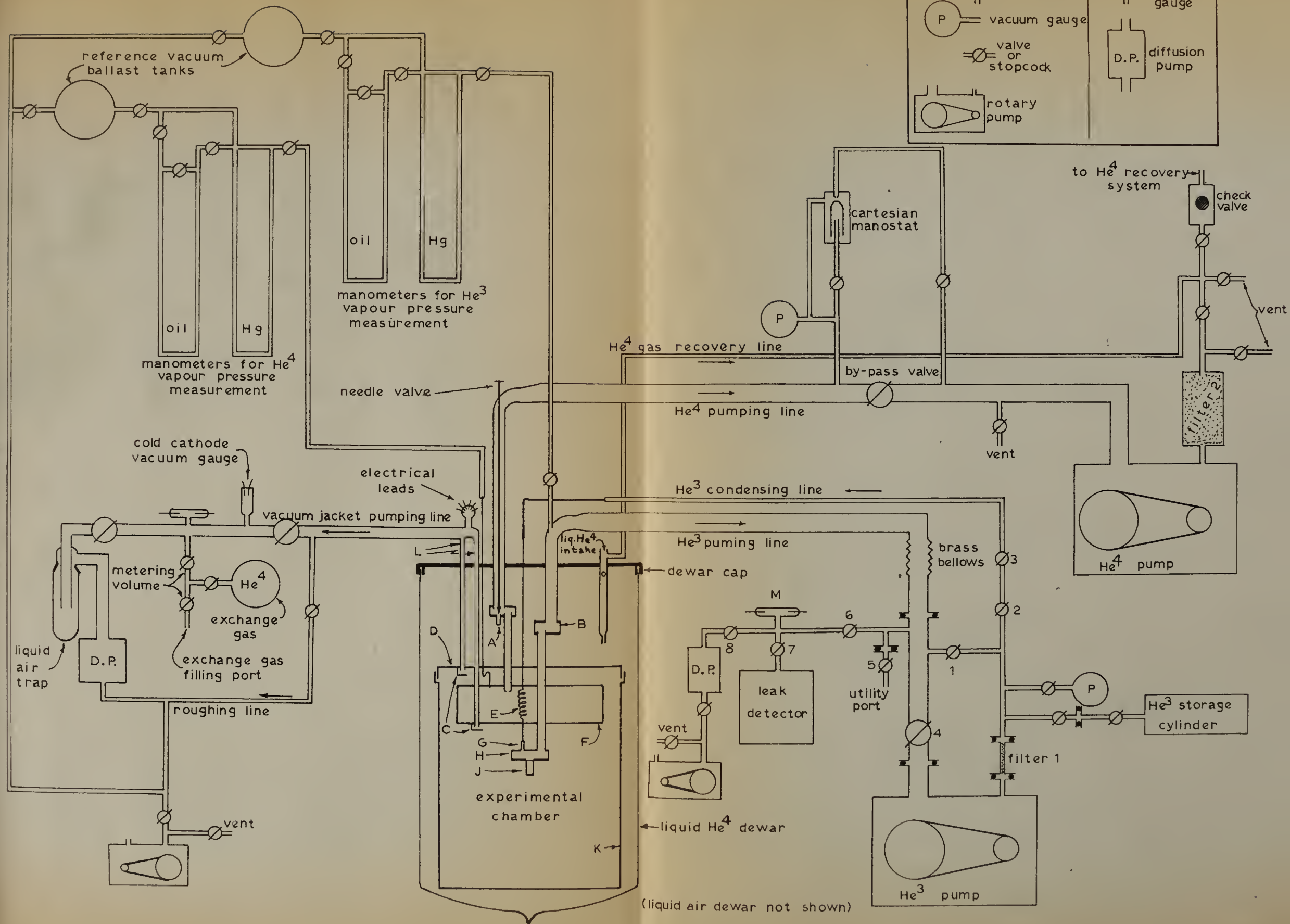
D. Description of the He^3 Cryostat

A complete schematic diagram of the He^3 cryostat and auxillary systems is given in Fig. 4.2. A set of machine drawings of the cryostat appears in Appendix III. The experimental chamber of the cryostat is enclosed by a brass can K. This can is soldered to a brass plate, D,

FIGURE 4.2

Schematic diagram of the He³ Cryostat.

manometer reference vacuum line



(liquid air dewar not shown)

using Wood's alloy, so that it can readily be removed for changing specimens. The experimental chamber can be evacuated through two pumping tubes, L. These tubes are made of 3/8 inch diameter stainless steel having a wall thickness of 0.004 inch. The reason for using such thin walled tubing is to minimize the heat influx into the He⁴ in the dewar. The vacuum inside the experimental chamber serves to thermally isolate its contents from the surrounding He⁴ dewar (the helium in this dewar is allowed to boil at atmospheric pressure, so that $T \doteq 4^{\circ}\text{K}$). The electrical leads are brought to the experimental chamber through one of these pumping tubes. They enter the pumping tube through a Kovar to glass seal at the top of the cryostat. These wires are thermally anchored to the He⁴ bath at 4^oK. This anchoring is achieved by tightly wrapping several feet of wire around a copper post which is soldered to D. The wires are also thermally anchored to the He⁴ chamber, F, with an intervening length of about one foot of wire freely suspended in the vacuum jacket. Lengths of manganin wire which have been tinned with 50/50 tin-lead solder linked these wires to the specimen or carbon resistance thermometers. This provides a superconducting link of low thermal conductivity. Small pieces of blackened copper foil, C, serve as radiation traps for the two pumping tubes. Provision is made on the vacuum system

to admit low pressure He^4 gas to the experimental chamber. This exchange gas is used to achieve thermal equilibrium between the liquid He^4 in the dewar and the contents of the specimen chamber.

Chamber F contains liquid He^4 . The chamber is filled through a combination needle valve and radiation trap, A, a detailed view of which appears in Fig. A-2, Appendix III. A short length of Tygon tubing attached to A and extending several inches below plate D allows one to fill chamber F even if the liquid helium level is below plate D. The temperature of chamber F can be reduced from 4°K to 1.25°K by pumping with the He^4 pump. Intermediate temperatures can be maintained by using a Cartesian manostat of the type described by Gilmont (1951). The He^4 which has been pumped from chamber F passes from the exhaust of the pump through cotton wool filter 2 into the helium recovery system. An estimated 25 cubic feet of He^4 gas (N.T.P.) are recovered from this chamber each run. The He^4 chamber is connected by means of a $1/8$ inch Inconel tube to a mercury and an oil manometer. These manometers are used to determine the vapour pressure from which the temperature of the He^4 bath can be deduced. The thermomolecular pressure correction had to be applied only at the lowest temperatures ($T \approx 1.25^\circ\text{K}$)

and was of the order of 1%. For this correction the values of Roberts and Sydoriak (1956) were used.

The He^3 part of the system was built around a Welch model 1402 KBG vacuum pump. This is a rotary pump with a speed of about 70 liters per minute at $1\ \mu$ pressure. It has a specially designed shaft seal (cf. Reich and Garwin 1958) whose leak rate is about 200 times lower than that of a conventional pump. Such a modified pump is necessary to avoid contamination or loss of the He^3 . The He^3 (1.12 liters N.T.P.) is stored partly in the pump body and partly in a brass storage vessel at a pressure of about $2/3$ of an atmosphere. Low pressure storage is used in order to minimize potential loss due to small leaks. Any air collected through such small leaks can readily be separated from the He^3 by freezing and then released later. The exhaust side of the He^3 pump plays the role of the compressor in the refrigerator system. The compressor pressure is always below one atmosphere, and about equal to the saturated vapour pressure of the He^3 at the condensation temperature ($T \doteq 1.25^\circ\text{K}$). Filter 1 (glass wool) collects oil vapours from the He^3 gas as it leaves the pump. Condensation takes place by letting the He^3 gas pass through valves 2 and 3 into a 1.0 millimeter capillary (condensing line). After passing through

the He^4 bath at 4°K the capillary narrows to a diameter of 0.5 millimeters and feeds coil E which consists of a one meter length of 0.5 millimeter capillary wound into a coil with a diameter of $1/8$ inch. This coil is located in the He^4 chamber and is at a temperature of 1.25°K . The He^3 liquifies inside this coil provided the compressor pressure is 25 millimeters of mercury or more (vapour pressure of He^3 at 1.25°K). The He^3 thus liquified passes through a porous plug, G, into the He^3 chamber. This plug serves to limit the injection rate of He^3 into the chamber. Too rapid an injection rate will raise the ultimate temperature because flow resistance of the tubes connecting the He^3 chamber to the pump finally limits the refrigeration rate. The plug is made by inserting a piece of porous stainless steel which has been ground down to 0.050 inch diameter into a copper tube having an inside diameter of $1/16$ inch.* The copper tube was then drawn down until it fitted tightly around the stainless steel. The plug used in this cryostat had a flow rate for He^4 gas of about $1.6 \text{ cm}^3/\text{min}$ under a pressure difference of $1/2$ atmosphere at room temperature. The specimen is attached to post J, which together with the He^3 chamber

* I wish to acknowledge the advice of Dr. R.B. Dove of the Cryogenic Physics Section of the National Bureau of Standards, Washington, D.C. in the construction of such plugs.

is machined from one piece of copper (see Appendix III). Some control of the temperature of the He^3 chamber is obtained by reducing the pumping speed with valve 4. In this way the cryostat operates in a continuous cycle as a refrigerator. Single shot operation is achieved by closing valves 2 and 3 and opening valve 1 so that the He^3 condenses down the pumping tube. This temporarily raises the temperature of the He^4 chamber but when equilibrium is re-established valve 1 is closed and valve 4 opened to cool the He^3 . A system for leak detection preceding every run is also incorporated in the apparatus. The details of this system are discussed in Section G.

E. Discussion of Some of the Design Parameters of the Liquid He^3 Cryostat

Due to the scarcity and price of He^3 at the time the cryostat was designed, we adopted the basic philosophy of keeping the number of joints, particularly at the low temperature end of the cryostat, to a minimum. This has resulted in a performance which is somewhat less than optimum, in particular the ultimate attainable temperature is only 0.47°K . Modifications to remedy this situation are proposed in Section H. In the present section we concern ourselves only with the design parameters of the existing system. The design problems encountered in

building a He^3 cryostat are in many respects similar to those of constructing an adiabatic demagnetization cryostat. The major fundamental difference between the two systems is that the low temperature part of the apparatus (salt pill) in a demagnetization cryostat has a much higher heat capacity, than does a He^3 chamber and its content. This results in He^3 systems having a much more rapid equilibrium time than that of demagnetization systems, as well as greater temperature instabilities than demagnetization cryostats under similar heat influxes.

(i) Pumping Speed of the He^3 system:

The equations governing the flow of gases through pipes are discussed in detail by Dushman (1949). There are however a number of problems peculiar to cryogenic equipment which make difficult accurate estimation of the size of pumping tubes required for particular applications. In an isothermal situation the equations of gas conductance can be solved exactly in two limiting cases. The first case, free molecular flow, occurs when the mean free path of the molecules is larger than the lateral dimensions of the gas passage. In this case conduction is determined entirely by the geometry of the tubes. The second case, Poiseuille flow, arises when the mean free path of the molecules is much less than the lateral dimensions of the

gas passage. The pumping speed then depends on the gas viscosity, pressure gradient, and geometry of the pumping tube. Even in these two cases exact calculations can only be made for pumping tubes whose lengths are about fifty times their diameter (infinite tubes) or for orifices (zero length). In practical applications of the type considered here neither of these cases is applicable and the corrections which must be made for end effects are large. Over the pressure and temperature ranges involved the type of flow is neither viscous nor free molecular flow, and unfortunately no satisfactory interpolation formula between these two types of flow exists. An added difficulty arises due to the fact that most of the pumping tubes are under a temperature gradient. In calculating the required pumping tube diameter on the basis of free molecular flow for an ultimate temperature of 0.35°K , a diameter of about $1/4$ inch is sufficient for the section of the He^3 pumping tube between the 4°K bath and the He^3 chamber. It is further found that the $2\frac{1}{2}$ inch diameter section of the pumping tube at room temperature limits the ultimate pumping speed of the whole He^3 pumping line. The section of the He^3 pumping line between 4°K and the He^3 chamber was made $3/4$ inch in diameter in order to avoid extra solder joints. This results in a

large heat leak to the He^3 bath and limits the ultimate temperature. Because of this it is impossible to maintain intermediate temperatures (between 0.47°K and 1.25°K) using a single shot process. Remedies for this situation are given in section H.

(ii) The dead volume:

In order to make the most efficient use of the available He^3 , the dead volume, that is the volume which contains He^3 gas when the maximum amount has been condensed, must be kept to a minimum. For this reason the volume of the condenser side of the cryostat was made of capillary tubing. Most of the dead volume is in the pumping tubes and this is difficult to reduce without impairing the pumping speed. The distribution of He^3 by weight, when all the condensable He^3 is in liquid form at 1.25°K is shown below:

Amount at room temperature	6%
Amount between 295°K and 4°K	2%
Amount at 4°K	8%
Amount at 1.25°K but not in the He^3 chamber	18%
Amount in He^3 chamber	66%

(iii) Heat Influx:

Estimates of the heat flow to the He^3 chamber were made assuming the temperature to be below 0.5°K and the He^4 bath to be at 1.25°K . The biggest source of heat influx to the He^3 arises from the conduction by He^3 gas between the He^4 and He^3 baths. This mechanism can contribute as much as 40 microwatts; this upper limit is obtained by calculating the conduction of a static gas column. The $3/4$ inch pumping tube joining the He^3 and He^4 baths and the electrical leads conduct about 15 microwatts each. Initially the heat leak through the electrical leads was very large due to improper anchoring of the wires at 4°K and at 1.25°K . Estimates of the heat leak due to inefficient anchoring obtained from observations of the warming rate of the cryostat show this contribution to be about 2 microwatts.

A major source of heat influx is mechanical vibration. This is minimized to some extent by mounting the cryostat on a pillar which is mechanically de-coupled from the floor. The He^3 pump is connected to the cryostat by means of a bellows, while the He^4 pump is de-coupled using flexible vacuum hose. Despite such precautions slight mechanical vibrations are transmitted to the cryostat and result in additional heat influx.

(iv) The Kapitza Resistance:

Kapitza (1941) showed that in the case of liquid He^4 below about 1°K there is a temperature discontinuity at the boundary between the liquid helium and the solid surface of the container. At the present time no proper theory of this effect exists. The experiments of Fairbank and Lee (1957) show that this phenomenon also occurs with He^3 . Their results indicate that with He^3 the thermal resistivity, W , is given by

$$W = 130/T^2 \quad \text{cm}^2 \text{ deg K watt}^{-1},$$

where T is the absolute temperature at the boundary. The temperature discontinuity, ΔT , is then given in terms of the rate of heat transfer, \dot{Q} , in watts across the boundary by

$$\Delta T = 130 \dot{Q}/AT^2,$$

where A is the surface area in cm^2 across which heat transfer takes place. The He^3 chamber was designed to have a surface area which is large enough that this effect is not too important. For a heat load of about 10^{-4} watts the maximum temperature discontinuity is calculated to be three millidegrees K.

F. Thermometer Calibration

Two types of commercial carbon resistors were used as resistance thermometers, one was a 10 ohm Allen-Bradley resistor, the other a 220 ohm Speer. The resistances of these thermometers were determined using an isolating potential comparator similar in principle to that described by Dauphinee (1953).^{*} These thermometers were calibrated against the He⁴ vapour pressure scale at several temperatures between 4.2°K and 1.25°K, and an additional comparison was made with the He³ vapour pressure scale at 1.25°K. The range from 1.25°K to 0.47°K was covered using an extrapolation of the three constant equation of Markham, Netzel and Dillinger (1957):

$$\ln R/T = a(\ln R)^2 + b(\ln R) + c .$$

Here R is the thermometer resistance, T is the absolute temperature, and the constants a, b, and c are determined by a least squares fit to the calibration points. In order to determine the validity of such an extrapolation two different thermometers were attached to the specimen post and calibrated in the manner described above. At the same time a piece of high purity cadmium wire was also attached to the specimen post. The cadmium had both current and potential leads attached to it. The resistance

* We wish to thank Dr. F. D. Manchester for the loan of this device.

of the cadmium was determined as a function of temperature. The resistance measurements were made by comparing the voltage drop across a standard resistor in series with the specimen to the voltage drop across the specimen. The voltage measuring system was that described by Adler and Woods (1962). The temperature at which the cadmium became superconducting was determined with both resistance thermometers. The superconducting transition temperature of cadmium obtained by extrapolation of the two thermometers was $0.52 \pm 0.015^\circ\text{K}$. This is in good agreement with the value of $0.52 \pm 0.01^\circ\text{K}$ obtained calorimetrically by Martin (1961a) for cadmium of similar purity. The reason that the temperature scale was not established using the He^3 vapour pressure scale is that this would have required at least one additional liter of He^3 (N.T.P.) for filling a separate manometer system.

G. Operating Procedure of the He^3 Cryostat

This type of cryostat differs considerably from conventional He^4 cryostats in that a rather labourious leak testing procedure must be carried out in the process of cooling down the apparatus. Leak testing is performed using a Veeco leak detector. This instrument is a mass spectrometer which is sensitive only to He^4 , and is capable of detecting very small amounts of this gas (2×10^{-10} std cm^3/sec) leaking into the system to which it is attached.

Before every run the He^4 chamber, the experimental chamber, and the He^3 system are evacuated. The He^3 system is evacuated through the auxiliary vacuum system shown in Fig. 4.2. This auxiliary system is used in order to avoid contaminating the leak detector's vacuum system. When the pressure in the He^3 system has been reduced to below 10^{-4} mm of Hg (black-out on discharge gauge, M) valve 7 is opened. He^4 from a cylinder is sprayed on all the exposed parts of the He^3 system. If the leak indication then remains below about 10^{-9} std cm^3/sec the system is assumed to be leak tight. The He^4 chamber is then filled with about 1/2 atmosphere of He^4 gas from a cylinder, and the He^4 system is sealed. If no increase in the leak-rate is evident after about five minutes the He^3 condensing coil and length of He^3 pumping tube are assumed to be leak tight. A similar procedure is carried out filling the experimental chamber with He^4 exchange gas to a pressure of about 10^{-3} mm of Hg. This tests the He^3 chamber and porous plug for leaks. With the He^4 in the two chambers as described above the apparatus is then cooled down to liquid air temperatures. If no leak indication appears in the ensuing hour the apparatus is then cooled down to liquid helium temperature. The He^4 in the dewar serves to test the pumping tubes for leaks. When the liquid helium level in the dewar is

sufficiently high needle valve, A, is opened several turns. This admits liquid helium into the He^4 chamber. When the pressure in the He^4 chamber (as monitored either by the manometers or by the Bourdon gauge) reaches atmospheric pressure, the vent near the He^4 pump may be opened. At this point if no increase in the leak rate is noted the experimental chamber is evacuated to a gauge pressure of about 10^{-6} mm of Hg. This takes about one hour to one and one half hours. If the leak rate has remained unaltered, the vent near the He^4 pump and the needle valve may be closed and the system pumped down to 1.25°K . At this temperature superleaks in the He^3 system should become evident. If none appear the leak detector is removed from the system.

Before condensing the He^3 through the capillary it is allowed to condense down the pumping tube by opening valve 1. A few minutes later it is pumped off again. This process must be carried out several times at the beginning of every run. The reason for this is that He^3 system collects small amounts of air between runs. This condensation process freezes the air in the large pumping tube where it can not create a blockage. The air collected in the large pumping tube may be released at the end of the run through the He^3 manometer system. During cyclic operation the temperature is regulated by adjusting the ten

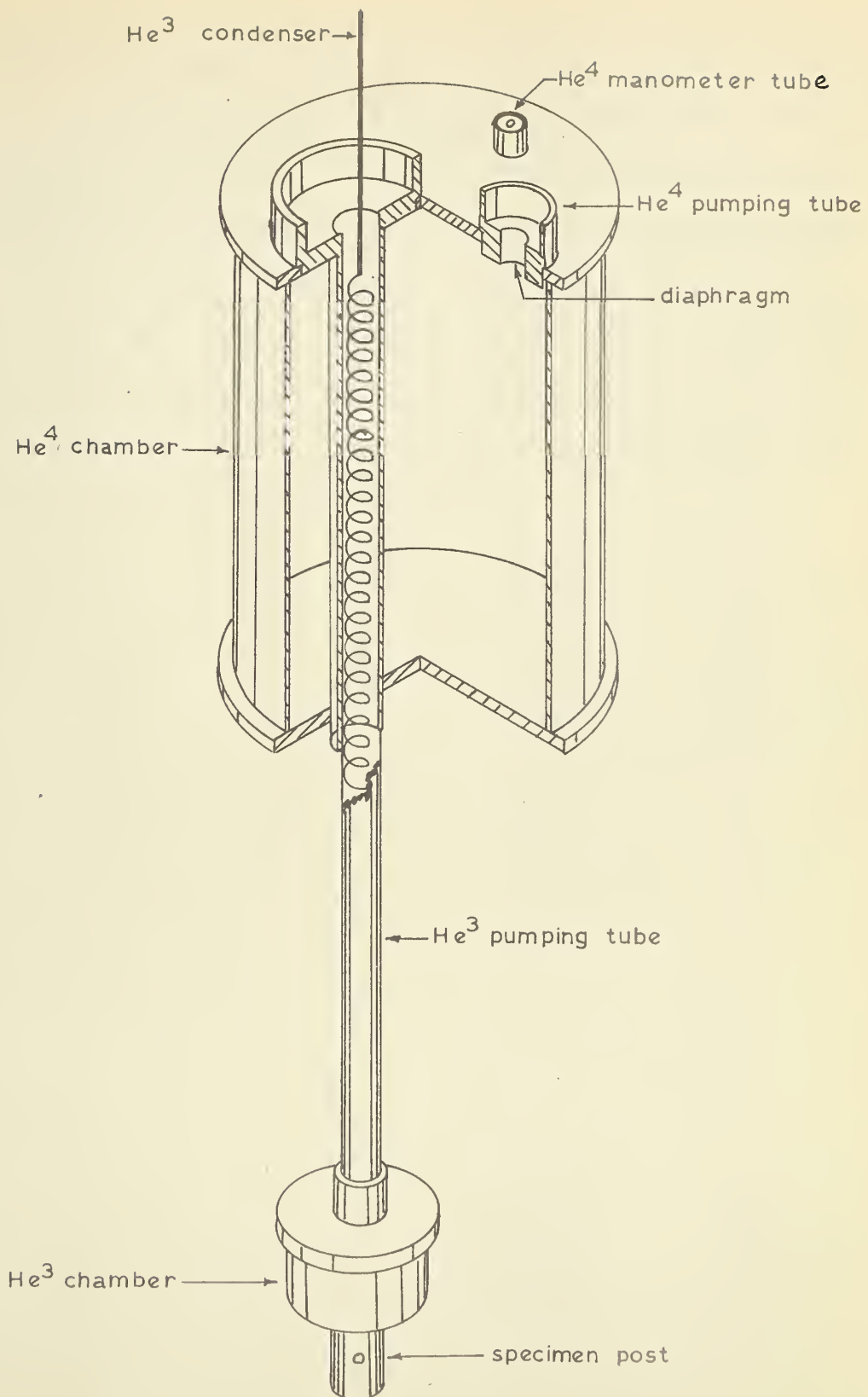
turn metering valve (valve 3) in the condensing line, and also adjusting the pumping speed using valve 4. During single shot operation the He^3 is condensed through the large pumping tube, and a final temperature of 0.47°K may be obtained with valve 4 wide open. It is not possible to maintain intermediate temperatures in the single shot process because the heat influx down the $3/4$ inch pumping tube leading to the He^3 chamber is too large at all but the lowest pressure. Temperatures between 4°K and 1.25°K are obtained by regulating the pressure of the He^4 chamber using the cartesian manostat; the specimen is then linked thermally to the He^4 bath by means of the He^3 in the He^3 pumping tube.

H. Proposed Modifications to the He^3 Cryostat

At the time the He^3 cryostat was originally designed, allowances were made so that future modifications might be incorporated without undue difficulty. A schematic diagram of a proposed modification of the cryostat is shown in Fig. 4.3. This modification would reduce the influx to the He^3 bath, reduce the dead volume by 16 percent, and provide for good heat exchange between the incoming and evaporating He^3 . The latter is achieved by placing the condensing coil in the He^3 pumping tube. In the modified cryostat the condensing capillary would enter the He^3

FIGURE 4.3

Schematic diagram showing proposed modifications to the He³ cryostat. Although not a scale drawing this figure is approximately true size.



pumping line through a ferrule in the He^3 radiation trap (Fig. A-3, Appendix III). Both the modified He^3 and the He^4 chambers are made of copper. The diaphragm in the He^4 pumping line is similar to the one in the present cryostat and serves to limit film flow. The pumping tube joining the He^3 and He^4 chambers is to be 3/16 inch thin wall inconel tubing. It is expected that this modification will enable temperatures of 0.35°K to be reached, and will allow the cryostat to handle larger heat loads.

CHAPTER V

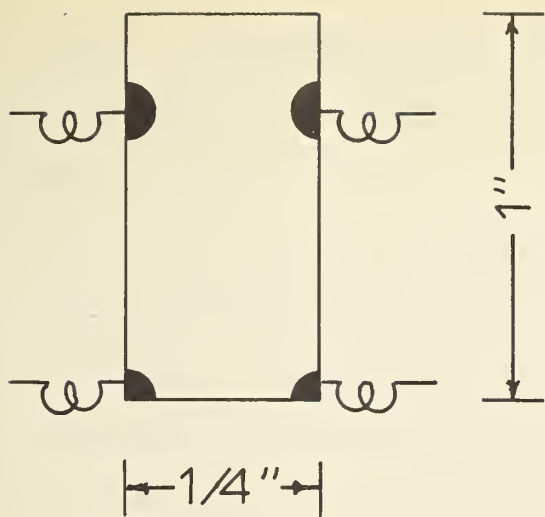
EXPERIMENTAL METHODA. Preparation of Tunnel Junctions

All tunnel junctions used in these experiments involved thin evaporated metal films. These films were deposited on 1/4" x 1" thin soda glass slides. The various stages of specimen preparation are shown schematically in Fig. 5.1. The glass slide (a portion of a standard microscope slide) was thoroughly cleaned using household detergent and water. After drip drying it was heated in a Bunsen flame to a temperature at which the edges just became fire polished. This anneals the slide as well as removing minor surface irregularities.* Four copper wires were then attached to the clean glass surface using pure indium solder as shown in Fig. 5.1 (a). The copper wires were tinned with 50/50 tin-lead solder. This tinning insured that the specimen leads were superconducting at liquid helium temperatures, thus reducing the heat input to the tunnel junction. The glass slide was then mounted in the evaporator. The first metallic layer (usually aluminum) was then evaporated through an aluminum mask; Fig. 5.1 (b) shows such a layer on the

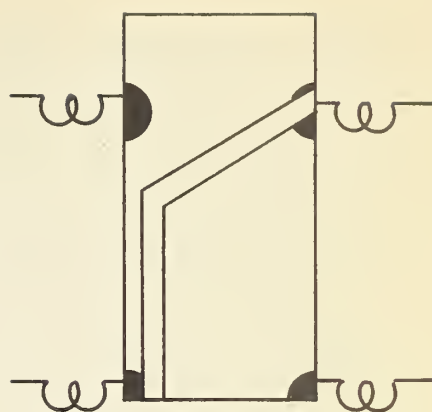
* Metal films deposited on slides which had not been flamed often lacked continuity.

FIGURE 5.1

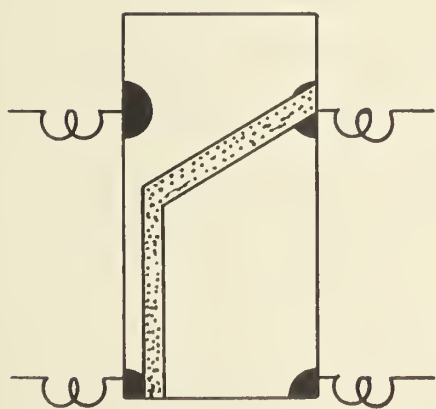
Schematic showing the various stages of specimen preparation.



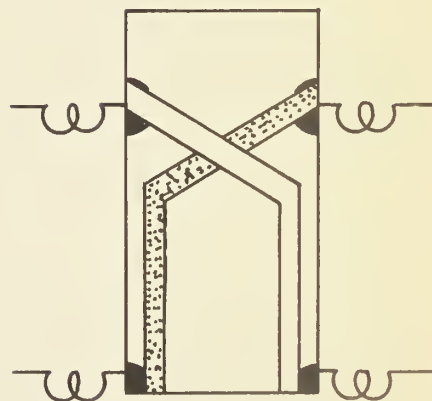
(a)



(b)



(c)



(d)

glass. Different kinds of filaments were tried, the generally used types being a tungsten helix, and molybdenum wire wound in a spiral to form a basket. Pressures of about 10^{-5} mm of Hg (sometimes lower) were maintained during evaporation. Care was taken to let some of the material evaporate onto a shutter plate before any was allowed to reach the glass plate. This decreased the probability of contamination of the metal film on the glass. Evaporation was allowed to proceed until the filament was no longer visible through the glass. The resulting films all had mirrorlike finishes. Air was then admitted into the evaporation chamber to allow the specimen to oxidize. Oxidation procedures varied, due to the varying moisture content of the air. When the moisture content of the air was low, the air was allowed to pass over water before entering the evaporator. The specimen with both the metal and metallic oxide layer is shown in Fig. 5.1 (c). Finally a second metallic layer was evaporated, completing the specimen as shown in Fig. 5.1 (d).

If the specimen showed tunneling characteristics, it was mounted and used in the experiments. The criteria used to determine whether the major contribution to the current was due to tunneling was that given by Fisher and Giaever (1961). The ratio of useless to useful specimens was about 6/1. Typical current-voltage characteristics

for an Al - Al_2O_3 - Al junction are shown in Figs. 5.2, 5.3, 5.4, and 5.5. Other tunnel junctions behaved much the same way except that those of type A - A_xO_y - B (A different from B) had their center of symmetry displaced by a few tenths of millivolts from the origin along the abscissa. Fig. 5.3 shows a comparison of I-V characteristics between our specimens and those reported by Fisher and Giaever (1961).

The following types of tunnel junctions were successfully made and used in these experiments:

Pb - Al_2O_3 - Al, Zn - Al_2O_3 - Al, Al - Al_2O_3 - Al, and In - Al_2O_3 - Al. Attempts were made at using various other oxide layers but all of these failed. Among those tried were: Cu - Cu_xO_y - In, Fe - Fe_xO_y - In, In - In_xO_y - In, Sn - Al_2O_3 - Al, Pb - PbO - Pb, Al - Al_2O_3 - Tl, and Mg - MgO - In. One of the difficulties with the magnesium was that even though evaporated through a mask the magnesium spread out and covered an area much larger than that of the mask, and in many cases the whole glass slide. This occurred even when the mask was only separated by about 2 mm from the glass slide. A possible cause for this behaviour is the rather high vapour pressure of magnesium at the temperatures at which we attempted evaporation. This is unfortunate because magnesium might have provided a metal substrate which does not become superconducting and

FIGURE 5.2

Current-voltage curves for a typical Al-Al₂O₃-Al tunnel junction at three different temperatures.

CURRENT - VOLTAGE CURVES
of an $\text{Al-Al}_2\text{O}_3\text{-Al}$ tunnel junction

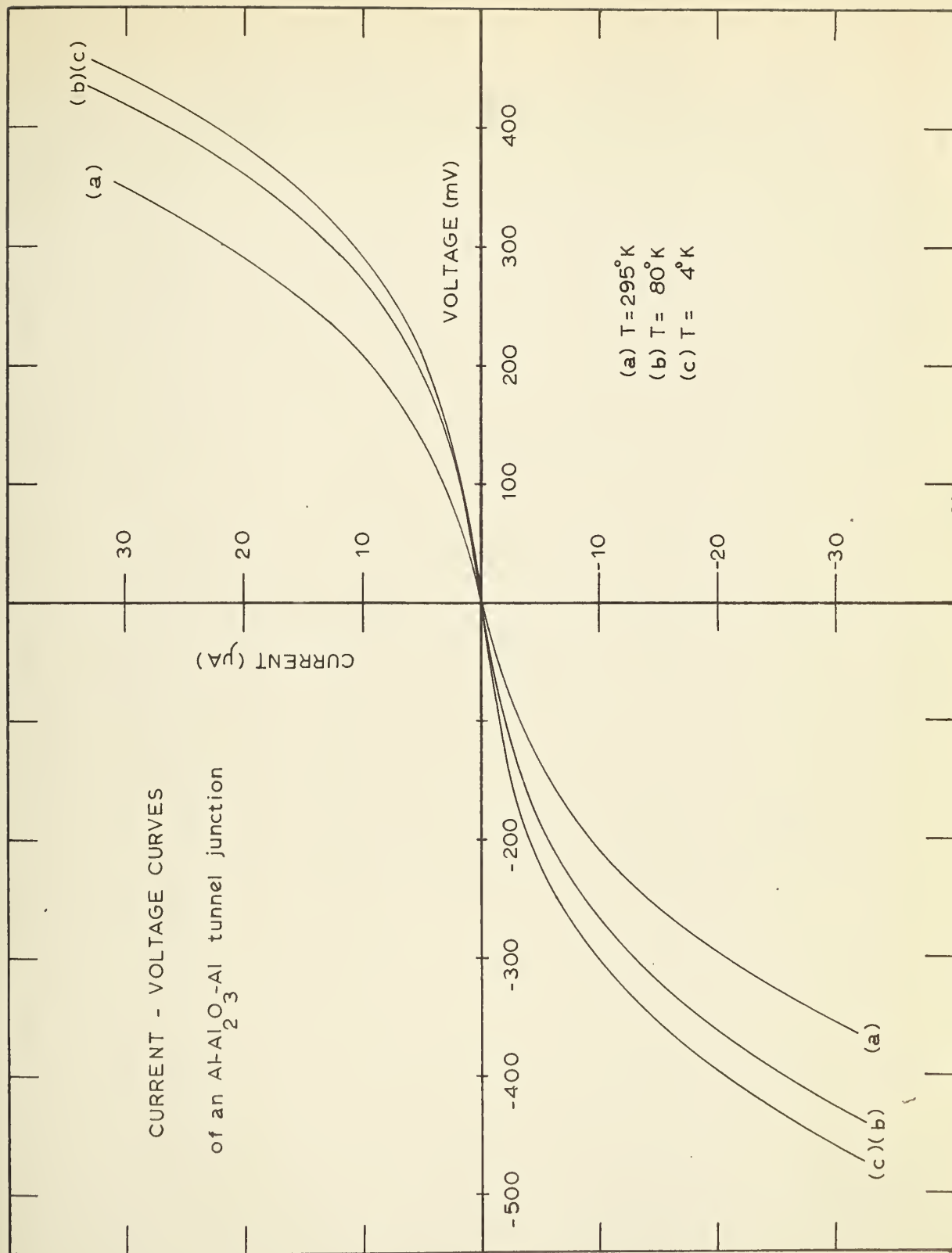




FIGURE 5.3

Semi-log plot of the I-V curves of typical
Al-Al₂O₃-Al tunnel junctions.

- (a) This work $T = 295^{\circ}\text{K}$
- (b) This work $T = 79^{\circ}\text{K}$
- (c) This work $T = 4.1^{\circ}\text{K}$
- (d) Fisher and Giaever (1961) $T = 295^{\circ}\text{K}$
- (e) Fisher and Giaever (1961) $T = 77^{\circ}\text{K}$

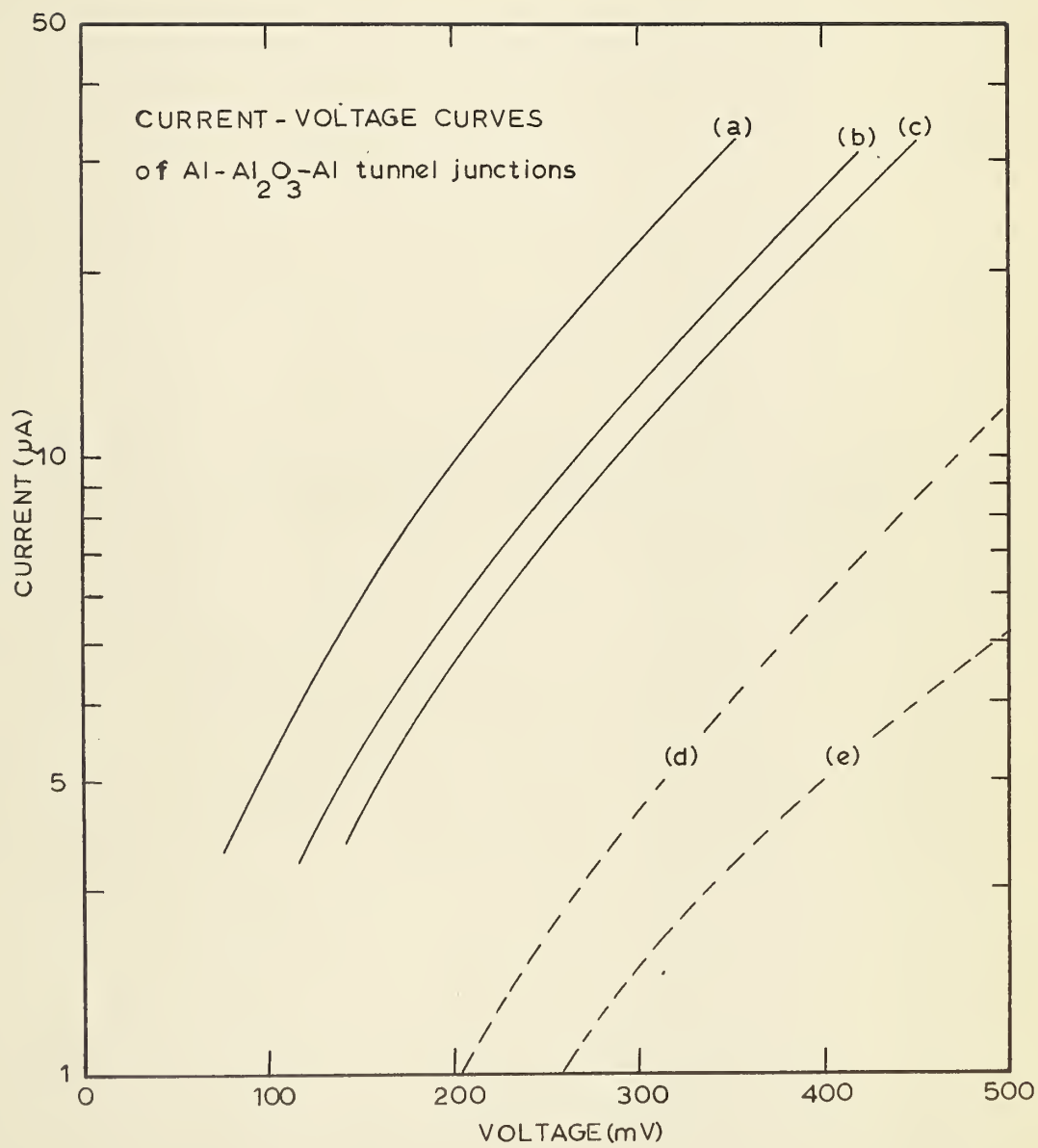


FIGURE 5.4

Linearity of a typical Al-Al₂O₃-Al tunnel junction.

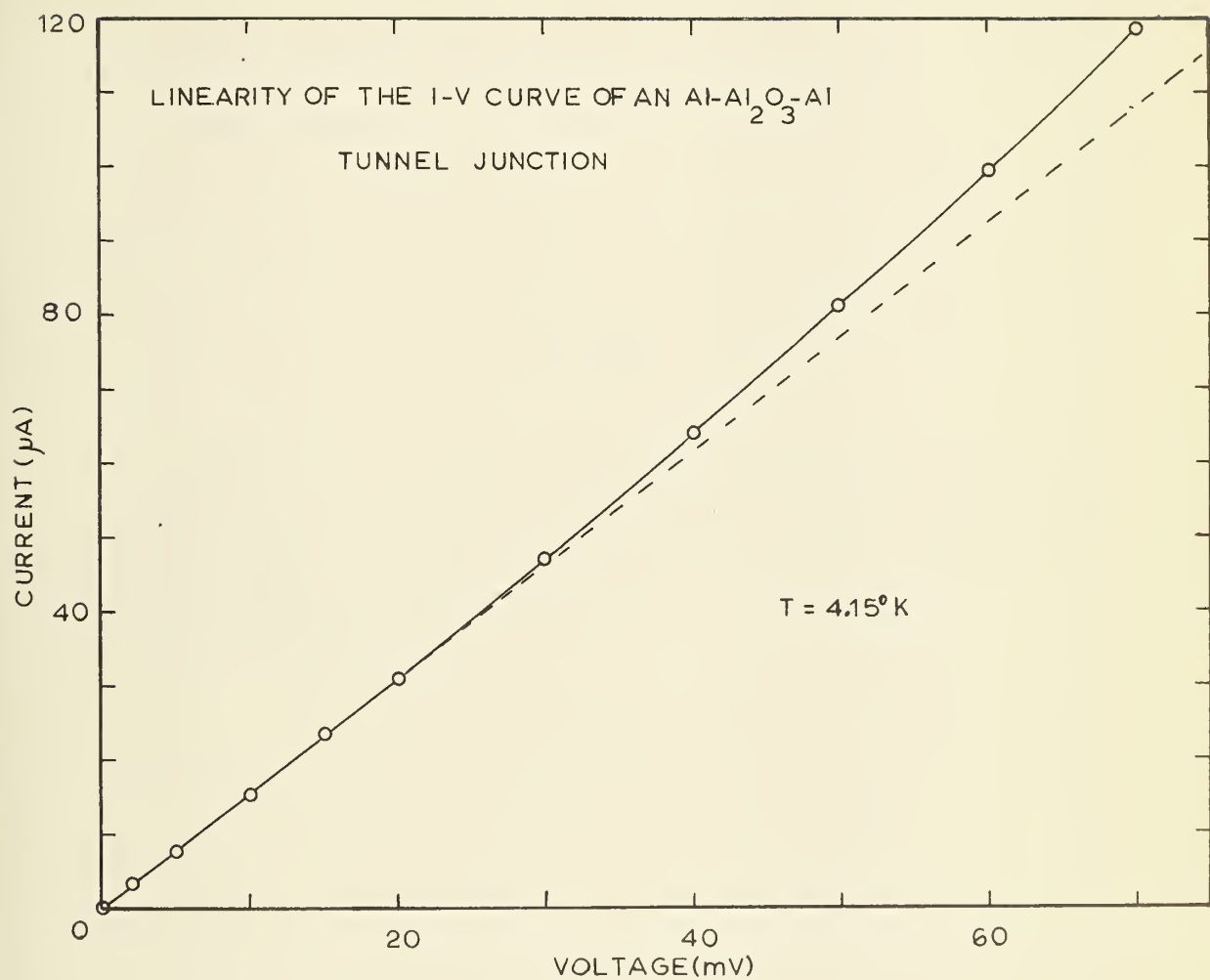
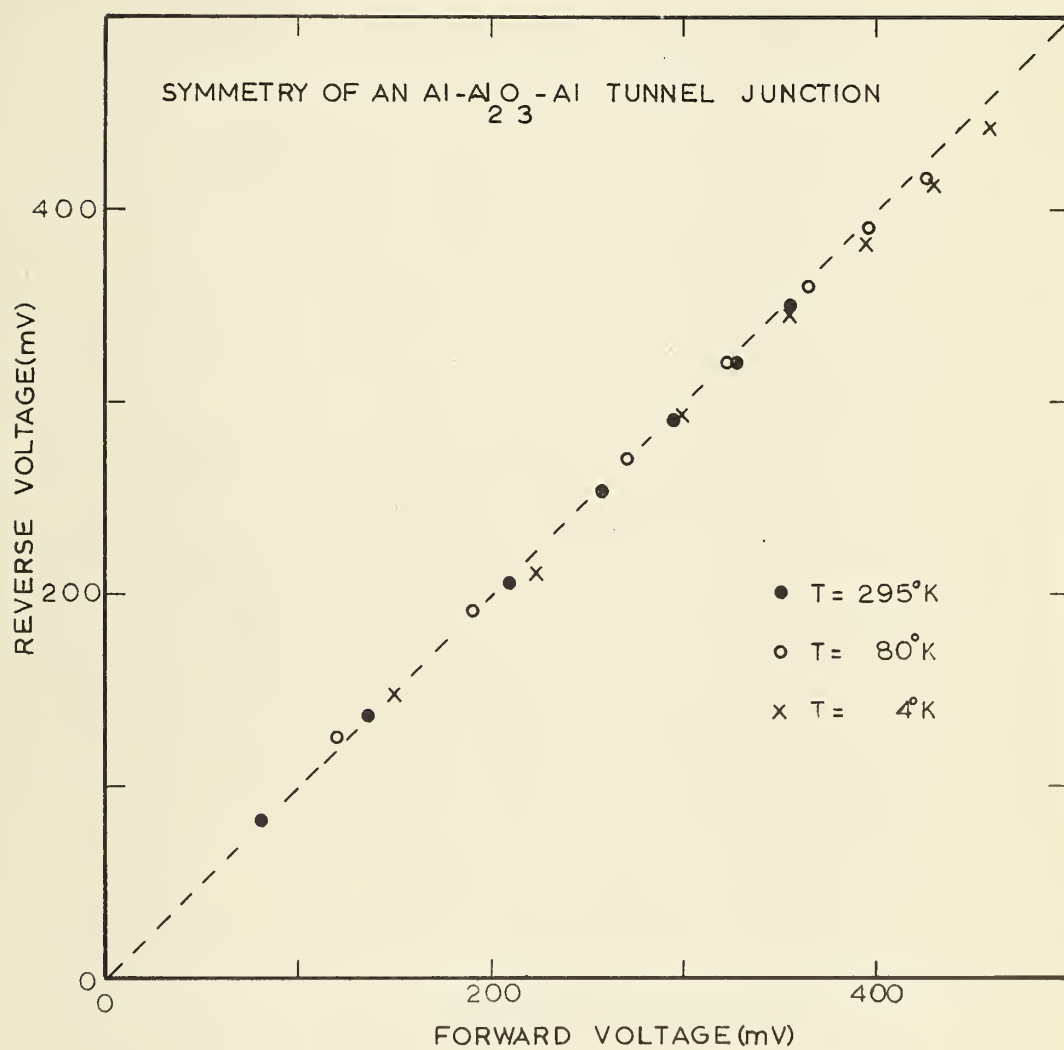


FIGURE 5.5

Symmetry of a typical Al-Al₂O₃-Al tunnel junction.
(Forward voltage is with the aluminum film nearest
the glass made positive).



at the same time is similar to aluminum in its oxide properties. The advantage of a normal metal substrate is that measurements can then be carried out with only one component of the junction superconducting and then the relative conductance gives the ratio of the densities of states of the superconducting to normal phases directly.

Some attempts were also made to produce tunnel junctions with mercury as one of the metals. One such junction was made using a "Kovar" tube that had an oxidized surface, and was subsequently filled with mercury. The oxide layer was too thick and although conduction through the "Kovar" oxide was partly due to tunneling, the bulk of the conduction was due to a semiconductor effect. This mercury-"Kovar" oxide-"Kovar" junction had a room temperature resistance of $1/4$ ohm, while its resistance at 1.25°K was about $1/2$ megohm. All that this experiment demonstrated was that "Kovar" oxide is a semiconductor. Other attempts involved mechanically polished copper, coated with a very thin layer of polyvinyl formvar which floated in a pool of mercury that was subsequently frozen. This type of junction could be made to exhibit tunneling properties down to 79°K , but would breakdown after about an hour. The reason for the breakdowns were not ascertained. Further attempts at producing tunnel junctions with mercury should be made because mercury is an interesting superconductor, since the electron-phonon interaction in this metal is very strong.

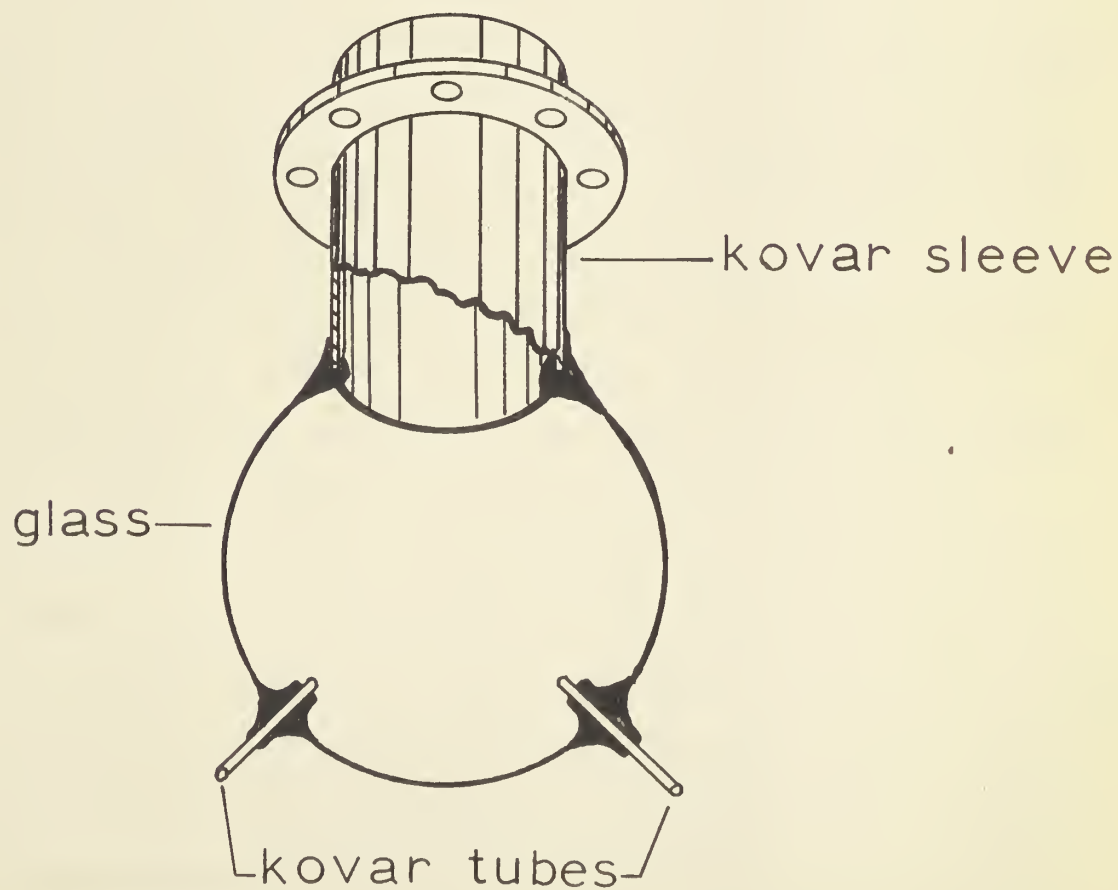
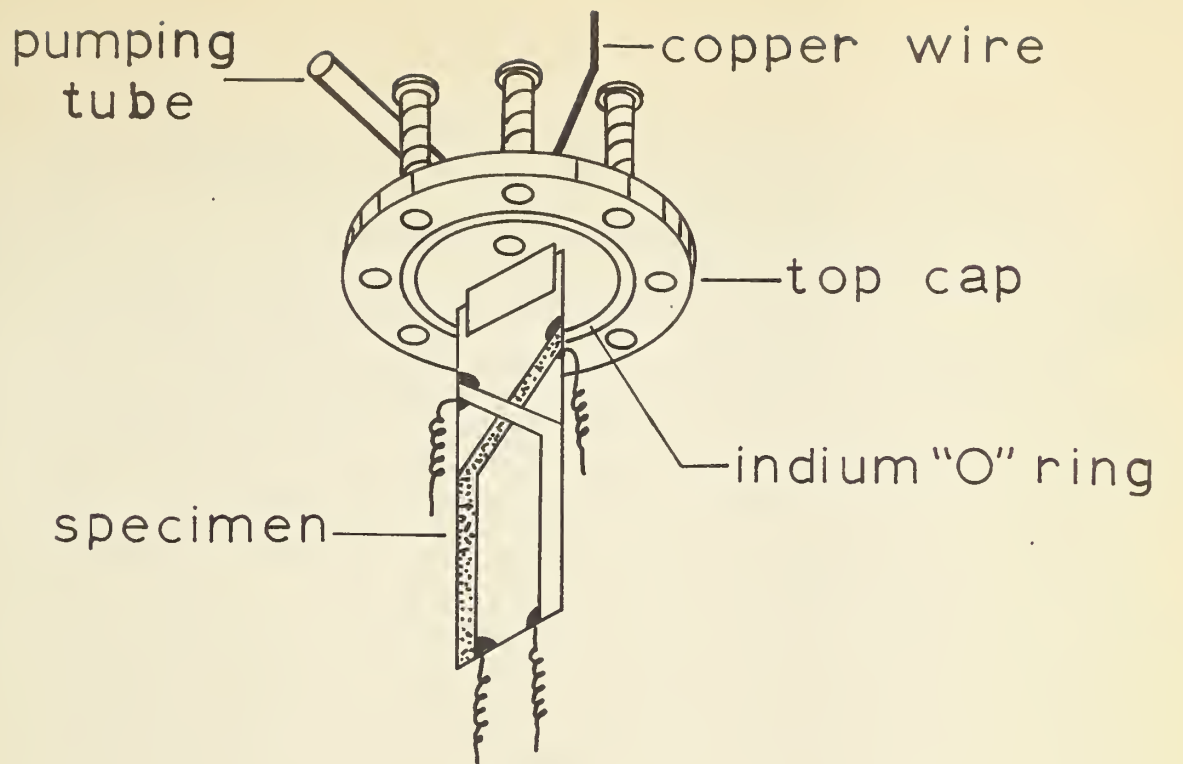
B. Specimen Mounting

The specimens on glass slides were mounted, one at a time in a "Kovar" to glass seal shown in Fig. 5.6. The top cap of the seal holds the specimen, while the current and potential leads are brought out through four small "Kovar" tubes at the bottom. These small tubes are sealed by allowing solder to flow into them. The top cap contains an indium "O" ring seal (Vacuum seal). There is a small tube in the top cap which allows the assembly to be evacuated and then filled with He^4 gas to atmospheric pressure. A few pellets of solder which had been placed in the small pumping tube before evacuation are melted to seal the assembly. This holder with the He^4 gas and specimen inside, was then soldered onto the specimen post of the cryostat. The copper (about 0.040 inch diameter) joining the top cap and the cryostat specimen post provided thermal contact between these two components. Thermal contact between the top cap and the specimen is established by the helium gas inside the "Kovar" to glass seal. We have found that thermal contact is somewhat improved at temperatures below the lambda point of He^4 . The reason for this is that at temperatures above the lambda point thermal contact is maintained by gas conduction, while at lower temperatures a film of superfluid He^4 acts as the thermal link.

FIGURE 5.6

Schematic showing the method of specimen mounting.

This drawing is approximately two times actual size.



C. Procedure

The operation and cool-down procedure of the cryostat has already been described in chapter IV. The specimen resistance as well as one resistance thermometer calibration point was obtained at 4°K before the exchange gas was pumped out of the experimental chamber of the cryostat. After pumping out the exchange gas for about one hour (to a gauge pressure of about 10^{-6} mm of Hg.), the apparatus was cooled to a temperature below the superconducting transition temperature of the specimen. This was done with most the He^3 in the cold part of the cryostat. The He^3 gas in the pumping tube between the He^3 and He^4 chambers acted as a thermal link. Somewhere between 4°K and 2°K a second resistance thermometer calibration point was obtained. The third resistance thermometer calibration point was normally obtained at about 1.25°K . If temperatures below 1.25°K were required, the temperature was further reduced to 0.5°K by pumping on the He^3 . Measurements on a specimen were first carried out with it in the superconducting state. Measurements with the specimen in the normal state were obtained at the end of the run, at 4°K , with exchange gas in the cryostat. Since normal state measurements were only required for relative conductance measurements this procedure enabled us to examine

the oscilloscope photographs of δV - V curves obtained with the specimen in the superconducting state and then to take photographs of oscilloscope traces with the specimen in the normal state using the same scale. Thus the scale used was determined by the finest structure visible on δV - V in the superconducting state. At the end of the run, with exchange gas in the experimental chamber of the cryostat all the He^3 was pumped back into storage and all the valves of the He^3 system were closed. The warm-up procedure from then on was the same as that for any He^4 cryostat.

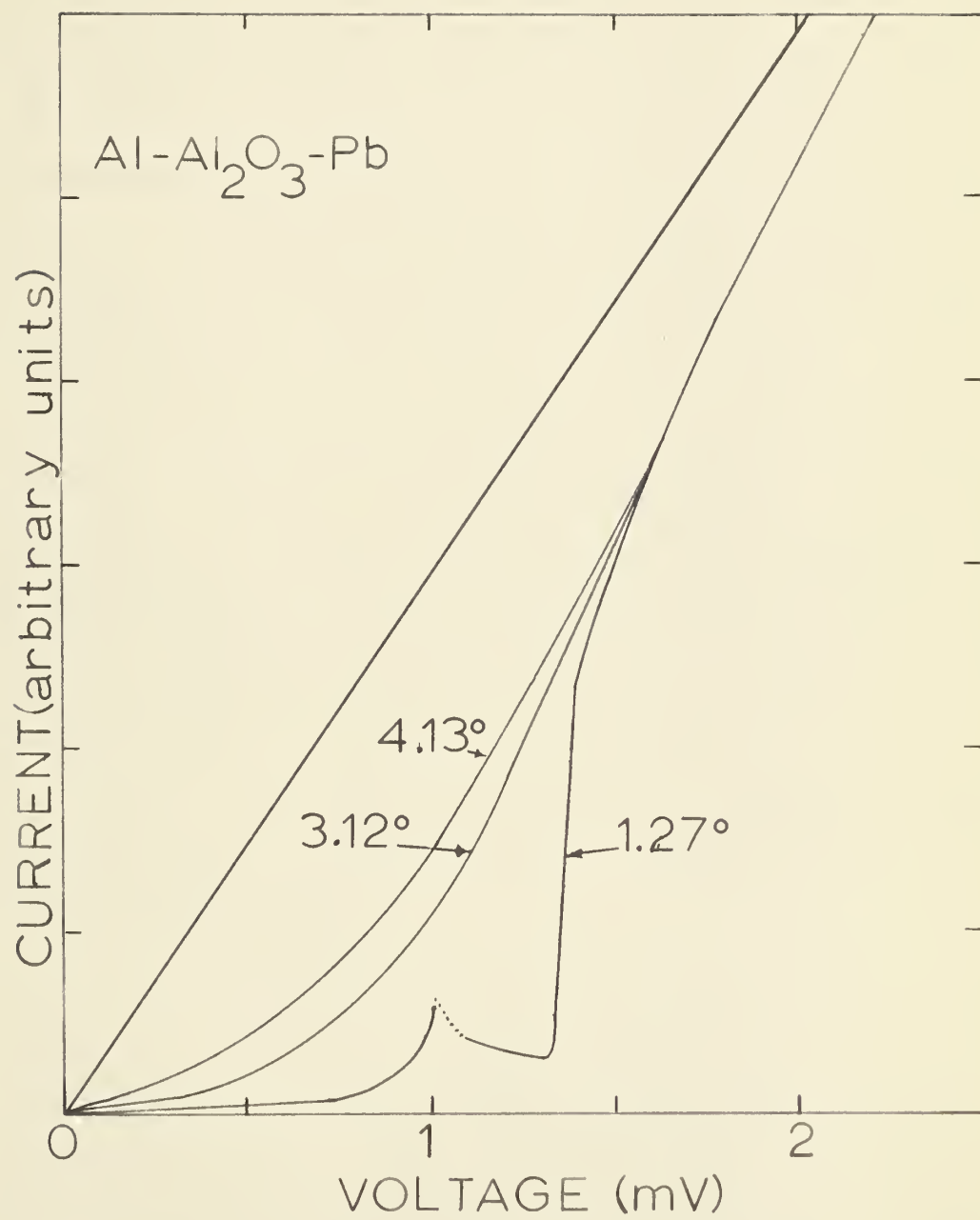
CHAPTER VI

EXPERIMENTAL RESULTSA. Current-Voltage Curves(1) Pb-Al₂O₃-Al:

This type of junction was the first to be attempted. Since the transition temperature of lead is 7.2°K we were able to familiarize ourselves with the method and with the characteristics of good specimens by immersing the junction in liquid helium in a storage dewar. For these immersion experiments the specimen was mounted in a stainless steel tube filled with He⁴ gas at low pressure. Specimens cooled without such mounting were invariably ruined even when dipped into liquid air. The sudden thermal shock that occurs when the unmounted specimen is dipped creates a rapid differential contraction between the metal film and the glass substrate which breaks the film. When we developed our experimental technique sufficiently, a junction was mounted as described in the previous chapter and soldered to the outside surface of the He⁴ chamber. The I-V curves obtained with this specimen are shown in Fig. 6.1. The specimen resistance, recorded in the normal state, during warm-up was about 4000 ohms. The room temperature resistance obtained preceeding the run was about 1250 ohms.

FIGURE 6.1

Current-Voltage curves for a Pb-Al₂O₃-Al tunnel junction.



This change in resistance arises because more than one conduction mechanism across the barrier is present. One conduction mechanism is provided by electrons either in the valence band or impurity levels of Al_2O_3 that are thermally excited into the conduction band at room temperature thus enhancing the conductance of the tunnel junction. This mode of charge transfer is greatly reduced at liquid air or lower temperatures since the thermal energy available for excitation is much lower. The second conduction mechanism, provided by tunneling through the barrier, is almost temperature independent. A thorough discussion of electron tunneling through thin insulating films is given by Holm (1951) and by Fisher and Giaever (1961). In most of our specimens the resistance at liquid air temperatures was two to four times the room temperature resistance, while there was a further increase in resistance of only about ten percent between liquid air and liquid helium temperatures.

An estimate of the thickness of the insulating barrier was also made. It was assumed that the equivalent circuit of the tunnel junction could be represented by a resistor in parallel with a parallel plate capacitor, the distance between the plates being the thickness of the oxide layer. The data for this calculation were obtained from the I-V curves at a number of frequencies. These

measurements showed a capacity of about $0.24\mu\text{F}$. Using the value of 6.4 obtained by Feldman and Hacskeylo (1962) for the dielectric constant of Al_2O_3 we obtain an estimate of about 20\AA for the barrier thickness. It must be pointed out that this estimate is probably extremely crude, because of the following major uncertainties:

(i) Measurements of dielectric constants of films of thicknesses comparable to these would be difficult to make; in fact they would involve a parallel plate capacitor arrangement, not unlike our tunnel junctions and the determination of film thickness would be uncertain. The value of dielectric constant used has been obtained by Feldman and Hacskeylo on material which was 100μ thick, they also pointed out that extrapolation to thinner films is uncertain.

(ii) Since capacitance measurements yield some average thickness for the barrier, while tunneling is exponentially dependent on the barrier thickness, any width inferred from capacity measurements is likely to be larger than the effective tunneling width. It is probably safe to conclude that the thickness of the Al_2O_3 layer is less than 30\AA . This takes into account the possibility of having underestimated the dielectric constant by 50%.

Finally it should be mentioned that the resistance of the tunnel junctions was found to increase with time at

room temperature. This increase was fairly rapid during the first few hours after the junction was made. For example, one newly made junction with a resistance of 10 ohms had a resistance between 100 and 1000 ohms a few hours later. The rate of increase of resistance decreased with time, but no actual saturation was observed. This type of behaviour occurred in all our specimens to a greater or lesser degree, not just in Pb-Al₂O₃-Al junctions. If the specimens were kept at liquid air or lower temperatures their resistance remained constant. Storing the specimens in an inert atmosphere (helium gas) at room temperature did not inhibit the resistance increase. It seems evident that whatever process caused the resistance to increase depends on the amount of thermal energy available. Assuming that the increase in resistance is due to a thickening of the barrier layer, two tentative explanations are offered:

(i) Oxygen trapped between the two metal films combined with the metal substrate to form more oxide, thus increasing the barrier thickness.

(ii) Assuming that the interface between the metals and the oxide layer is initially not very sharp, a diffusion process in which the metal moves in one direction while the oxide moves in the other in such a way as to sharpen the boundary would also have the effect of

increasing resistance.

One or both of the above explanations are possible because each of these mechanisms would slow down as the temperature is lowered.

(2) Zn-Al₂O₃-Al:

Measurements on this type of junction were carried out since no measurements of the energy gap in the density of electron states could be found in the literature for superconducting zinc. The I-V characteristics obtained at 0.5°K are shown in Fig. 6.2.

(3) Similar measurements were also carried out for aluminum and indium using Al-Al₂O₃-Al, (see Fig. 6.3) and In-Al₂O₃-Al tunnel junctions.

B. The Energy Gap

Values of the energy gap in the density of electronic states of a superconductor can be obtained from the current-voltage curves. For combinations of a normal metal and a superconductor the voltage, $V_1 = \Delta/e$, corresponds to the point at which the relative conductance is unity. In the case of two dissimilar superconductors the voltage, $V_2 = (\Delta_1 + \Delta_2)/e$, is given by the point where the I-V curve is steepest, while the sharp peak preceding the

FIGURE 6.2

Current-Voltage curves for a $\text{Zn-Al}_2\text{O}_3$ -Al tunnel junction at $T = 0.5^\circ\text{K}$.

CURRENT-VOLTAGE CURVES

for a $\text{Zn-Al}_2\text{O}_3\text{-Al}$ tunnel junction at $T=0.5^\circ\text{K}$

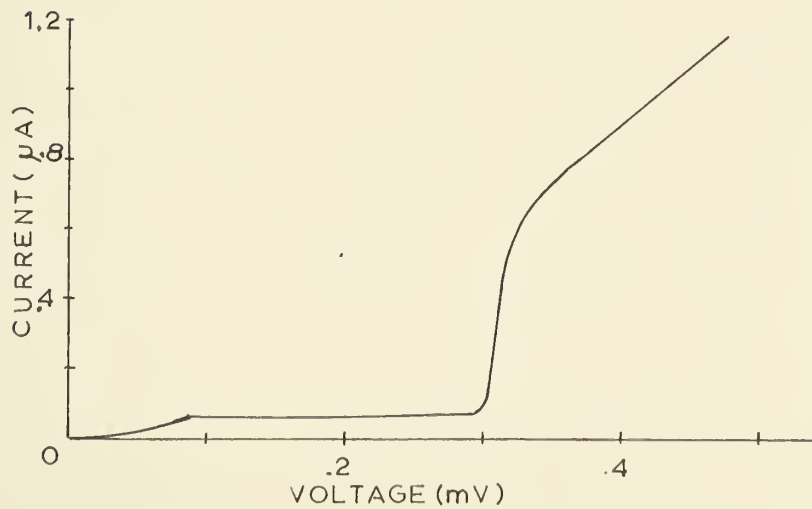
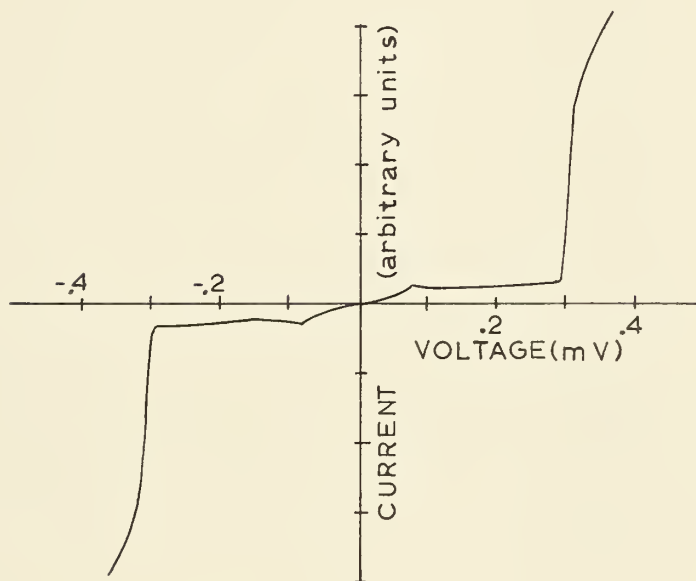
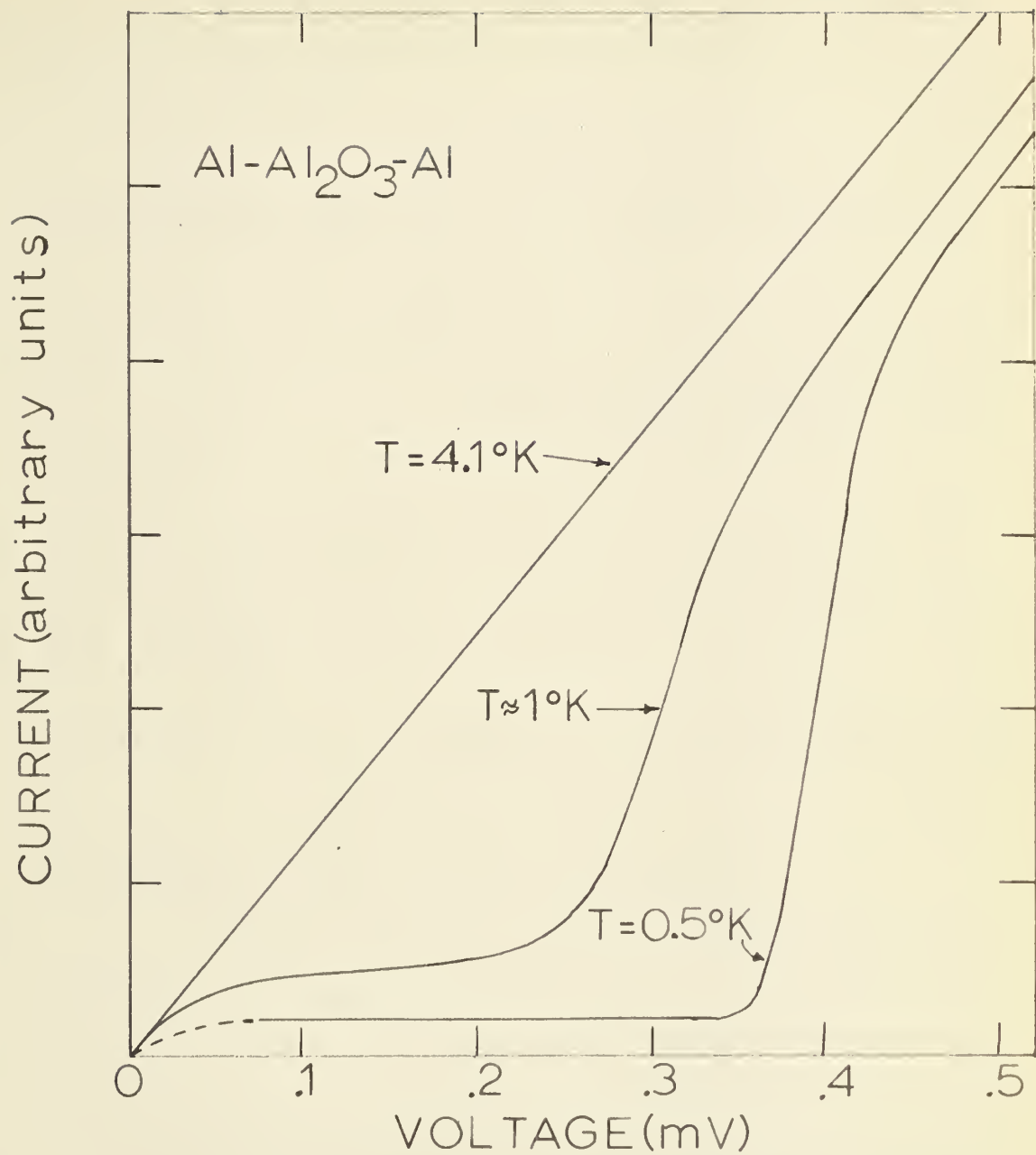


FIGURE 6.3

Current-Voltage curves for an Al-Al₂O₃- Al tunnel junction at T = 0.5°K.



negative resistance region occurs at a voltage,

$V_3 = (\Delta_1 - \Delta_2)/e$. Values of the energy gap so obtained are tabulated below.

TABLE I

Values of the energy gap (2Δ) in units of (10^{-3}eV) at
 $T = 0.5^\circ\text{K}$

Metal	This Work	Calculated from the BCS theory*	Giaever and Megerle (1961)
Pb**	2.47 ± 0.10	2.20	2.68 ± 0.06
In	1.09 ± 0.05	1.03	1.05 ± 0.03
Al	0.39 ± 0.03	0.355	0.42 ± 0.06
Zn	0.23 ± 0.02	0.234	- - - - -

C. Measurements of Relative Conductance

Giaever, Hart, and Megerle (1962) and Rowell, Chynoweth, and Phillips (1962) have reported structure in the relative conductance curve of lead. The observed

* In these calculations the transition temperatures given by Cochran and Mapother (1961) were used.

** The gap energy in lead was obtained at 1.24°K but is not expected to change significantly at lower temperatures because of the high transition temperature of lead.

structure was found to be harmonic, occurring at energies $\Delta + n E_t$, where E_t is the energy of the transverse acoustic phonon in lead and n is an integer. Since this structure has until now only been observed in lead it is of interest to examine other superconductors. Since such multiphonon effects should be easiest to observe in superconductors having a strong electron-phonon interaction the most logical metal to investigate is mercury. Since we were not successful in making tunnel junctions with mercury we decided to investigate indium and aluminum, in which the electron-phonon interaction is not quite as strong.

(1) Indium:*

The relative conductance of indium was measured using an In-Al₂O₃-Al tunnel junction. Specimens used had tunneling resistances of 30, 140, and 230 ohms. A small depression appears (between -12 and -16 mV) inside the dotted square in Fig. 6.4 (a). This corresponds to structure in the relative conductance of indium. There is an exactly similar effect occurring in the positive half of the curve, but is not as readily visible due to the steepness of the δV - V curve there. The asymmetry in the δV - V curves occurs in all tunnel junctions of the type A-A_xO_y-B,

* See also Appendix IV

FIGURE 6.4

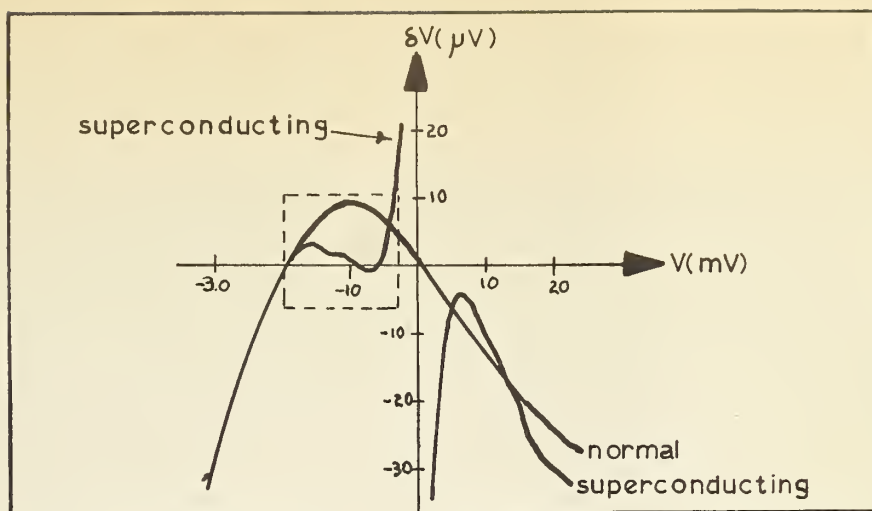
Relative conductance of an In-Al₂O₃-Al tunnel junction.

- (a) δV - V traced from an oscilloscope photograph.

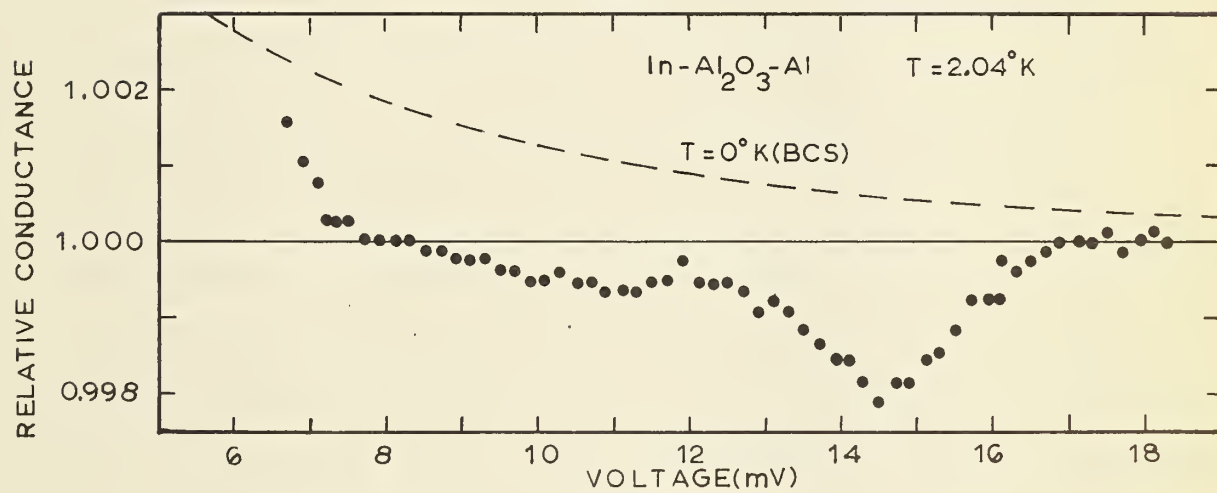
This photograph was taken with small sensitivity in order to show a large voltage range.

- (b) Relative conductance of a 230 ohm specimen at $T = 2.04^{\circ}\text{K}$. Indium but not the aluminum is superconducting.

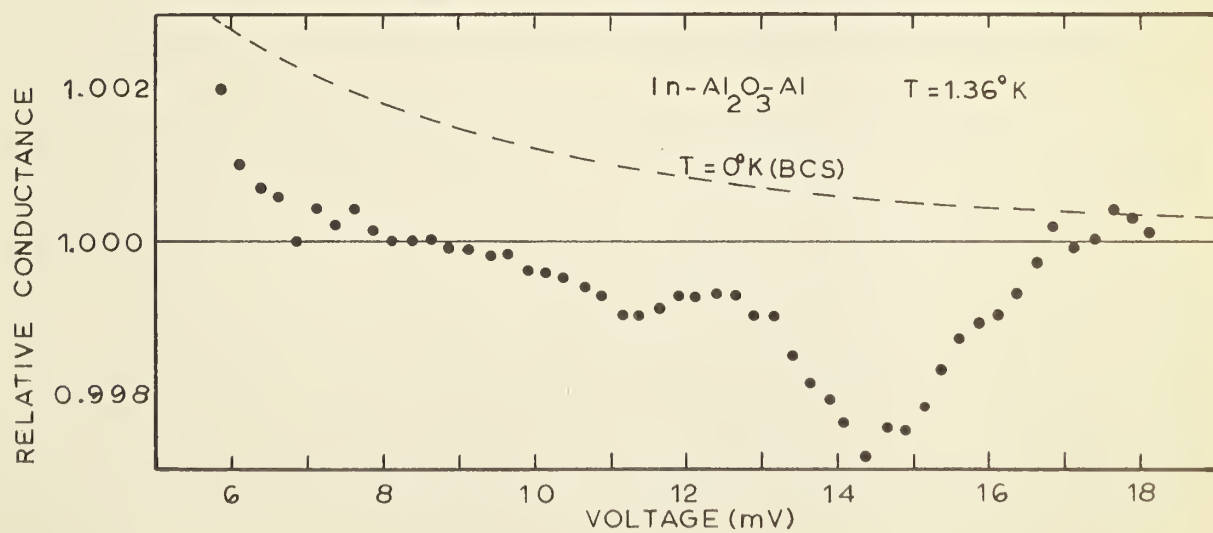
- (c) Relative conductance of a 30 ohm specimen. Both indium and aluminum are superconducting.



(a)



(b)

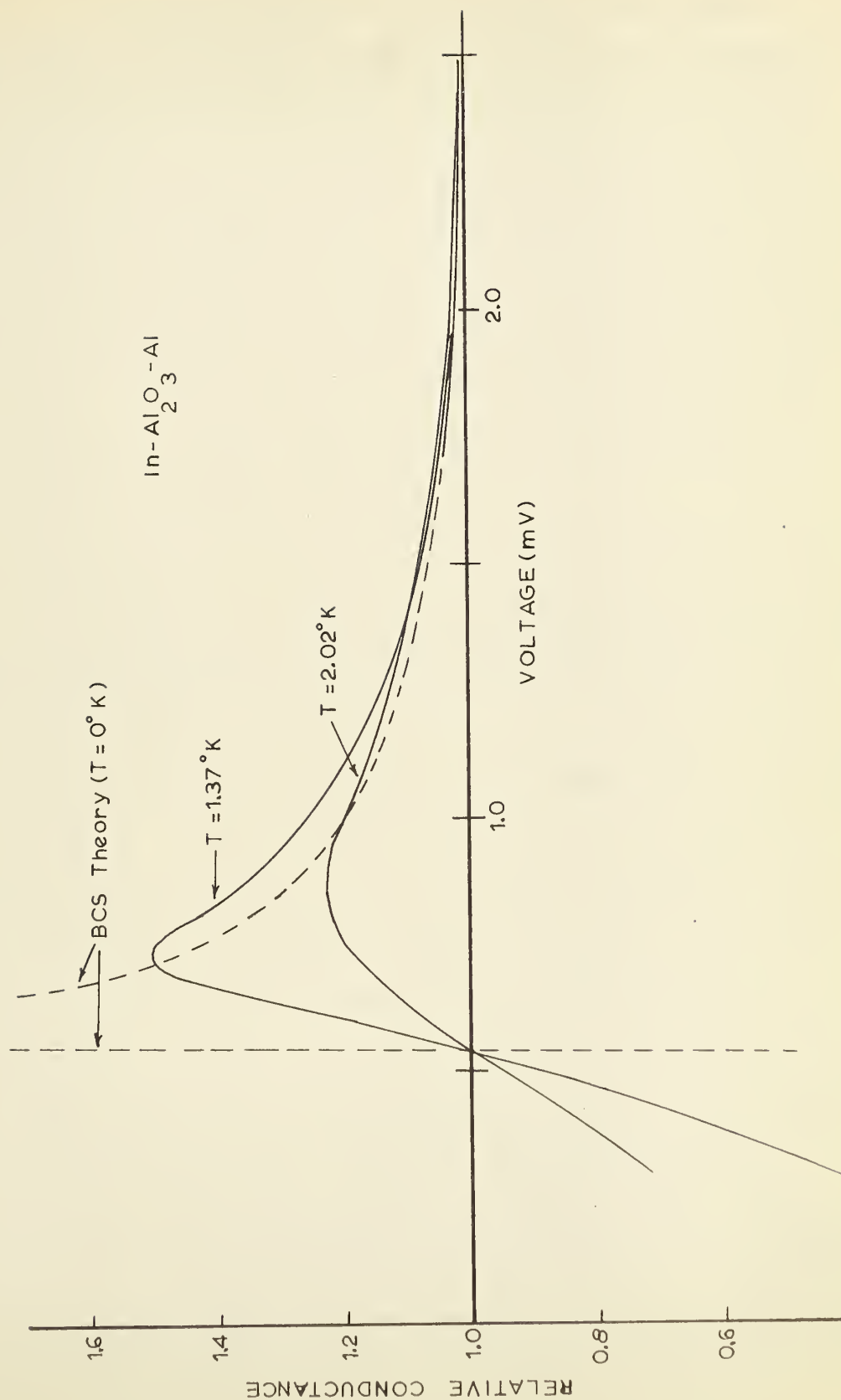


(c)

where A and B are dissimilar metals, and probably arises because of the difference in work function of the two metals. The same asymmetry appears in both the normal and superconducting states and hence does not affect the results. The relative conductance curves Fig. 6.4 (b) and (c) were evaluated from δV -V curves using the sensitivity of $1 \mu\text{V}/\text{cm}$ for δV . The relative conductance is then determined to an accuracy of ± 0.0001 . The level of the whole relative conductance curve with respect to unity can be ascertained only within ± 0.0005 , because the steepness of the δV -V curves at the higher voltages makes accurate measurement of $\delta V_s - \delta V_n$ difficult. The dashed line is the theoretical curve calculated from the BCS theory for $T = 0^\circ\text{K}$. The curve seems to remain asymptotic to unity for voltages greater than $\pm 20 \text{ mV}$, but above about 30 mV heating effects become noticeable. Heating effects cause discrepancies between the trace obtained with increasing sweep voltage and that obtained with decreasing sweep voltage. If heating effects are present then the slower the sweep the larger the discrepancy. Of the specimens used none showed heating effects below $\pm 20 \text{ mV}$. The specimen with the highest tunneling resistance (Fig. 6.4 (b)) was the least affected by heating, this is because the power input to the junction varies inversely with junction resistance.

FIGURE 6.5

Relative conductance of an In-Al₂O₃-Al tunnel junction
in the vicinity of the energy gap.



We also examined the relative conductance in the vicinity of the energy gap. Our results are in agreement with those of Giaever, Hart, and Megerle (1962) and are shown in Fig. 6.5. Because of the steepness of the relative conductance curve in this region we cannot obtain as great an accuracy at these small biases as we can at higher voltages (~ 6 to ~ 20 mV). Nevertheless the data in Fig. 6.5 are accurate to about $\pm 5\%$ for voltages below ~ 1 mV, and becomes more accurate as the voltage across the tunnel junction increases.

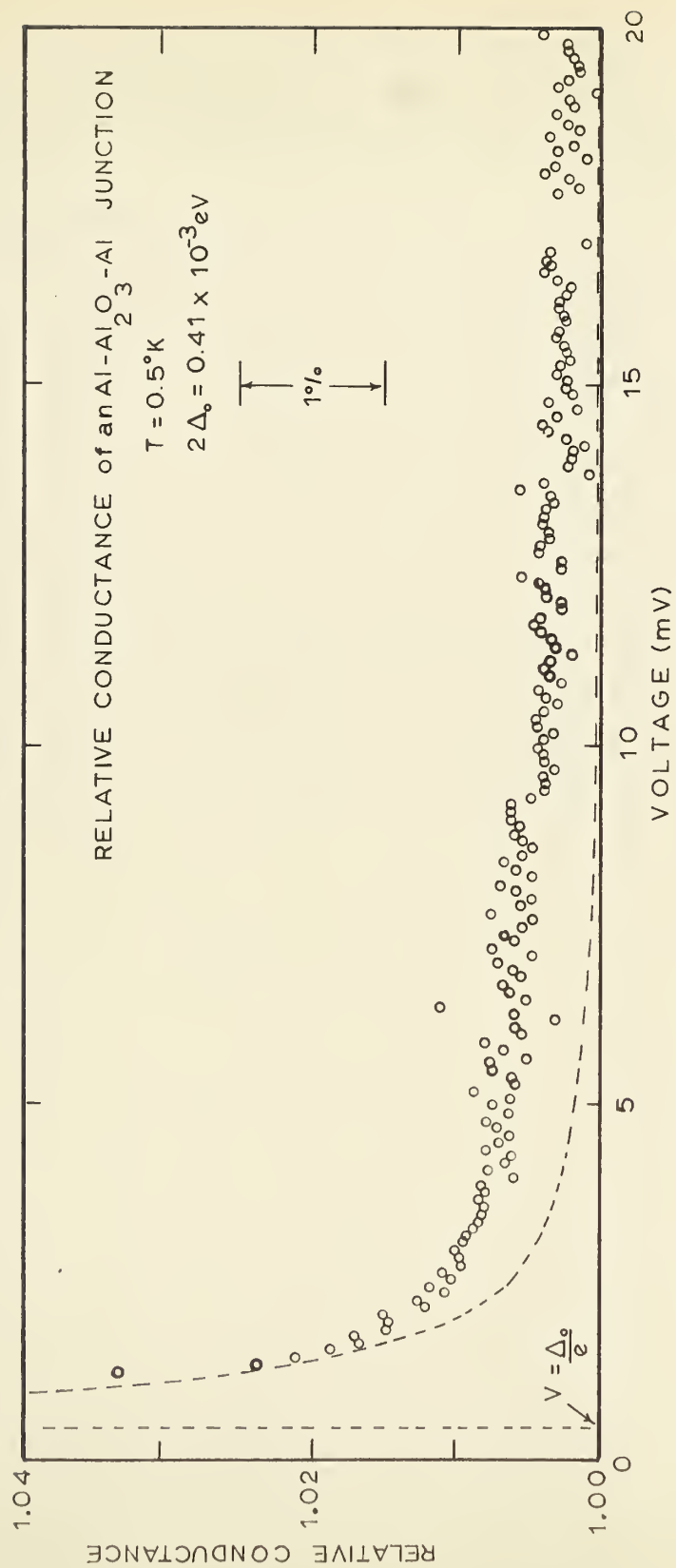
(2) Aluminum:

Relative conductance measurements were made on Al-Al₂O₃-Al tunnel junctions, a portion of one of the resulting curves is shown in Fig. 6.6. Since we wanted to carry our measurements out to voltages which correspond to energies higher than the Debye energy of aluminum, tunnel junctions were made having high resistances (200 to 2000 ohms) to minimize heating effects*. As can be seen from Fig. 6.6 agreement with the BCS theory is surprisingly good. (The dashed line is the relative conductance calculated using equation (A-6)). Small humps and depressions in the relative conductance appear throughout the whole curve out to about 60 mV. The amplitude of these effects varies starting from a rather

* The Debye temperature of aluminum is 430°K which corresponds to a voltage of 37 mV.

FIGURE 6.6

Relative conductance curve for an Al-Al₂O₃-Al tunnel junction at $T = 0.5^{\circ}\text{K}$. Dashed curve indicates the behaviour predicted by the BCS theory at the absolute zero.



small amplitude near the gap region and increasing somewhat at larger biases. Several attempts to find significant regularities or periodicities in the energies at which the humps occurred were unsuccessful. These humps were clearly visible on the δV - V curves and occurred only when the aluminum was in the superconducting state. They were quite reproducible and several photographs showed exactly the same structure on separate occasions, as long as the specimen was kept at liquid helium temperatures. The same humps persisted on different specimens, but humps having the same character appeared at higher energies (never more than 10^{-3} eV) in a specimen that was allowed to warm up to room temperatures between runs.

CHAPTER VII

CONCLUSIONS AND DISCUSSIONA. The Energy Gaps

Table I shows that the values obtained for the energy gap in the density of electron states are in remarkable accord with the values predicted by the BCS theory. This good agreement with the BCS theory seems characteristic of thin film experiments, such as those of Giaever and Megerle (1961), Giaever, Hart and Megerle (1962), Townsend and Sutton, (1962), and of Ginsberg and Tinkham (1960). On the other hand measurements of the energy gap in single crystals, done by e.g. Morse, Olsen, and Gavenda (1959), Morse and Bohm (1960), Mackintosh (1960), using ultrasonic attenuation indicate dependence of the energy gap on crystalline orientation. Such anisotropy is not surprising when one considers the complex Fermi surfaces of metals which become superconductors. It may be that anisotropy does not manifest itself very strongly in thin film experiments because of film thicknesses that are less than the coherence length. In such a case the wave functions for the electrons in the superconducting state might be affected to an extent large enough to mask any anisotropy effects. Such a geometrical

restriction of the electronic wave functions might be expected to modify some of the parameters which are characteristic of the superconducting state, such as the energy gap.

As can be seen from Table I, our results for the energy gap of lead are about 12% higher than those predicted by the BCS theory. This is because the theory is only applicable in the weak coupling limit, that is for metals in which the electron-phonon interaction is moderately weak. A measure of the strength of this interaction is usually expressed in terms of the coupling constant, T_c/θ_D , where θ_D is the Debye temperature. The weak coupling limit of the BCS theory implies $T_c/\theta_D \lesssim 0.01$, whereas for lead $T_c/\theta_D = 0.075$.

For each of our aluminum tunnel junctions we found that the superconducting transition temperature was higher than that of bulk aluminum. This is in accord with the observations of Giaever, Hart, and Megerle (1962) which showed that the transition temperature increased as the film thickness decreased. These workers also noted that the energy gaps obtained from their tunneling measurements were somewhat higher than those predicted by the BCS theory for aluminum.* They attributed this behaviour to the effect of internal stresses on their films. Our results

* For aluminum $T_c/\theta_D = 0.0027$, thus the weak coupling limit of the BCS theory should apply.

(Table I) are in general accord with those of Giaever and his co-workers, but we feel that a more satisfactory explanation of the high transition temperatures might be found in terms of the coherence length. In the BCS theory the relation for the coherence length, ξ_0 , in terms of the energy gap parameter, Δ_0 , is

$$\xi_0 = \frac{\hbar v_0}{\pi \Delta_0} \quad , \quad (7.1)$$

where v_0 is the Fermi velocity. Since these films all have a thickness which is less than the coherence length, the bulk coherence length might be replaced by a new coherence length $\xi(t) \leq \xi_0$, where t is the film thickness. The transition temperature would then still be linked to the energy gap by the BCS relation $2\Delta_0 = 3.52 kT_c$. Both indium and zinc show extremely good agreement with the energy gap value predicted by the BCS theory, indeed so good that in the light of what has been said above it may be somewhat fortuitous.

B. The Relative Conductance Measurements

A discussion of the relative conductance of indium, which has been accepted for publication, is given in Appendix IV, and only the results for aluminum will be discussed here. A portion of the relative con-

ductance curve for an Al-Al₂O₃-Al tunnel junction is shown in Fig. 6.6. The agreement between the theoretical curve and the experimental points is extremely close, being better than one percent throughout. Measurements were made to biases of about 60 mV, but only a portion of the results were plotted as the remainder are asymptotic to unity and show about the same scatter. As mentioned above (Chapter VII, Section C) we were unable to find any regularity in the observed structure. It is at first sight tempting to attribute this structure to multiphonon effects similar to those observed by Rowell, Chynoweth, and Phillips (1962)*, but which appear at various energies due to the real lattice spectrum not conforming to an Einstein approximation. However if these were in fact multiphonon effects one would expect the amplitude of the peaks to diminish as the electron energy increased, particularly above the Debye energy, since the probability of a two phonon process is less than that of a single phonon process. An explanation for these small bumps in the relative conductance curve is not apparent.

C. Suggestions for Further Investigation

The above investigations in this relatively new field of electron tunneling into superconductors are naturally of somewhat preliminary nature. The experience

* See Chapter II, Section D.

gained thus far has however clarified the scope of the technique and stimulated ideas for further experiments that should provide definitive information. Some of these are briefly listed below:

(i) The measurement of energy gaps by electron tunneling into bulk superconductors, using single crystals of known orientation. Such measurements should reveal the anisotropy of the energy gap and its relation to the Fermi surface of the metal in its normal state.

(ii) Electron tunneling experiments with the transition metal superconductors ruthenium and osmium. Such experiments are of interest from a theoretical standpoint because these metals show no isotope effect, which is an indication that superconductivity in them does not arise from the electron-phonon interaction.

(iii) Electron tunneling experiments with superconducting alloys. These experiments would provide information about the effects of alloying on the attractive interaction which gives rise to superconductivity.

(iv) Measurements of the energy gap in thin films along with a careful determination of both the transition temperature and film thickness, to establish the correlation between these parameters.

(v) A careful re-examination of the relative conductance of lead to determine whether any further

multiphonon structure besides that observed by Rowell et al. exists. Neither this group, nor Giaever and his co-workers have indicated the sensitivity with which they are able to observe the relative conductance, and it is quite possible that our bridge technique is an order of magnitude more sensitive. Furthermore efforts should be made to produce tunnel junctions in which one component is mercury and determine if it exhibits multiphonon effects as well.

D. A Proposed New Application of Electron Tunneling to Normal Metals

The value of electron tunneling techniques as a solid state research tool stems from the fact that by virtue of the barrier layer one can inject electrons of a known energy and direction of motion into a metal. Consider a tunnel junction of the type A/ barrier/ A', where A is a single crystal of known orientation and A' is an evaporated film of metal A. If we apply a positive voltage to metal A, then only electrons with a direction of travel that is essentially perpendicular to the barrier layer will tunnel from A' to A because of the exponential dependence of the tunneling probability on the barrier thickness. Thus the direction of motion with respect to the crystalline axes of metal A is known. The wave-vector

of the electron is now fully determined and if it corresponds in energy to the Brillouin zone boundary for this wave vector, the electron will suffer a Bragg reflection, that is it will not be permitted to tunnel at all. In a practical situation there will be some contribution to the current even at these energies for two reasons. (i) The electron may be scattered by impurities or lattice imperfections. (ii) The electron may be scattered by lattice vibrations. For this reason such experiments must be carried out at low temperatures (liquid helium) where the phonon density is low. Also the single crystal of material A must be very pure and have a very carefully prepared surface so that lattice irregularities scatter only a small fraction of the tunneling electrons. Such an experiment enables one to determine the energies involved in umklapp processes (Bragg reflections) directly. This information would be of use in determining the umklapp contribution when calculating transport coefficients. If such measurements are carried out in many crystal directions and if one assumes a general form for the dispersion relation (i.e. energy as a function of wave vector) one can in principle determine the Fermi surface.

BIBLIOGRAPHY

- Adler, J. G. and Woods, S.B., 1962. Can. J. Phys. 40, 550.
- Adler, J.G. and Rogers, J. S., 1963. Phys. Rev. Letters 10, **217**
- Aldrich, I.L.T. and Nier, A.O., 1948. Phys. Rev. 74, 1590.
- Ambler, E. and Dove, R.B., 1961. Rev. Sci. Instr. 32, 737.
- Bardeen, J., 1950a. Phys. Rev. 79, 167.
- Bardeen, J., 1950b. Phys. Rev. 80, 567.
- Bardeen, J., 1956. Handbuch der Physik XV Springer-Verlag, Berlin pp. 274-368.
- Bardeen, J., Cooper, L.N., and Schrieffer, J.R., 1957a. Phys. Rev. 106, 162.
- Bardeen, J., Cooper, L.N., and Schrieffer, J.R., 1957b. Phys. Rev. 108, 1175.
- Bardeen, J. 1961. Phys. Rev. Letters 6, 57.
- Bardeen, J. and Schrieffer, J.R., 1961. Progress in Low Temperature Physics, 3, North Holland Publishing Co., Amsterdam.
- Blevins, G.S., Gordy, W., and Fairbank, W.M. 1955. Phys. Rev. 100, 1215.
- Biondi, M.A., Forrester, A.T., Garfunkel, M.P., and Satterthwaite, C.B., 1958. Revs. Mod. Phys. 30, 1109.
- Casimir, H.G.B. and Gorter, C.J., 1934. Physik, z. 35, 963.
- Cochran, J.F. and Mapother, D.S., 1961. Phys. Rev. 121, 1688.
- Cohen, M.H., Falicov, L.M., and Phillips, J.C., 1962. Phys. Rev. Letters 8, 316.
- Cooper, L. N., 1956. Phys. Rev. 104, 1189.
- Corak, W.S. and Satterthwaite, C.B., 1956. Phys. Rev. 102, 662.

- Culler, G.J., Fried, B.D., Huff, R.W., and Schrieffer, J.R., 1962. Phys. Rev. Letters, 8, 399.
- Daunt, J.G., Probst, R.E., and Johnston, H.L., 1947. J. Chem. Phys., 15, 759.
- Daunt, J.G., Probst, R.E., and Johnston, M.L., 1948. Phys. Rev., 73, 638.
- Dauphinee, T.M., 1953. Can. J. Phys. 31, 577.
- de Bruyn Ouboter, R., Taconis, K.W., LePair, C., and Beenakker, J.J.M., 1960. Physica 26, 853.
- Decker, D.C., Mapother, D.E., and Shaw, R.W., 1958. Phys. Rev., 112, 1888.
- Fairbank, H.A. and Lee, D.M., 1957. Proceedings of the Symposium on Solid and Liquid He³, Ohio State University, p. 27, 32.
- Feldman, C. and HacsKaylo, M., 1962. Rev. Sci. Instr., 33, 1459.
- Fisher, J.C. and Giaever, I., 1961. Journ. Appl. Phys. 32, 172.
- Frölich, H. 1950a. Phys. Rev. 79, 845.
- Frölich, H. 1950b. Proc. Phys. Soc. A63, 778.
- Frölich, H. 1962. Reports of Progress in Physics XV, 1.
- Geballe, T.H., Matthias, B.T., Hull, G.W., and Corenzwitt, E., 1961. Phys. Rev. Letters 6, 275.
- Giaever, I., 1960a. Phys. Rev. Letters 5, 147.
- Giaever, I., 1960b. Phys. Rev. Letters 5, 464.
- Giaever, I. and Megerle, K., 1961., Phys. Rev. 122, 1101.
- Giaever, I., Hart, H.R., Megerle, K., 1962. Phys. Rev. 126, 941.
- Ginsberg, D.M. and Tinkham, M., 1960. Phys. Rev. 118, 990.
- Glover, R.E. and Tinkham, M., 1956. Phys. Rev. 104, 844.

- Glover, R.E. and Tinkham, M. 1957. Phys. Rev. 108, 243.
- Harrison, W.A., 1961. Phys. Rev. 123, 85.
- Hastings, C. 1955. Approximations for Digital Computers, Princeton University Press.
- Hebel, L.C. and Slichter, C.P., 1959. Phys. Rev. 113, 1504.
- Holm, R. 1951. J. Appl. Phys. 22, 569.
- Jahnke, E. and Emde, F., 1945. Tables of Functions, Dover, 4th edition.
- Kapitza, P., 1941. J. Exptl. Theoret. Phys. (U.S.S.R.) 11, 1.
- Lewis, R.R., 1956. Phys. Rev. 102, 1508.
- London, F., 1950. Superfluids, Vol. 1., Dover.
- Mackintosh, A.R., 1960. Proceedings of the VIIth Conference on Low Temperature Physics, Toronto.
- Mackinnon, L., 1955. Phys. Rev. 98, 1181.
- Magnus, W. and Oberhettinger, F., 1954. Formulas and Theorems for the Functions of Mathematical Physics, Chelsea Publishing Co., New York.
- Marcus, P.M., 1952a. Phys. Rev. 86, 649.
- Marcus, P.M., 1952b. Phys. Rev. 88, 373.
- Marcus, P.M., 1953. Phys. Rev. 90, 346.
- Markham, A.M., Netzel, R.G., and Dillinger, J.R., 1957. Rev. Sci. Instrum., 28, 382.
- Martin, D.L., 1961. Proc. Roy. Soc. A263, 378.
- Martin, D.L., 1961a. Proc. Phys. Soc. 78, 1482.
- Mason, H.E. and Bommel, W.P.J. Acoust. Soc. Am. 28, 930.
- Mattis, D.C. and Bardeen, J., 1958. Phys. Rev. 111, 412.

- Meissner, W. and Ochsenfeld, R., 1933. Naturwissenschaften, 21, 787.
- Morse, R.W., Tamerkin, P. and Bohm, H., 1956. Phys. Rev. 101, 1610.
- Morse, R.W., Olsen, T., Gavenda, J.D., 1959. Phys. Rev. Letters 3, 15.
- Nicol, J., Shapiro, S. and Smith, P.H., 1960. Phys. Rev. Letters 5, 461.
- Peshkov, V.P. and Zinov'eva, K.N., 1959. Reports of Progress in Physics 22, 504.
- Reich, H.A. and Garwin, R.L., 1958. Proceedings of 1st Conference of Institut International du Froid, Delft.
- Reynolds, C.A., Serin, B., Wright, W.H., and Nesbitt, L.B., 1950. Phys. Rev. 78, 487.
- Richayzen, G., 1958. Phys. Rev. 111, 817.
- Rickayzen, G., 1959. Phys. Rev. Letters 2, 90.
- Roberts, R.R. and Sydoriak, S.G., 1955. Phys. Rev. 98, 1672.
- Rogers, J.S., 1962. M.Sc. Thesis, University of Alberta.
- Rowell, J.M., Chynoweth, A.G., and Phillips, J.C., 1962. Phys. Rev. Letters 9, 59.
- Schiff, L.I., 1955. Quantum Mechanics, McGraw-Hill Co., New York.
- Seidel, G. and Keesom, P.H., 1958. Rev. Sci. Instrum. 29, 606.
- Shapiro, S., Smith, P.H., Nicol, J., Miles, J.L. and Strong, P.F. 1962. IBM J. Research and Develop. 6, 34.
- Sommerfeld, A. and Bethe, H., 1933. Handbuch der Physik, Springer Verlag., Berlin.

- Swihart, J.C. 1962. IBM J. Research and Develop. 6, 14.
- Sydoriak, S.G. and Roberts, T.R. 1957. Phys. Rev. 106, 175.
- Taylor, B.N. and Burstein, E., 1963. Phys. Rev. Letters 10, 14.
- Townsend, P. and Sutton, J., 1962. Phys. Rev., 128, 591.
- van den Meijdenberg, C.J.N., Taconis, K.W., and LePair, C. 1961. Physica, 27, 117.
- van Dijk, M., Durieux, M., Clement, J.R., and Logan, J.K. 1958. Reprinted in: J. Res. Nat. Bur. Stand. (U.S.A.) 64A, 1.

APPENDIX I

EVALUATION OF SOME INTEGRALS OCCURRING IN
TUNNELING PROBLEMS

Evaluation of $I = \alpha \int_{-\infty}^{\infty} Q(E) \rho_1(E) \rho_2(E+eV) [f(E) - f(E+eV)] dE$,
 at $T = 0^\circ K$ for small applied voltage, V , and arbitrary $Q(E)$.
 At $T = 0^\circ K$:

$$\begin{aligned} f(E) &= 0 && \text{for } E > 0 \\ f(E) &= 1 && \text{for } E < 0 \\ f(E+eV) &= 0 && \text{for } E > -eV \\ f(E+eV) &= 1 && \text{for } E < -eV \end{aligned}$$

Without loss of generality V is assumed positive throughout.

$$\begin{aligned} \therefore I &= \alpha \int_{-\infty}^0 Q(E) \rho_1(E) \rho_2(E+eV) dE - \alpha \int_{-\infty}^{-eV} Q(E) \rho_1(E) \rho_2(E+eV) dE \\ &= \alpha \int_{-eV}^0 Q(E) \rho_1(E) \rho_2(E+eV) dE. \end{aligned}$$

Carrying out a Taylor expansion about the Fermi level:

$$\begin{aligned} I &= \alpha \int_{-eV}^0 Q(E) [\rho_1(0) + E(\partial \rho_1 / \partial E)_{E=0} + \dots] [\rho_2(eV) + E(\partial \rho_2 / \partial E)_{E=eV} + \dots] dE \\ &= \alpha \int_{-eV}^0 Q(E) \rho_1(0) \rho_2(eV) dE + \dots \end{aligned}$$

Assuming the densities of states (ρ_1 and ρ_2) to be approximately constant in the vicinity of the Fermi surface, higher order terms may be neglected, furthermore if $eV \ll \epsilon_F$, where ϵ_F is the Fermi energy, the integral reduces to:

$$I = \alpha \rho_1(0) \rho_2(0) \int_{-eV}^0 Q(E) dE. \quad (A-1)$$

(i) For both metals in the normal state we set $Q(E) = 1$
 hence $I_{nn} = \alpha \rho_1(0) \rho_2(0) eV. \quad (A-2)$

(ii) For the case in which one of the metals is in the normal state while the other is in the superconducting state, one obtains on the basis of the BCS* theory:

$$\begin{aligned} Q(E) &= RP |E| (E^2 - \Delta^2)^{-1/2} \\ \int_{-eV}^0 Q(E) dE &= RP \int_{-eV}^0 |E| (E^2 - \Delta^2)^{-1/2} dE \\ &= RP \int_0^{eV} E (E^2 - \Delta^2)^{-1/2} dE \\ &= RP [(eV)^2 - \Delta^2]^{1/2} \end{aligned}$$

Substituting into equation (A-1) we have

$$I_{ns} = 0 \quad \text{for } eV < \Delta \quad (A-3)$$

$$I_{ns} = \alpha \rho_1(0) \rho_2(0) [(eV)^2 - \Delta^2]^{1/2} \quad \text{for } eV > \Delta \quad (A-3a)$$

(iii) For the case of two identical superconductors, at $T = 0^\circ K$, we again assume the BCS theory.

$$\begin{aligned} Q(E) &= RP \frac{|E| |E + eV|}{\sqrt{(E^2 - \Delta^2) [(E + eV)^2 - \Delta^2]}} \\ \int_{-eV}^0 Q(E) dE &= RP \int_{-eV}^0 \frac{|E| |E + eV| dE}{\sqrt{(E + \Delta)(E - \Delta)(E + eV - \Delta)(E + eV + \Delta)}} \\ &= RP \int_0^{eV} \frac{E (eV - E)}{\sqrt{(-E + \Delta)(-E - \Delta)(-E + eV - \Delta)(-E + eV + \Delta)}} dE \end{aligned}$$

* This is the original BCS theory, Bardeen, Cooper, and Schrieffer (1957), in which the energy gap parameter, Δ , is independent of energy.

$\int_{-eV}^0 Q(E) dE = 0$ for $eV < 2\Delta$ because the denominator becomes imaginary. For $eV > 2\Delta$ we have:

$$J = \int_0^{eV} Q(E) dE = \text{RP} \int_0^{eV} \frac{[(1/2eV - E) + 1/2eV] dE}{\sqrt{[(1/2eV - E) + (\Delta - 1/2eV)][(1/2eV - E) - (\Delta + 1/2eV)]}}$$

$$\cdot \int_0^{eV} \frac{[1/2eV - (1/2eV - E)] dE}{\sqrt{[(1/2eV - E) + (\Delta + 1/2eV)][(1/2eV - E) - (\Delta - 1/2eV)]}}$$

put: $u = 1/2eV - E$

$\alpha = 1/2(2\Delta - eV)$

$\beta = 1/2(2\Delta + eV)$

then:

$$J = \text{RP} \int_{-1/2eV}^{1/2eV} \frac{[(1/2eV)^2 - u^2] du}{\sqrt{(u+\alpha)(u-\beta)(u+\beta)(u-\alpha)}}$$

$$= \text{RP} \int_{-1/2eV}^{1/2eV} \frac{[(1/2eV)^2 - u^2] du}{\sqrt{(u^2 - \alpha^2)(u^2 - \beta^2)}}$$

$$= \text{RP} \frac{1}{\alpha\beta} \int_{-1/2eV}^{1/2eV} \frac{[(1/2eV)^2 - u^2] du}{\sqrt{(u^2/\alpha^2 - 1)(u^2/\beta^2 - 1)}}$$

$$= \frac{\alpha^2}{\beta^2} \int_{-1/2eV}^{1/2eV} \frac{[(eV/2\alpha)^2 - (u/\alpha)^2] d(u/\alpha)}{\sqrt{(1 - u^2/\alpha^2)(1 - \alpha^2/\beta^2 \cdot u^2/\alpha^2)}}$$

put: $t = u/\alpha$ and $-k = \alpha/\beta = (2\Delta - eV)/(2\Delta + eV)$

$$J = \text{RP} \quad 1/2 \quad \frac{(2\Delta - eV)^2}{(2\Delta + eV)} \int_{\frac{-eV}{eV - 2\Delta}}^{\frac{eV}{eV - 2\Delta}} \frac{t^2 dt}{\sqrt{(1 - t^2)(1 - k^2 t^2)}}$$

$$+ \frac{(eV)^2}{eV + 2\Delta} \int_{\frac{-eV}{eV - 2\Delta}}^{\frac{eV}{eV - 2\Delta}} \frac{dt}{\sqrt{(1 - t^2)(1 - k^2 t^2)}}$$

Since $eV > 2\Delta$ and both Δ and eV are real and positive, the real part of the integral has contributions only in the range $0 \leq t < 1$, hence:

$$J = (2\Delta + eV)k^2 \int_0^1 \frac{t^2 dt}{\sqrt{(1-t^2)(1-k^2 t^2)}} + \frac{(eV)^2}{eV + 2\Delta} \int_0^1 \frac{dt}{\sqrt{(1-t^2)(1-k^2 t^2)}}$$

using the relations: $\frac{1}{k^2}[K(k) - E(k)] = \int_0^1 \frac{t^2 dt}{\sqrt{(1-t^2)(1-k^2 t^2)}}$

and $K(k) = \int_0^1 \frac{dt}{\sqrt{(1-t^2)(1-k^2 t^2)}}$

where K and E are complete elliptic integrals of the first and second kind respectively.

Thus:

$$J = \frac{(eV)^2}{eV + 2\Delta} K\left(\frac{eV - 2\Delta}{eV + 2\Delta}\right) + (eV + 2\Delta) \left[E\left(\frac{eV - 2\Delta}{eV + 2\Delta}\right) - K\left(\frac{eV - 2\Delta}{eV + 2\Delta}\right) \right]$$

$$I_{ss} = 0 \text{ for } eV < 2\Delta \quad (A-4)$$

$$I_{ss} = \alpha p^2(0) \frac{(eV)^2}{eV + 2\Delta} K\left(\frac{eV - 2\Delta}{eV + 2\Delta}\right) + (eV + 2\Delta) \left[E\left(\frac{eV - 2\Delta}{eV + 2\Delta}\right) - K\left(\frac{eV - 2\Delta}{eV + 2\Delta}\right) \right] \quad eV > 2\Delta \quad (A-4a)$$

which agree with those obtained by Giaever Hart, and Megerle (1962).

The evaluation of the I-V characteristics for non-zero temperatures are much more difficult and can only be solved by numerical methods. Shapiro, Smith, Nicol, Miles, and Strong (1962) discuss such numerical integrations.

* Magnus and Oberhettinger (1954), pp. 112-3

APPENDIX II

NUMERICAL EVALUATION OF THE NORMALIZED CURRENT
AND RELATIVE CONDUCTANCE FOR THE CASE OF TWO
IDENTICAL SUPERCONDUCTORS AT THE ABSOLUTE ZERO.

Defining the normalized current, $J_{ss} = I_{ss}/I_{nn}$, and the relative conductance $G_{ss} = (dI/dV)_{ss}/(dI/dV)_{nn}$, for the case of two identical superconductors equation (A-4a) becomes:

$$J_{ss} = \frac{x}{x+2} K(k) + \frac{x+2}{x} E(k) - K(k) \quad (A-5)$$

$$G_{ss} = \frac{x(x+4)}{(x+2)^2} K(k) + \left[\frac{x^2}{x+2} - (x+2) \right] \frac{dK(k)}{dx} \\ + (x+2) \frac{dE(k)}{dx} + E(k) - K(k). \quad (A-6)$$

Where $x = eV/\Delta$ and $k = (x-2)/(x+2)$.

$K(k)$ and $E(k)$ may be evaluated numerically using the approximation formulae given by Hastings (1955). In order to evaluate the relative conductance the numerical results of (A-5) may not be differentiated. The reason for this being that the approximation formulae used for K and E are in the form of Chebyshev series which oscillate with small error about the true values. If one puts $y = (x-2)^2/(x+2)^2$ then:

$$\frac{dK}{dy} = \frac{1/2(y-1)K+E}{y(1-y)}$$

$$\frac{dE}{dy} = \frac{1/2(E - K)}{y}$$

may be substituted into G_{ss} (cf. Jahnke and Emde 1945, p. 76) in order to evaluate (A-6) numerically. The IBM 1620 digital computer was used in order to compile the table of J_{ss} and G_{ss} given below.

TABLE II

Energy in units of Δ_0 *	$\frac{I_{ss}}{I_{nn}}$	$\frac{(dI/dV)_{ss}}{(dI/dV)_{nn}}$
2.1	.80376	1.16424
2.2	.81986	1.15195
2.3	.83406	1.14100
2.4	.84664	1.13119
2.5	.85784	1.12238
2.6	.86786	1.11443
2.7	.87686	1.10723
2.8	.88497	1.10069
2.9	.89231	1.09473
3.0	.89897	1.08929
3.1	.90503	1.08430
3.2	.91056	1.07972
3.3	.91562	1.07550
3.4	.92026	1.07161
3.5	.92454	1.06801
3.6	.92848	1.06467
3.7	.93212	1.06158
3.8	.93549	1.05870
3.9	.93862	1.05602

* Δ_0 is the half width of the energy gap at $T = 0^\circ\text{K}$

Table II (Continued)

4.0	.94152	1.05351
4.1	.94422	1.05117
4.2	.94674	1.04898
4.3	.94910	1.04693
4.4	.95130	1.04500
4.5	.95336	1.04319
4.6	.95529	1.04148
4.7	.95711	1.03988
4.8	.95882	1.03836
4.9	.96042	1.03693
5.0	.96194	1.03558
5.2	.96472	1.03309
5.4	.96721	1.03084
5.6	.96944	1.02882
5.8	.97146	1.02699
6.0	.97328	1.02533
6.2	.97493	1.02381
6.4	.97643	1.02243
6.6	.97780	1.02116
6.8	.97906	1.01999
7.0	.98021	1.01892
7.2	.98127	1.01793
7.4	.98224	1.01702
7.6	.98314	1.01617
7.8	.98398	1.01539
8.0	.98475	1.01466
8.2	.98547	1.01398
8.4	.98614	1.01334
8.6	.98676	1.01275
8.8	.98734	1.01220

Table II (Continued)

9.0	.98789	1.01168
9.2	.98840	1.01119
9.4	.98888	1.01073
9.6	.98933	1.01030
9.8	.98975	1.00990
10.0	.99015	1.00952
10.2	.99052	1.00916
10.5	.99105	1.00865
11.0	.99183	1.00790
11.5	.99251	1.00724
12.0	.99311	1.00666
12.5	.99364	1.00615
13.0	.99411	1.00569
13.5	.99453	1.00529
14.0	.99491	1.00492
14.5	.99525	1.00459
15.0	.99556	1.00430
15.5	.99584	1.00403
16.0	.99609	1.00378
16.5	.99632	1.00356
17.0	.99654	1.00336
17.5	.99673	1.00317
18.0	.99691	1.00300
18.5	.99707	1.00284
19.0	.99722	1.00270
19.5	.99736	1.00256
20.0	.99750	1.00244
20.5	.99762	1.00232
21.0	.99773	1.00222
22.0	.99793	1.00203
23.0	.99811	1.00186

Table II (Continued)

24.0	.99827	1.00171
25.0	.99841	1.00158
26.0	.99853	1.00147
27.0	.99864	1.00136
28.0	.99874	1.00127
29.0	.99883	1.00119
30.0	.99891	1.00111
31.0	.99898	1.00105
32.0	.99904	1.00099
33.0	.99910	1.00093
34.0	.99916	1.00088
35.0	.99921	1.00083
36.0	.99925	1.00079
37.0	.99930	1.00075
38.0	.99934	1.00072
39.0	.99937	1.00068
40.0	.99941	1.00065
41.0	.99944	1.00062
42.0	.99946	1.00059
43.0	.99949	1.00057
44.0	.99952	1.00055
45.0	.99954	1.00052
46.0	.99956	1.00050
47.0	.99958	1.00048
48.0	.99960	1.00047
49.0	.99962	1.00045
50.0	.99963	1.00043
51.0	.99965	1.00042

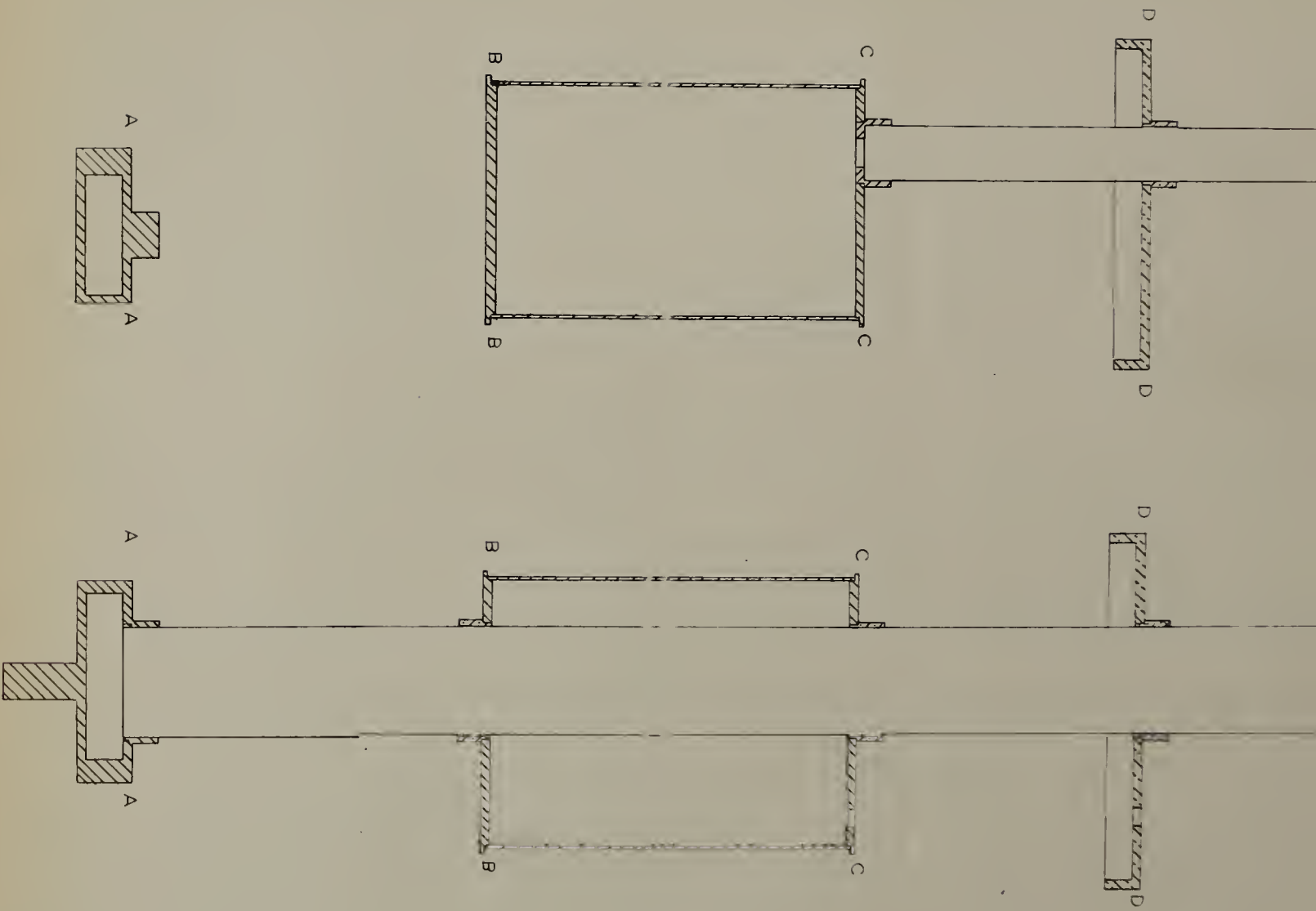
APPENDIX III

MACHINE DRAWINGS OF THE LOW TEMPERATURE PART
OF THE He³ CRYOSTAT

This appendix contains the machine drawings of the various parts of the He³ cryostat. These drawings are those which were submitted to the machine shop. It is a pleasure to acknowledge the work of Mr. G. Sanders in machining all these pieces. Various ferrules and flanges used in the room temperature part of the apparatus are of standard design and construction and do not appear in this appendix.

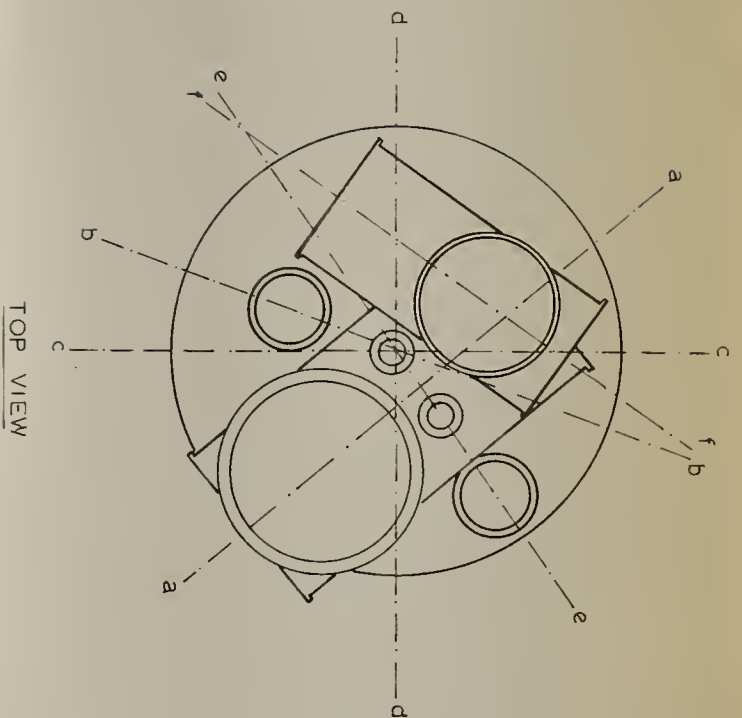
FIGURE A-1

Two sections showing assembled view of lower parts
of the He³ cryostat.



SECTION f-f

SECTION a-a



TOP VIEW

He³ CRYOSTAT

SECTIONS a-a & f-f

brass
copper

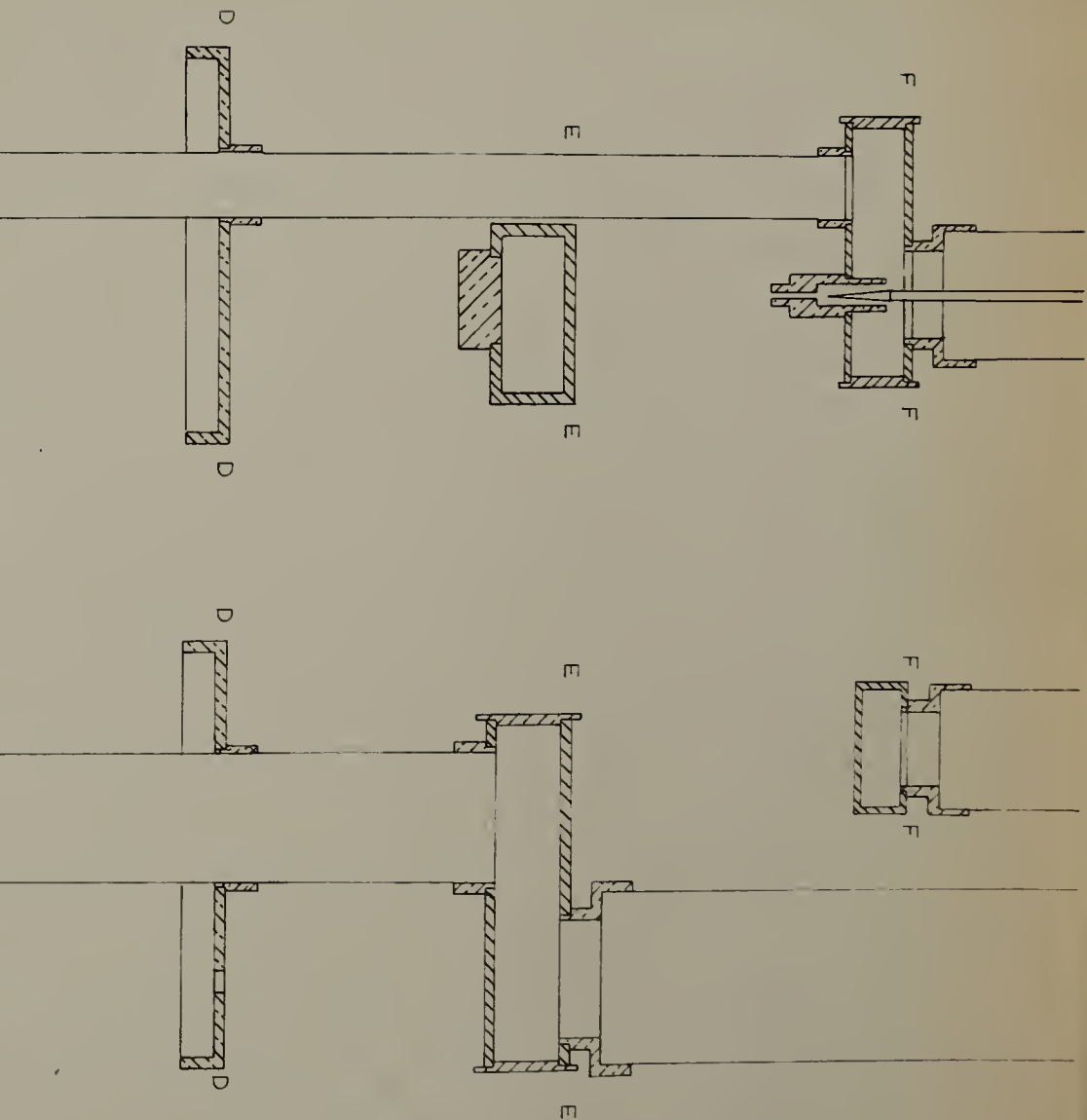
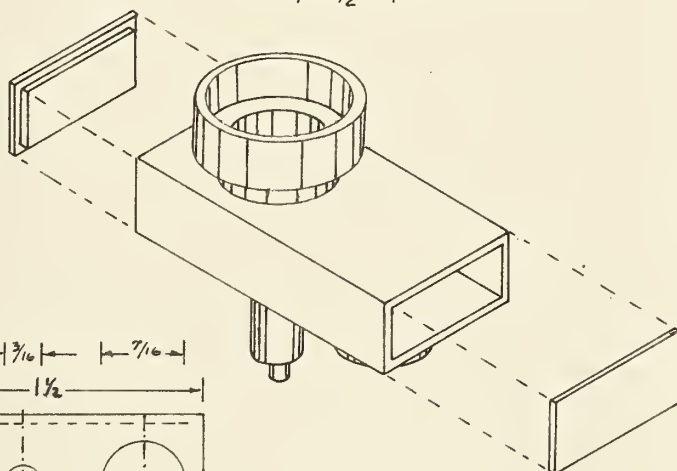
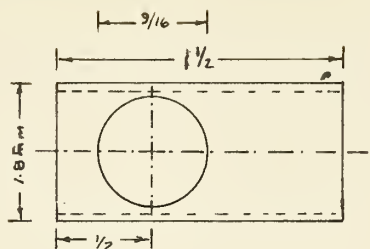
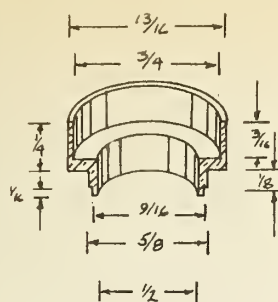


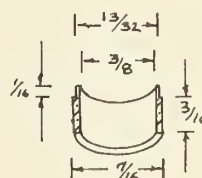
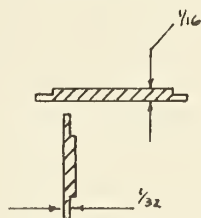
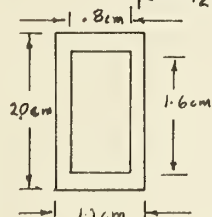
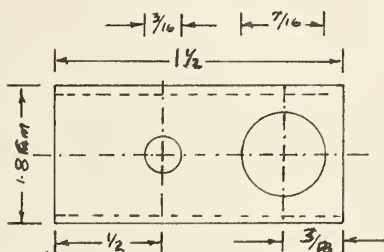


FIGURE A-2

He^4 radiation trap showing He^4 needle valve construction.
This is shown as A in Figure 4.2.



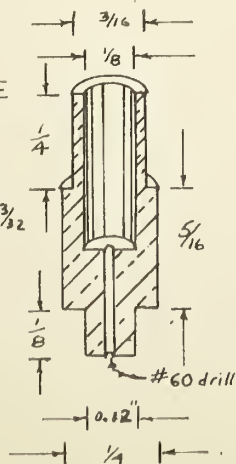
*Note: See plan view of end pieces (not pictorial view)
End pieces are to be bigger on the outside than waveguide material



SECTION F-F

NEEDLE VALVE SEAT

Use a sharp $\frac{1}{8}$ " milling cutter to provide a flat seat - depth $\frac{13}{32}$ "



He³ CRYOSTAT

He⁴ RADIATION TRAP

Notes:

- (1) Check sample in low temp. 1. Rm. & before starting
- (2) All ferrules & valve seat & brass
- (3) copper waveguide material supplied.

J. Adler

Aug. 3, 1961

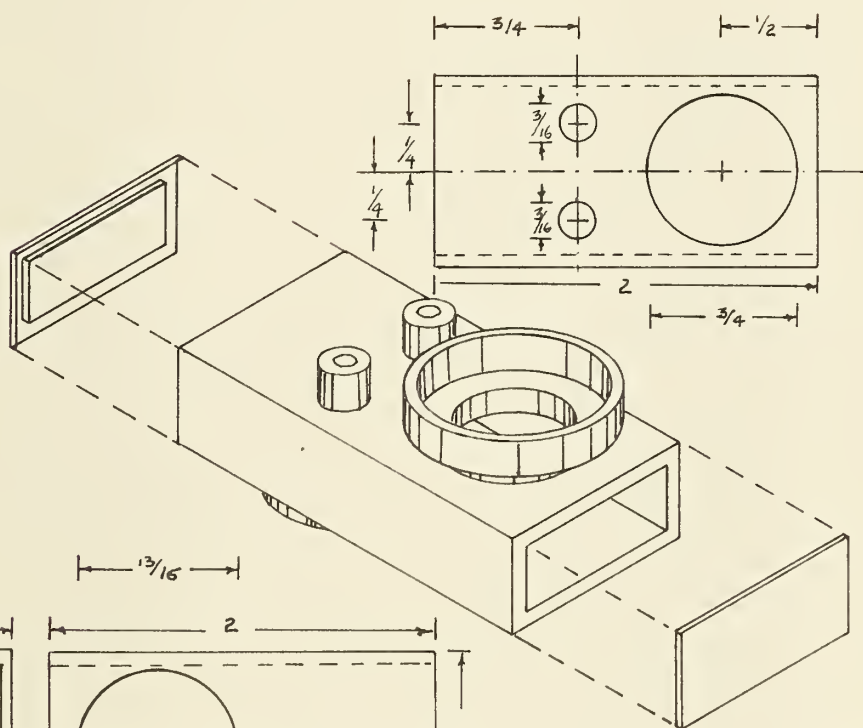
FIGURE A-3

He³ radiation trap. The two 1/8 inch ferrules were not made. One of these is to be used in the modification proposed in Chapter II, Section H, to enable the He³ condensing capillary to enter the He³ pumping tube. This radiation trap is shown as B in Fig. 4.2.

[illegible]

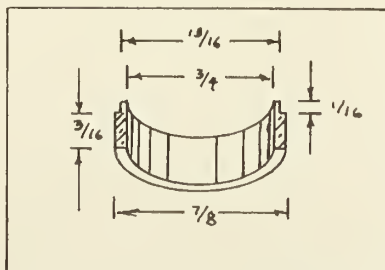
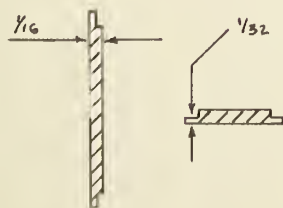
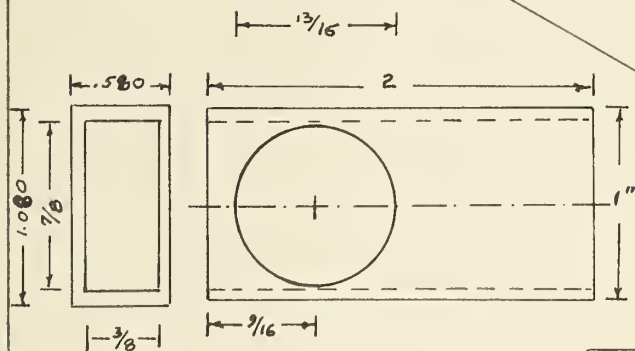
Technical drawing of a semi-circular arch. The drawing includes the following dimensions:

- Top horizontal dimension: $1\frac{1}{8}$
- Second horizontal dimension: 1
- Left vertical dimension (from top to bottom): $3\frac{1}{16}$, $1\frac{1}{4}$, and $1\frac{1}{16}$
- Right vertical dimension: $1\frac{1}{8}$
- Bottom horizontal dimension (from left to right): $1\frac{1}{16}$, $3\frac{1}{4}$, and $1\frac{1}{16}$



See note(*) on section
F.F

SECTION E-E



He³ Radiation Trap

Note: (1) copper waveguide material supplied.

(2) all ferrules brass.

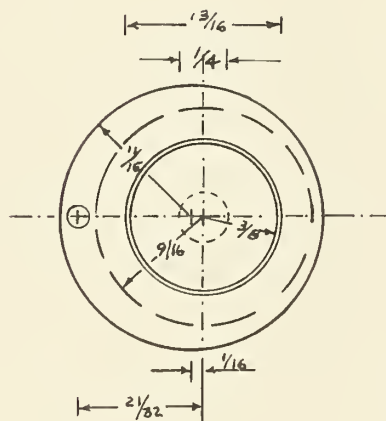
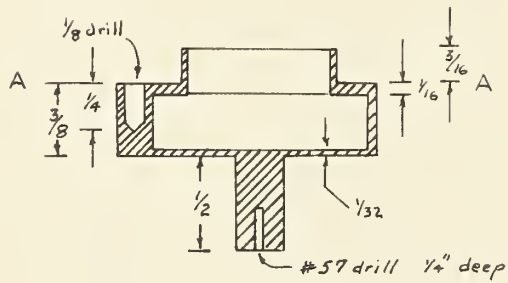
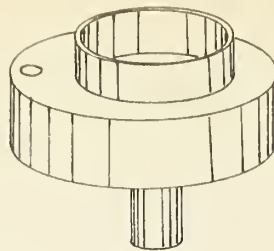
(3) check sample in low temp. lab. Rm 4

J. Adler

Aug. 2, 1961.

FIGURE A-4

The He^3 Chamber. Shown as H and J in Figure 4.2.



SECTION A-A

He^3 CRYOSTAT He^3 CHAMBER

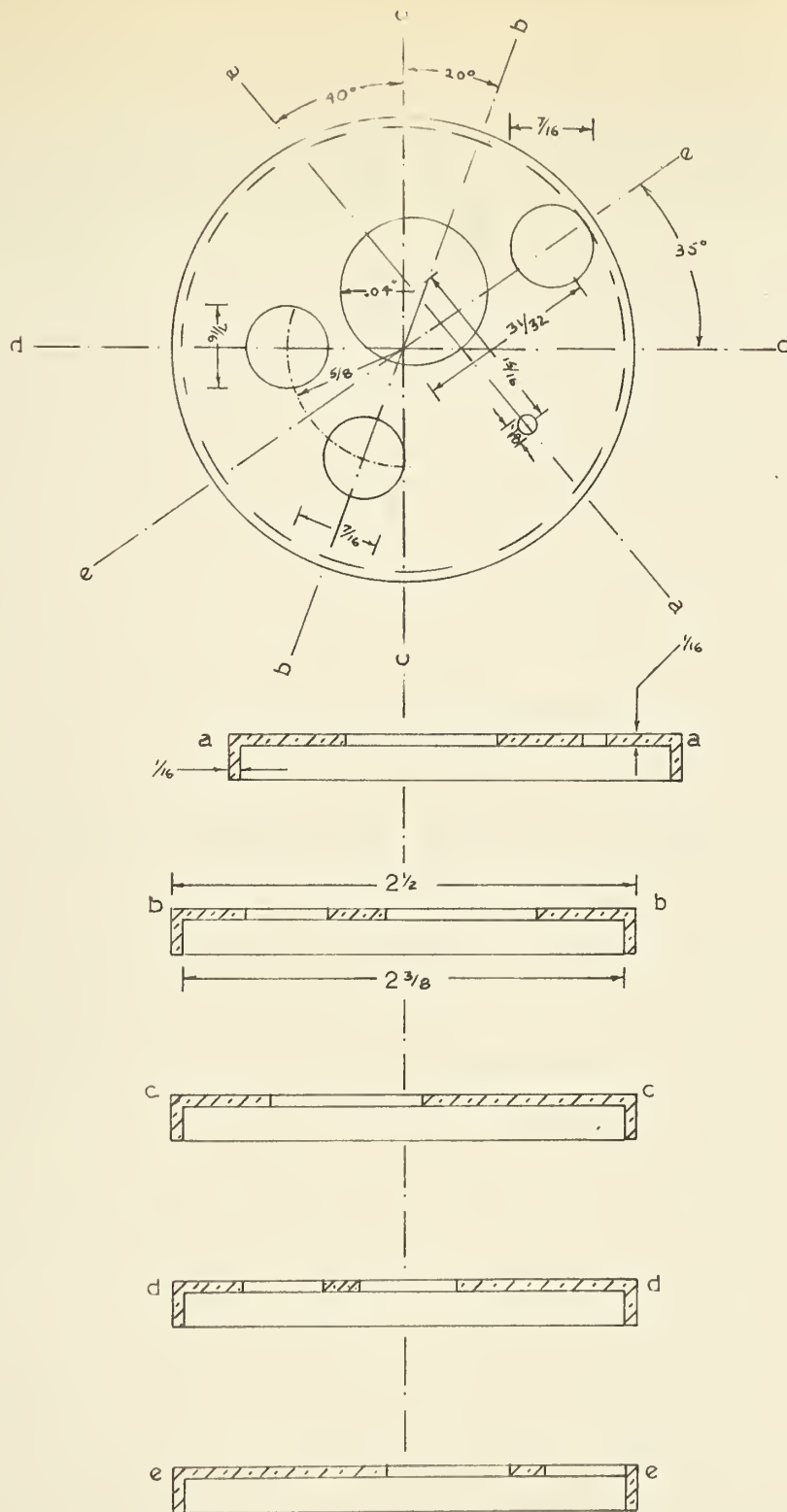
Notes: (1) All copper
 (2) One piece

J. Adler

Aug. 3, 1961.

FIGURE A-5

Top of outer brass can, shown as D in Figure 4.2.




SECTION D-D

He³ CRYOSTAT

TOP OF OUTER CAN

Scale $\frac{1}{4}$

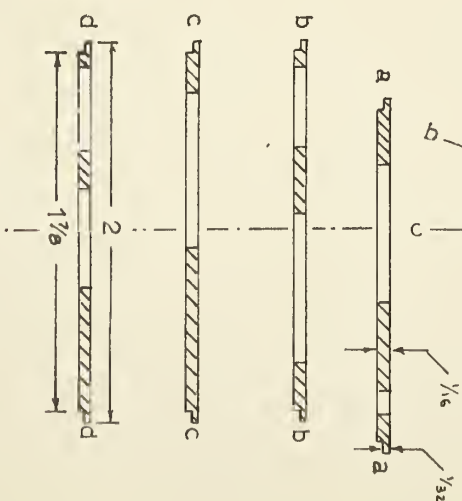
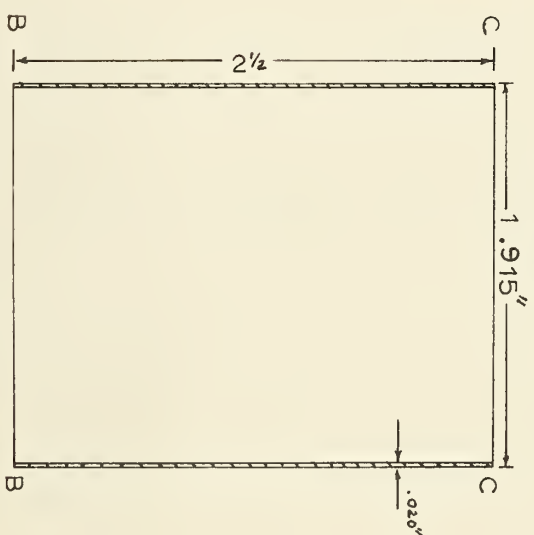
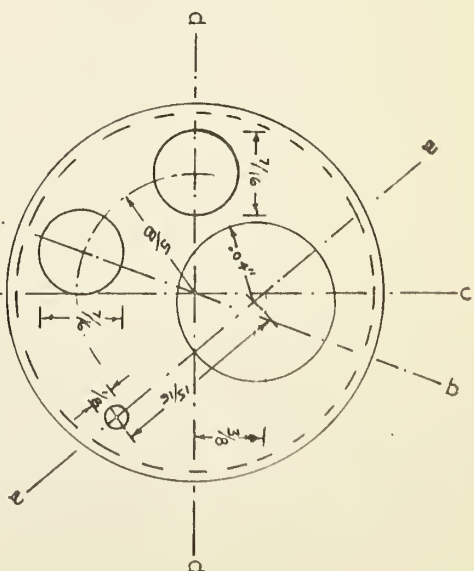
 brass

J. Adler

Aug. 3, 1961.

FIGURE A-6

The He^4 chamber, shown as F in Figure 4.2.

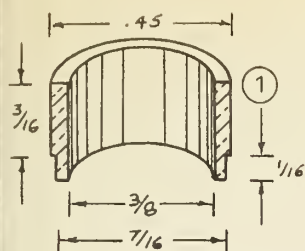
He³ CRYOSTATHe⁴ CHAMBER

Scale %

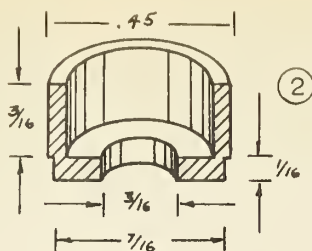
 copper

FIGURE A-7

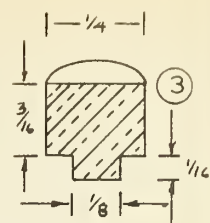
Various ferrules and their location.



7 required

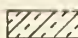


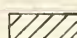
1 required

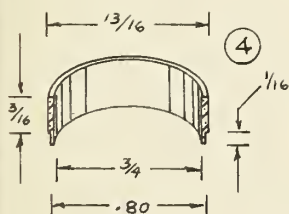


5 required

SCALE $\frac{2}{1}$

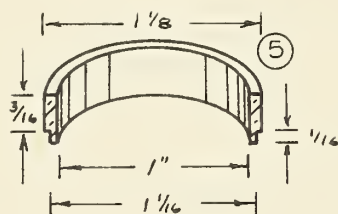
 BRASS

 COPPER

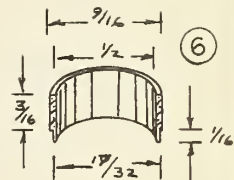


4 required

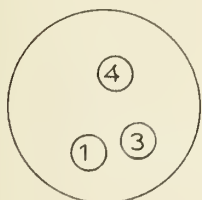
SCALE $\frac{1}{1}$



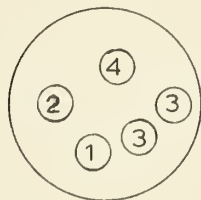
1 required



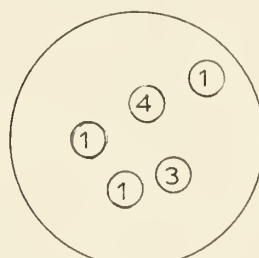
1 required



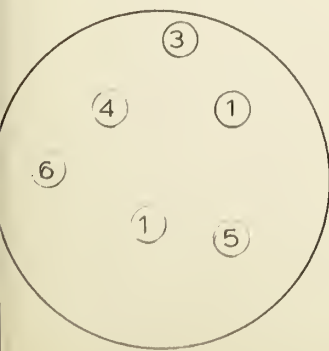
B-B



C-C



D-D



G-G

He³ CRYOSTAT
FERRULES

J. ADLER

Aug. 17, 1961

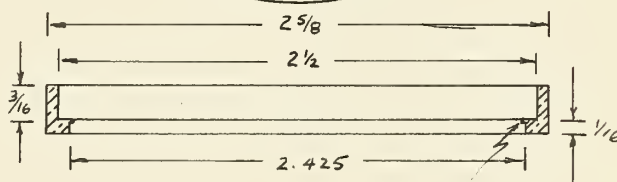
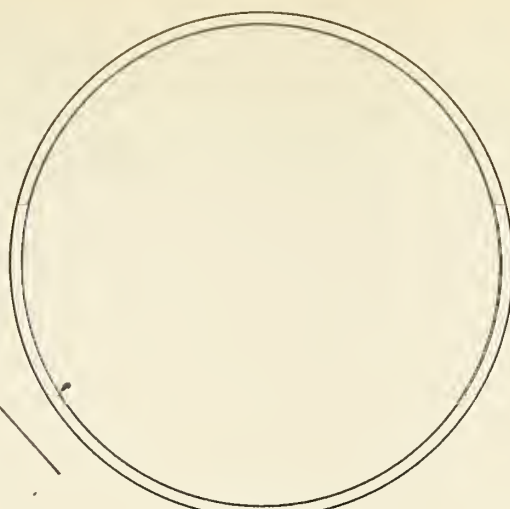
FIGURE A-8

Outer can, shown as K in Figure 4.2.

OUTER BRASS CAN



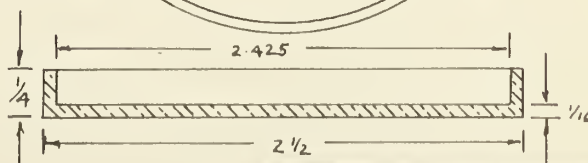
SCALE $\frac{1}{4}$



small retaining top diameter 2.40"

NOTES:

- (1) Long cylinder to be 12.5" long turned down to 2.425" O.D. on a mandrill starting with $2 \frac{3}{8}$ I.D. brass tubing
- (2) Parts to be a light press fit.
- (3) The top of can to fit loosely around plate D-D. (sliding fit)



He³ CRYOSTAT
OUTER CAN

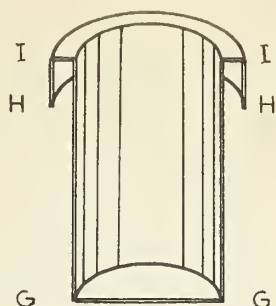
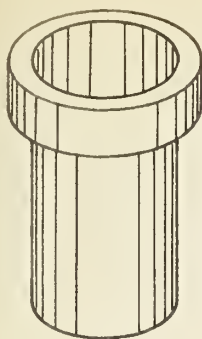
J. Adler

Aug 15, 1961

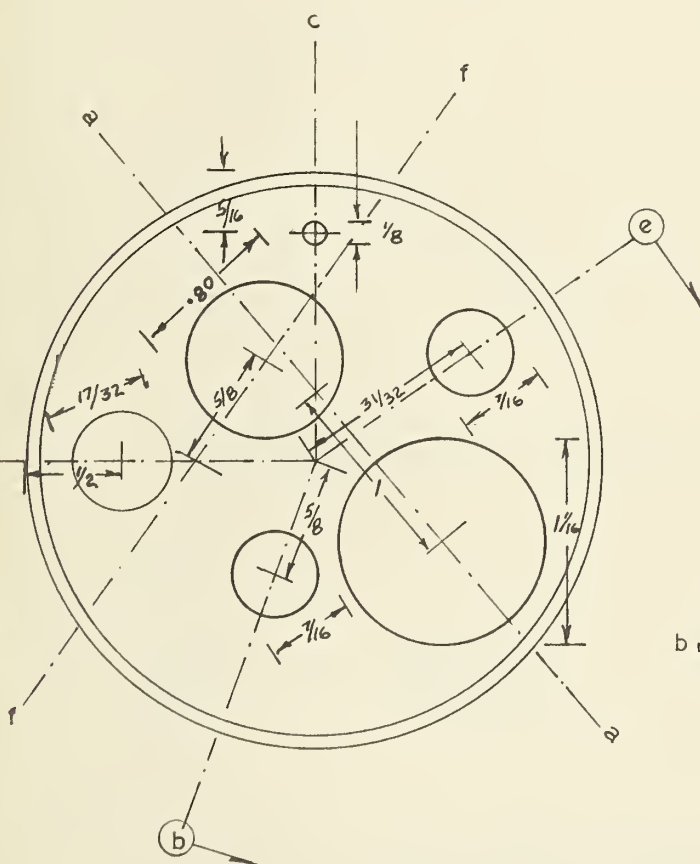
FIGURE A-9

Two drawings showing the construction of the dewar cap.

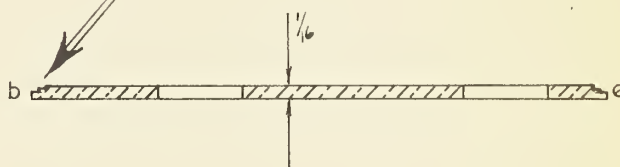
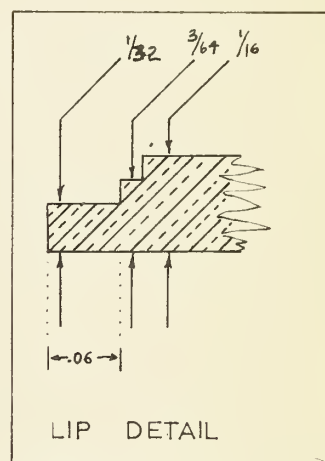
DEWAR CAP



SCALE 1/4



SECTION G-G



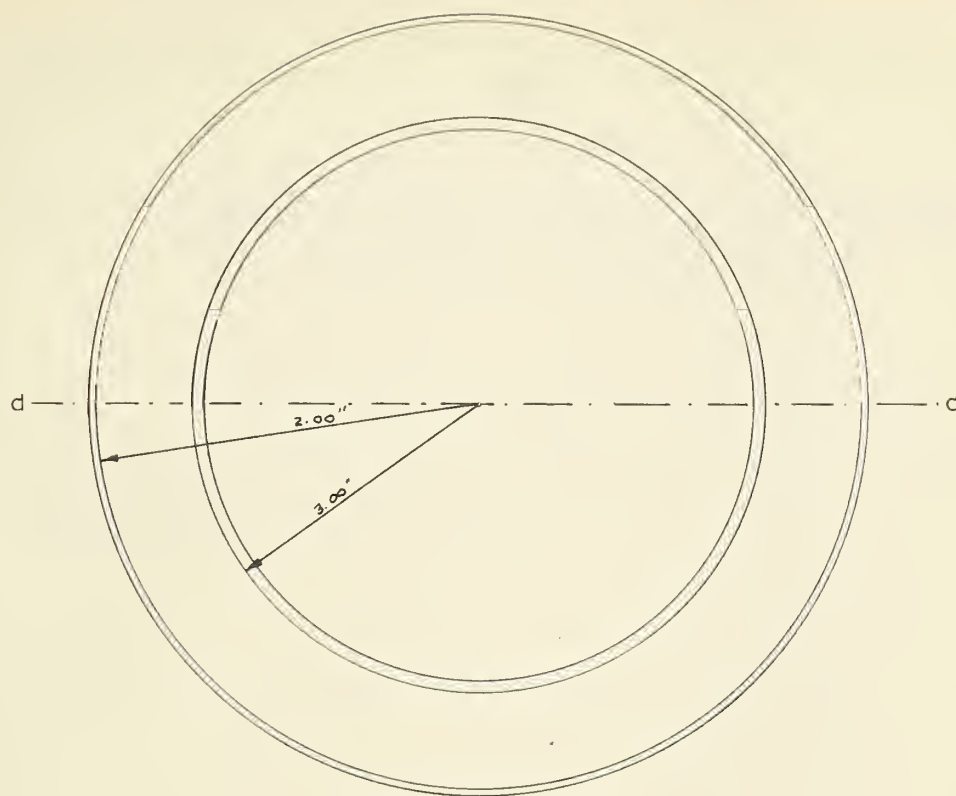
NOTES:

- (1) O.D. of section GG is 3"
- (2) Lip of section GG machined to be a light press fit in Stainless Steel tube H-G (tube supplied)
- (3) Stainless Steel Section I-G to be 4 1/2" long (#316 S.S. tube supplied).

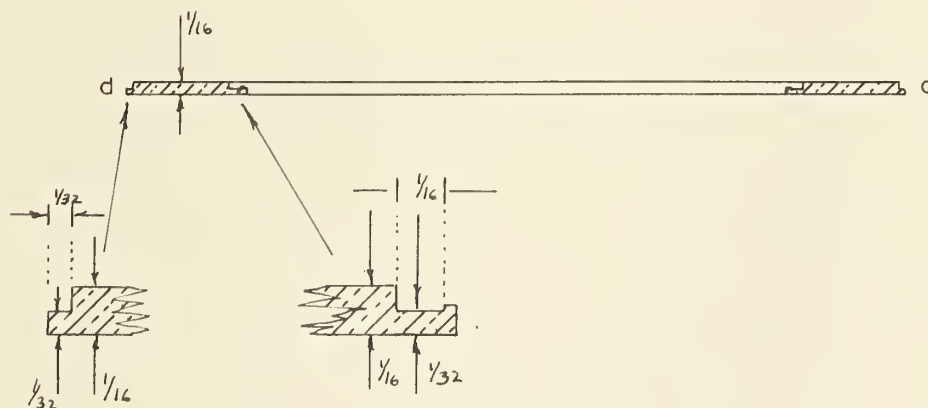
He³ CRYOSTAT

DEWAR CAP

(drawing 1)



SECTION I-I



NOTES:

- (1) Section I-I to be light press fit to S.S. tube I-G.
- (2) Section I-H to be made from $\frac{1}{32}$ " brass sheet bent around section I-I and silver soldered.
- (3) Inside diameter of section I-H to be 4.00".

He^3 CRYOSTAT

DEWAR CAP

(drawing 2)

J Adler

Aug 15, 1961.

APPENDIX IV

SUMMARY OF RESULTS AND CONCLUSIONS FOR THE
EXPERIMENTS INVOLVING INDIUM

This appendix contains the manuscript of an article submitted for publication in Physical Review Letters and is now in press.

Structure in the Density of States of Superconducting
Indium Films*.

by

J.G. Adler and J.S. Rogers

Department of Physics, University of Alberta

Edmonton, Alberta, Canada

(Received 16 January 1963)

Giaever, Hart, and Megerle¹, and more recently Rowell, Chrnaweth, and Phillips² have reported humps in the conductance vs. voltage curves for electrons tunneling between a normal metal and a superconductor through a thin insulating barrier. If one assumes (cf. Bardeen³) that the matrix element, M , that appears in the transition probability for electrons tunneling through the barrier is constant for small energy differences, then the reported humps in the conductance curves indicate structure in the density of states distribution. Solutions of the integral

equation which gives the energy gap parameter, Δ , as a function of the excitation energy E have been carried out by Swihart⁴ and Culler, Fried, Huff and Schrieffer⁵. Both of these predict structure in the density of states, in particular two humps occurring at energies near $k\Theta_D$ and $2 k\Theta_D$, where Θ_D is the Debye temperature. However, Rowell, Chynoweth, and Phillips² observed far more extensive harmonic structure in the density of states of lead than had been theoretically predicted. They observed this structure at energies $\Delta + nE_T$, where E_T is the energy of the transverse acoustic phonon in lead, and n is an integer. Since such structure has until now only been observed in lead it is of interest to examine other superconductors. As one expects such structure to be most readily observed in superconductors having a low Θ_D , the most suitable choices appear to be mercury, indium, and tin. The purpose of this letter is to describe the conductance vs. voltage curve for indium obtained from our tunneling experiments with In-Al₂O₃-Al junctions.

The relative conductance, $(dI/dV)_{ns}/(dI/dV)_{nn}$, was derived from measurements at temperatures where the indium, but not the aluminum was superconducting, along with similar measurements at 4°K where both metals were normal. Our method involved a bridge technique⁶ which

is very sensitive to the quantity $1 - (dI/dV)_{ns}/(dI/dV)_{nn}$, the latter being determined to within ± 0.0001 . The level of the relative conductance curve with respect to unity could only be determined to an accuracy of ± 0.0005 .

Measurements of the relative conductance at energies below about 6×10^{-3} eV were made at several temperatures, and agreed with those of Giaever, Hart, and Megerle¹. Our new results for higher energies are given in Fig. 1. The specimens were prepared in a manner similar to that described by Giaever⁷, they ranged in resistance from 50 to 230 ohms. Thermal contact was provided by helium gas at temperatures above the lambda point, while a film of superfluid helium formed the thermal link at lower temperatures. The relative conductance seemed to remain constant and equal to unity at voltages larger than 20 mV, this however could not be accurately ascertained since heating effects start to become noticeable at these voltages. The prominent structure, in particular the minimum at $V \approx 14.5$ mV, remained constant even at the lowest temperature available to us ($T = 0.5^\circ\text{K}$), which was well below the transition temperature of aluminum. This implies that the structure is not of the type observed by Rowell et al.², since there are no humps and there is no change in the energy at which the minimum appears as the temperature is varied (ie. the change in the size of the energy gap has no effect on the minimum).

It is evident from the scale on the ordinate of Fig. 1 that if any multiphonon effects of the type observed in lead² are present in indium then they must be smaller by more than an order of magnitude. This is not altogether unexpected since the electron-phonon interaction in indium is far weaker than in lead. The observed structure occurs at energies above the Debye energy ($k\theta_D \approx 9.5 \times 10^{-3}$ eV) and therefore an explanation in terms of the phonon spectrum seems unlikely. We have also considered the possibility that the effect may have been due to the volume change associated with the superconducting transition on the basis that the boundary of the Brillouin zone shifts and modifies the energy contours in its vicinity. This is again an unlikely explanation since in indium the superconducting phase has the larger volume. It appears that a better theoretical understanding of the factors affecting the density of electron states in a superconductor than is presently available is required in order to explain the observed effect in indium.

The authors wish to express their gratitude to Dr. S.B. Woods for his constant help and encouragement during the course of these experiments.

* This work was supported by the National Research Council of Canada.

¹I. Giaever, H.R. Hart, Jr., and K. Megerle,
Phys. Rev. 126, 941 (1962).

²J.M. Rowell, A.G. Chynoweth, J.C. Phillips,
Phys. Rev. Letters 9, 59 (1962).

³J. Bardeen, Phys. Rev. Letters 6, 57 (1961).

⁴J.C. Swihart, IBM J. Research Develop. 6, 14
(1962)

⁵G.J. Culler, B.D. Fried, R.W. Huff, and J.R.
Schrieffer, Phys. Rev. Letters 8, 399 (1962).

⁶J.G. Adler and J.S. Rogers (to be published).

⁷I. Giaever, Phys. Rev. Letters 5, 464 (1960).

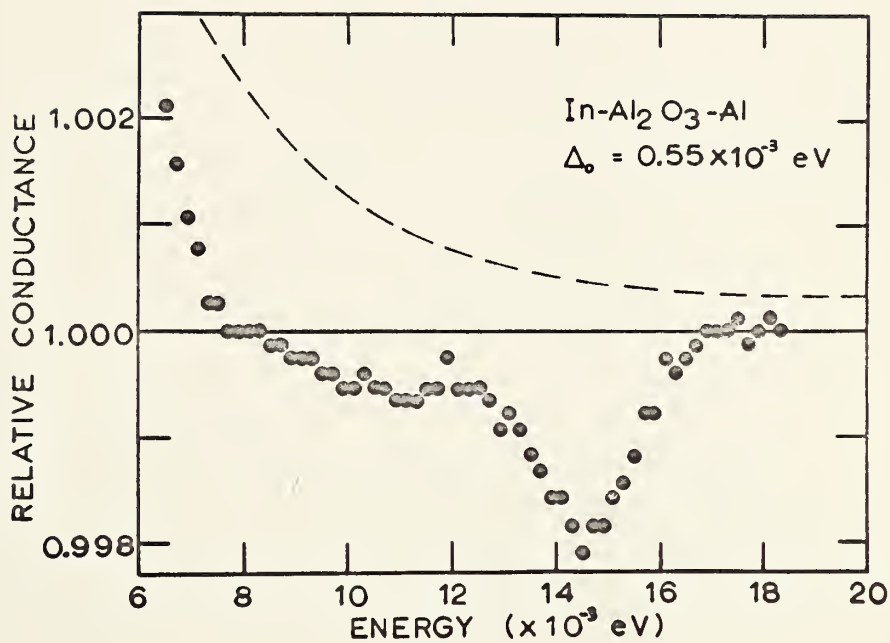


FIG. 1. Relative conductance, $(dI/dV)_{ns}/(dI/dV)_{nn}$, of an $\text{In-Al}_2\text{O}_3\text{-Al}$ tunnel junction, plotted against energy at 2°K . Δ_0 is the limiting value of the energy gap parameter obtained from measurement at $T = 0.5^\circ\text{K}$. The dashed line shows the ratio of superconducting to normal density of states calculated from the BCS theory for $T = 0^\circ\text{K}$.

B29808